ABSTRACT

Title of dissertation: THE ROLE OF THE ACTIN CROSSLINKER PALLADIN: FROM RECONSTITUTED NETWORKS TO LIVE CELLS

Brian James Grooman, Doctor of Philosophy, 2014

Dissertation directed by: Professor Arpita Upadhyaya
Department of Physics
Institute for Physical Sciences and Technology

Biophysics is a rapidly growing area of research. New discoveries continue to show the importance of mechanical phenomenon in biological processes, even at the cellular and sub-cellular levels. The complexity of living cells, coupled with their small size makes their study particularly difficult.

Palladin is an actin-crosslinker that has not yet been studied as much as other actin-crosslinkers. It localizes with alpha-actinin in stress fibers in many adult cell types. Palladin's exact purpose is still unknown. Through in-vitro studies of reconstituted actin networks we gain insight into the mechanical importance of this novel protein, and show that when partnered with α-actinin, palladin efficiently enhances the network stiffness.

Pancreatic Stellate Cells are responsible for maintaining organ integrity, and their malignant counterparts are responsible for one of the most deadly forms of cancer. Interestingly, palladin is shown to be up-regulated in tumors derived from these cells. By studying the stiffness of the cells with and without palladin (via genetic manipulation) we investigate the mechanical importance of palladin in vivo.

GFP labelled palladin can serve as a useful marker because it naturally localizes into a regular pattern along stress fibers. Combined with image processing, this makes tracking local strain rates within the cell possible. Pancreatic stellate cells will respond to an applied force by

actively contracting their stress fibers. The dynamics of these responses are quantified by tracking the spots of palladin. Through various pharmacological manipulations we study possible signaling pathways that lead from an applied force to stress fiber contraction.

Overall, this work explores the mechanical importance of palladin and also investigates the mechanical properties of tumor-associated pancreatic stellate cells, neither of which have been previously studied. Our work shows that palladin controls network stiffness in-vitro, but not in-vivo, suggesting a yet undiscovered purpose. We have also shown that pancreatic stellate cells are in the same range of stiffness as other fibroblasts, and can actively respond to external forces. All of these findings contribute to an increased understanding of the complex systems which govern the mechanical properties of living material.

THE ROLE OF THE ACTIN CROSSLINKER PALLADIN IN CYTOSKELETAL MECHANICS: FROM RECONSTITUTED NETWORKS TO LIVE CELLS

By

Brian James Grooman

Dissertation Submitted to the Faculty of the Graduate School of the
University of Maryland, College Park in partial fulfillment
of the requirements for the degree of
Doctor of Philosophy
2014

Advisory Committee:

Professor Arpita Upadhyaya, Chair
Professor Wolfgang Losert
Professor Joonil Seog
Professor Garegin Papoian
Professor Carol Keefer, Dean's Representative

Acknowledgements

First of all I would like to thank my advisor, Dr. Arpita Upadhyaya. Apart from giving me enormous freedom while studying here at Maryland she is also one of the nicest people I know. Together we have managed to succeed in pushing the boundaries of human knowledge.

I would also like to thank my committee, Dr. Wolfgang Losert, Dr. Joonil Seog, Dr. Garegin Papoian, and Dr. Carol Keefer for graciously giving their time to assist with my defense.

My fellow grad students have been a tremendous help over the years, both technically in the lab and personally outside of it. I enjoy their friendship, and hope that it will continue after I leave the lab. Christy Ketchum, Mike Azatov, King Lam Hui, you all are the best.

Shirong Zhang has been nothing short of amazing. As an undergraduate assistant she has taken care of the cells used in the experiments and learned to run many of the experiments herself. I owe her my gratitude for all of her hard work.

Some of my fellow classmates who helped me study for and pass the quals, Mike and Barbara.

I have also depended on many others outside the lab for materials and equipment. Ikoku (Ikko) Fujiwara from NIH supplied us with very high quality purified actin while asking nothing in return. The group at UNC (specifically Dr. Richard Superfine, Vinay Swaminathan and Tim O'brien) gave us the magnetic trap and have provided us with technical support over the years. Dr. Carroll Otey supplied us with the cell lines that we used in the experiments. These people have saved us loads of time and money with their support and have been a pleasure to work with.

Ed Cole let me borrow his tools and for helped me build a prototype device used for manipulating actin networks on a confocal microscope.

My future employer, for being so patient over the years and keeping a spot for me while I finish my degree. I would never have expected anyone to wait years for me to return. With the current sad state of the economy this has been an enormous weight off my shoulders.

Melissa Mandel took care of me while I was sick and helped me grow as a person in ways that I never thought possible.

My brother, Kevin, whom I picked on way too much growing up, but he still talks to me.

My Sifu, Derek Johnson, gave me an opportunity. I owe him my life. Also the rest of my kung fu brothers and sisters.

My grandfather, Bill Love, and my Mom for showing me the right way to be.

Anne, for keeping me sane and reminding me that there are great things ahead.

Table of Contents

List of Figures

1 Introduction and Background

1.1 The Structure of Life

A multi-cellular organism, such as a human, has many parts to help it survive. Its bones are rigid, and in combinations with its muscles, allow for large coordinated movements. Its teeth are even harder than the bones and are the first step of the digestive process. The skin provides a barrier against the outside world but is at the same time soft and flexible. Delicate structures in the ears detect vibrations in the air. Cells in the blood stream actively seek out invading pathogens. All of this begins as just a single cell. Its daughter cells differentiate and build all of the different parts of the body. After development completes, these cells also maintain the structural integrity of the different parts of the adult organism. Think of all the different materials that compose living objects. DNA transcription and chemical reactions give rise to highly organized structures, both within the cell itself and between them, as part of the larger organism. These structures are in fact organized and sustained by the physical interactions between them. Life, then, is a very mechanical phenomenon. Physical measurements are required for the complete study of living systems. Even cells, the fundamental building blocks of every organism, depend on their own mechanical properties as well as those of their environment. It is well known that the cytoskeleton is primarily responsible for regulating cell structure and translating external forces into chemical signals which the cell can use to modulate its behavior.

However, the complexity of this process currently places it beyond the scope of our understanding. Many thousands of scientists are trying to assemble a complete picture of the process of life. Every discovery is just another piece of the puzzle. This thesis is my own, small contribution towards completing the picture.

1.2 The Components of the Cytoskeleton and their Organization

1.2.1 The Cytoskeleton

Living cells have many parts. A lipid bilayer membrane separates the inside from the outside of the cell. The nucleus houses the DNA. The cytoskeleton is a collection of biopolymer filaments that dynamically assemble and disassemble to give cells their structure and allow them to change their morphology. Without the cytoskeleton, cells would be little more than pouches of cytoplasm floating around the body. However, the presence of the cytoskeleton enables cells to move, regulate their mechanical properties, change their shape, and much more. Actin, microtubules, and intermediate filaments are the three main components of the cytoskeleton, and through their organization and dynamic remodeling all of these mechanical feats are accomplished.

Actin filaments are comprised of monomer proteins (45 kDa), which arrange in a double helical pattern. Actin is one of the most highly conserved proteins, with a variation of less than 5% among its 375 amino acids, across all species of eukaryotic cells. Actin filaments have a persistence length of ~12μm and a diameter of approximately 7nm. The monomers have distinct ends which cause them to orient in the same direction within the filament. The resulting filament consequently has distinct ends, referred to as "plus" or "minus". Polymerization occurs more rapidly at the plus end of the filament, when the monomers have bound adenosine triphosphate (ATP). (ATP is a compound commonly used to make energy available to many different mechanisms within the cell). Shortly after binding to the filament, the ATP will hydrolyze. This changes the binding and unbinding rates, making the filaments more likely to depolymerize from the minus end. Actin monomers will nucleate on their own at sufficiently high concentrations, but nucleating proteins such as Arp 2/3 can start the growth process and allow the cell to control the location of new filament growth. The concentration needed for spontaneous polymerization (critical concentration) for an actin-only solution with ATP is approximately 0.1μM [1].

Monomers bind and unbind at different rates at each end, so a phenomenon known as treadmilling is possible, where the filament will grow at one end and shrink at the other [2]. The average length of the filaments depends on the total concentration of monomers. The amount of actin in excess of the critical concentration will be found in filaments. The length distribution of actin filaments is exponential in steady state in-vitro networks, but Gaussian in the presence of stabilizing proteins [3].

The polymerization of actin can also generate forces. Migrating Listeria monocytogenes, as well as the leading edge of lamellipodia (wide, flat protrusions of the cell) are thought to be driven by the same polymerization process[4]. This was directly observed by using empty vesicles coated with the virulence factor ActA. ActA promotes actin polymerization, which in turn pushes on the vesicle, causing it to move and change shape [5]. Force generation is described by the Brownian ratchet model proposed by Oster and colleagues. According to this theory, thermal fluctuations create a gap between the polymerizing filament and the object it touches, either by the object moving away or by compression or buckling of the existing filament. A new monomer can squeeze into the gap and lengthen the filament[4,6]. This continuing process is essentially a ratcheting mechanism that depends on new monomers having an on rate higher than the off rate of existing monomers. The polymerization stall force (1pN) has been directly measured with optical tweezers [7].

The polymerization process also depends on the organization of the monomers within the filaments. The double stranded structure of actin filaments allows them to grow to a much longer length than a single strand with the same monomer on/off rates. This is because double stranded actin only polymerizes and depolymerizes at its ends, whereas single strands are equally likely to sever at any point along their length. Consider a break in the middle of each type of filament. The single strand requires only one break, so the disassociation constant is the same at the ends

and the center. However, the double strand requires two bonds to sever the outermost protein, but three bonds to sever anywhere else on the filament[8].

In addition to actin, two other structural entities comprise the cytoskeleton: microtubules (MTs) and intermediate filaments (IFs). Microtubules are hollow tubes of alpha and beta tubulin responsible for cellular organization and organelle transport within the cell. They are the stiffest of the filaments, with a persistence length of ~6mm. Intermediate filaments are composed of a variety of different proteins but all share similar properties. They are typically 10nm wide and have a very short persistence length of 1μm. Unlike the other two types of filaments, IFs can be easily stretched. Intermediate filaments are thought to aid in strengthening animal cells by adding elastic resilience to the cells[9].

Although all three of these structural elements serve important roles within the cell, actin is the most dynamic and versatile of the three. Microvilli, muscle, lamellipodia, stress fibers, the actin cortex, contractile rings, filopodia, and membrane ruffles are all at least partially actin based structures. The breadth of uses for this protein are made possible by two things: a wide array of actin binding proteins (ABPs) that serve to organize and regulate filament growth and orientation, and the semi flexible nature of the individual filaments. It is therefore of great interest to examine the filaments' mechanical properties.

1.2.2 The Beam Equation and Semi flexible polymers

Physically, actin filaments can be thought of as slender bodies with their cross-sectional width being much smaller than their lengths. The elastic properties of slender bodies are best described by the Euler beam theory which relates the material properties of the filament to its geometry under applied loads. For small deflections, the beam equation describes the amount of deflection given an applied torque. In this case the torque is known as the bending moment, and can be described as

$$M = EI/R \tag{1.1}$$

R is the radius of curvature of the beam. The constant EI depends on the beam's material properties, as well as the beam's geometry. Combined, EI is the flexural rigidity, a parameter similar to a spring constant. It defines the linear relationship between the bending moment, and 1/R, the inverse of the radius of curvature. E is the Young's modulus, and describes the compressibility/extensibility of a material. *I* is the second moment of area, defined as:

$$I_{xx} = \iint_A y^2 dxdy \tag{1.2}$$

In this case, the beam lies in the z-direction, and is being bent in the y-direction. The beam remains in the x-z plane.

For actin, which has a double helical structure, the second moment changes depending on the location in the helix. However, the full repeat length of the double helical pattern is only 72 nm. Because of their symmetry, the structure repeats at half of this length: 36nm. Actin filaments are typically much longer than their repeat length, so the effective second moment depends on the geometric mean of the moment about the two principal axes. This simplifies to a dependence on the total area of the cross-section. For actin, the area is 19 nm^2; leading to a 2nd moment is then 29 nm^4. Combined with a Young's Modulus of E = 2.3 GPa, we find a flexural rigidity of 66 $nN*nm^2$ [8]. In order for the beam equation to hold, we must assume that the length of the filament is much longer than its other dimensions. If the strain is not too high, the beam will deform uniformly, following an arc. This regime holds while the internal stress/strain relationship is still linear. For actin, this equates to a 250nm radius of curvature[8].

Actin filaments are subject to thermal fluctuations, which bend the filaments in a stochastic manner. An effective measure of the resonse to thermal fluctuations is the persistence length. Persistence length is defined as the length at which there is no longer a correlation in direction between two ends of the filament during stochastic thermal fluctuations. Mathematically:

$$l_p = \frac{EI}{k_B T} \quad 1.3$$

Where l_p is the persistence length, E is the Young's modulus, I is the second moment of bending stiffness, k_B is the Boltzmann constant, and T is temperature. Here, k_BT at 37°C (typical body temperature) is approximately 4.3×10^{-21} Joules or 4.3 pN*nm. Combined with the value for EI listed above, we can estimate a persistence length of approximately 15μm. Therefore, actin filaments belong to a class of materials known as semi-flexible polymers, which means their length is approximately the same as their persistence length.

The persistence length may also be computed by directly observing a filament undergoing thermal fluctuations (Figure 1-1).

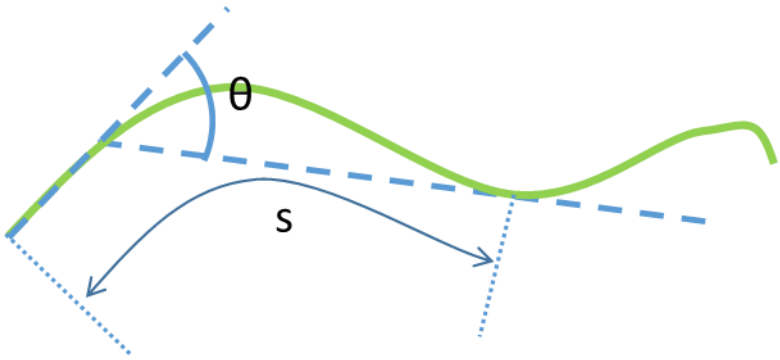

Figure 1-1: Diagram of persistence length measurement. The actin filament is shown in green.

$$\langle \mathrm{Cos}\,\theta(s) \rangle = e^{-\frac{s}{l_p}} \quad 1.4$$

Here, s is a distance along the contour of the filament. Θ is the angle between two vectors tangent to the filament, a distance s apart. The angled brackets denote the average over all of the measurements a distance s apart along the same stress fiber. This version of the equation assumes the filament is free to fluctuate in three dimensions. Using this method, [10] finds a persistence length of 16.7±0.2 μm when stabilized with rhodamine labeled phalloidin (very close to the 15μm calculated by equation 1.3).

Filament buckling occurs when a compressive load is applied lengthwise to the filament. Once a critical force is reached, the filament will bend outwards (buckle). After the filament has buckled, a force lower than the critical force is required to maintain the bend in the filament. The critical force depends on the length, Young's modulus, second moment as described below:

$$F_c = \frac{b\,EI}{L^2} \qquad 1.5$$

Where F_c is the critical force, E is the Young's modulus, I is the second moment of bending, L is the filament length and b is a constant of proportionality determined by whether the filament ends are allowed to pivot or are held at a fixed orientation. Using this equation we find that a 1μm actin filament free to rotate at both ends ($b = \pi^2$) would buckle under a 0.6pN load. This can be especially important for the arrangement of filaments in the cytoskeleton because the unsupported length of actin can determine the strength of the larger structure it is a part of. Cells actually exploit this fact to tune their mechanical properties by using other proteins to carefully organize actin filaments.

1.2.3 Actin Binding Proteins and Actin Networks

A wide variety of actin-based structures depend on actin-binding proteins (ABPs) that organize the actin filaments into intricate networks and bundles. In 1986 Pollard and Cooper characterized several dozen ABPs, and a 2003 review counted 162 unique types[11]. ABPs can serve as nucleation sites, cap filaments, sever filaments, sequester g-actin to prevent polymerization, bundle or cross-link, bind to other objects in the cell, regulate depolymerization, stabilize filaments, and in the case of motor proteins, use actin as a guide for transport. In the case of binding, ABPs may bind actin to focal adhesion sites, the membrane, microtubules and intermediate filaments, organelles, various trans-membrane receptors. In most cases, ABPs bind to actin at conserved sites, but the cross-linkers themselves may vary in size and shape. These variations allow for the great diversity of actin structures. Both calponin homology domains and immunoglobulin-like domains may bind to these conserved sites [11]. The wide variety of ABPs

make actin a versatile building block that can be used to form many different structures within the cell. Figure 1-2, illustrates several examples of ABP – actin interaction.

There are many examples of ABPs that regulate the cytoskeletal structure. A few will be discussed here to illustrate the wide variety of ABPs that can be found in a cell. This paragraph serves as a brief introduction, and many more examples will be discussed elsewhere in the thesis. The different actin based structures in the cell are a result of which ABPs are present. For instance, Arp 2/3 organizes actin into branched networks that polymerize towards the leading edge of lamellipodia [12]. Filamin, can organize actin into either bundles or a gel-like scaffold, depending on the filamin to F-actin ratio. The main reasons for this difference are the shape and structure of the filamin protein. Filamin is long and flexible. This allows it to bind two filaments at almost any orientation [13]. On the other hand, there are ABPs like fascin, which are short and rigid. Fascin forms tightly packed bundles of actin that grow into long protrusions known as filopodia [14]. In addition to these proteins which aid in growing structures, other proteins are used to disassemble the networks. Gelsolin is a severing and capping protein which prevents further growth at the plus end of an actin filament. This prevents uneccessary filament elongation away from the leading edge of lamellipodia. Cofilin severs actin filaments and in doing so creates more minus ends along the filament where depolymerization can occur. This allows for rapid disassembly of actin-fascin bundles in filopodia [15].

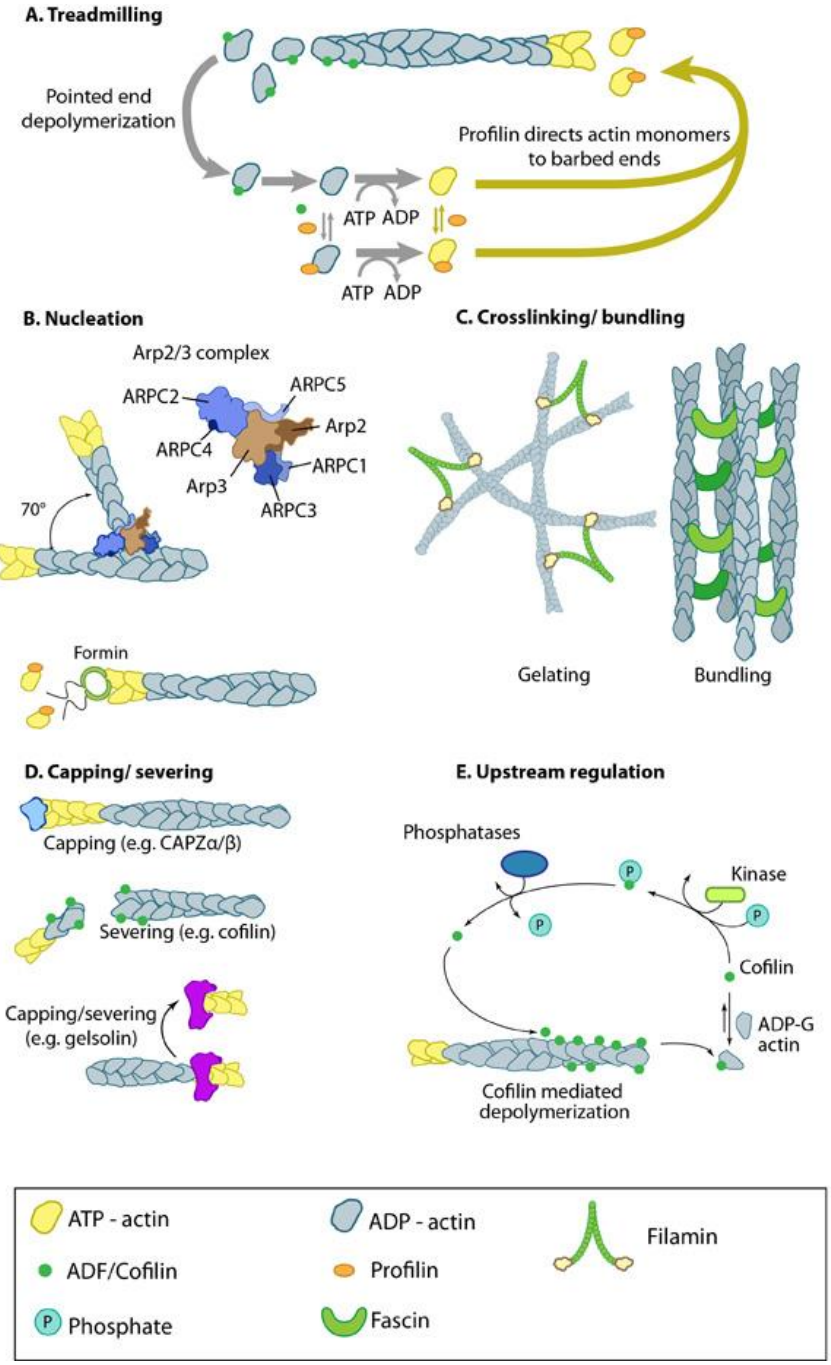

Figure 1-2: Representation of various actin associated proteins.

Figure used by permission from MBInfo: www.mechanobio.info; Mechanobiology Institute, National University of Singapore

It is possible to selectively purify actin and ABPs so that the interplay between them can be studied outside of a living cell. A common experimental procedure is to polymerize actin in the presence of a single species of cross-linker. This bottom-up approach removes the vast

complexity of a live cell and allows us to see how the properties of individual cross-linkers give rise to network morphology. The resulting structures vary morphologically depending on the type and concentration of cross-linker present. For example, α-actinin will form networks with short, straight bundles that are highly branched[16], whereas filamin-A at high enough concentrations will form networks with long, curved bundles[17]. Another crosslinker, palladin, will form networks very similar to those of alpha-actinin except that the spacing between the bundles is noticeably larger[18]. At higher concentrations of cross-linkers, the networks are no longer homogenous, but consist of discrete clusters of actin bundles. Thus, we see that network morphology must be governed by the concentration and physical properties of the cross-linking proteins.

1.2.4 Morphology and Mechanical Properties of *in vitro* Actin Networks

As discussed previously, cells can use actin to fulfill a variety of different roles. The mechanical requirements of these roles vary significantly. *In vitro* studies give us precise control over network parameters and help us to elucidate the origins of network elasticity.

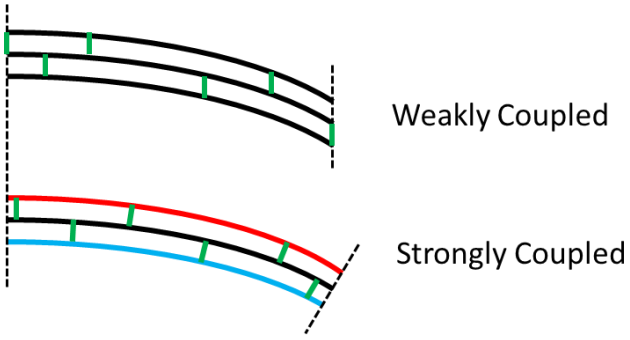

Figure 1-3: Diagram of coupled vs. uncoupled bending. Red and blue represent elongation and compression respectively. Black represents no change in length. Strongly coupled bundles require more energy to bend because their constituent filaments must change length.

The organization of the individual filaments within a network gives rise to varying mechanical properties. Even though actin filaments are semi-flexible polymers which can buckle under sub-piconewton forces, they can be utilized to form very rigid structures. Fascin, for example, forms

tightly bound actin bundles that are strongly coupled [14]. These bundles far exceed the stiffness of individual filaments and are used to stabilize and extend filopodia. Actin, although somewhat flexible, is not very compressible, with a Young's modulus of 2.3 GPa. Bending of strongly coupled bundles require the outer filaments to undergo large axial strains (See Figure 1-3). Therefore, tightly bound, highly coupled actin bundles have a much higher bending stiffness than their individual counterparts [8].

Individual bundle stiffness depends mainly on two factors: the number of filaments and how strongly the filaments are connected. Most models treat the filaments as beams and define a coupling parameter, which represents the shear stiffness of the cross-linkers between the filaments[19]. Using this model, strongly coupled bundles exhibit a stiffness dependence on n^2, while very weakly coupled bundles depend only on n (where n is the number of filaments) [20]. Species of cross-linkers couple the actin filaments by varying extents, from the crystalline structure in limulus sperm (fully coupled)[21] to hair cell stereocillia (decoupled). Likewise, in vitro bundles also display a broad range of bundle mechanics, dependent upon the cross-linker used. For example, plastin exhibits a linear dependence on the number of filaments [22], whereas fascin can strongly couple the filaments in the bundle at high enough concentrations[20]. One experiment used synthetic ABPs of various lengths but identical binding sites. The longer ABPs were naturally more flexible and allowed for greater shear movement between filaments. They found that more tightly bound bundles (strongly coupled) were indeed stiffer [23].

Just as the mechanical properties of individual bundles depend on the properties of the cross-linkers, so to do the mechanical properties of larger networks. *In vitro* actin networks are viscoelastic, meaning that they exhibit a restorative force when deformed, but also continuously deform under stress. The type of response observed depends on the rate of deformation. Over short time scales the material will behave elastically, meaning that the deformation is proportional to the applied force. On longer time scales the material will flow. Even though the applied force

is not changing, deformation continues. However, even if the material has transitioned to a flow state, there will still be an elastic recoil when the applied force is taken away. Materials of this type are called viscoelastic because they are simultaneously a viscous material and an elastic material. Another way to think of this is in terms of stored and lost energy. An elastic material stores all of the energy when it is deformed, while a viscous material dissipates it. There is no reason that a material has to be strictly one or the other, so there are in fact some materials that are both at the same time.

When measuring the properties of a viscoelastic material, we want to know how much energy the material stores and how much it dissipates. It is also important to know how long it takes for the material to transition from an elastic regime to a viscous one. To accomplish this, the stress strain relationship is measured at different strain rates. The most convenient way to do this is to drive the deformation as sinusoidal strains at varying frequencies. For biological samples this is accomplished with a cone-plate rheometer (the geometry of the rheometer allows for a consistent strain throughout the sample). Higher frequencies mean a higher strain rate. For purely elastic materials, the stress and strain will be perfectly in phase. For viscous samples, the stress and strain are 90 degrees out of phase because the sinusoidal strain means that the highest strain rate (and therefore highest drag forces) occur at zero displacement. This allows us to calculate the complex shear modulus, G*, which consists of two parts: the storage and loss moduli (G' and G" respectively), using the following relationship for oscillating stress and strain:

$$G^* = \frac{\sigma}{\gamma} = \frac{\sigma_0}{\gamma_0} e^{i\delta} = \frac{\sigma_0}{\gamma_0}(\cos\delta + i\sin\delta) = G' + iG'' \qquad 1.6$$

Where G* is the complex modulus, σ is the stress ($\sigma = \sigma_0 \sin(\omega t + \delta)$), γ is the strain, ($\gamma = \gamma_0 \sin(\omega t)$), and δ is the phase lag between the stress and strain. The storage modulus, G', and the loss modulus, G", represent the elastic and viscous components of the material's response to applied forces. The storage and loss moduli are not constants, but depend on the rate of

deformation (the driving frequency in the case of oscillating strain). Therefore, they are typically described over a range of frequencies.

Continuing with the bottom-up approach of studying in vitro actin networks, the next step is to add complexity by adding a second cross-linker to the network. Several studies have shown that multiple ABPs can exhibit cooperative effects. For example, filamin and fascin enhance network elasticity significantly more when used together than they would at higher concentrations separately [24]. Coffilin will disassemble actin filaments bound with fascin more quickly than those without [15]. Palladin and alpha actinin will bind to each other as well as actin [25,26], and low concentrations of palladin can stiffen an actin – alpha actinin network slightly more efficiently than additional alpha actinin [18].

These in vitro experiments do not even begin to approach the complexity that exists within a live cell, but nonetheless have revealed many interesting behaviors of the actin cytoskeleton. The study of any new ABP can benefit greatly from these techniques by allowing us to see the ABP's interaction with actin filaments without all of the other components present in living sample.

1.2.5 Cytoskeletal Organization in Vivo

In vitro experiments typically produce homogeneous networks of actin bundles. However, in a live cell there may be many distinct structures present at any given time. For example, Lamellipodia are driven by a highly branched network of polymerizing actin filaments. The force of the polymerization pushes the membrane forward during cell spreading and migration. Similar structures known as filopodia are much narrower protrusions, but are also driven by actin polymerization. In this case, fascin is the main cross-linker rather than the arp 2/3 complex, and it causes the actin to tightly bundle rather than branch. After the filopodium is no longer needed,

cofilin will rapidly sever the actin filaments. Thus, the difference in structure is determined by the mechanics of the abundant ABP (See Figure 1-2).

Actin is also found near the membrane and stabilizes the outer edge of the cell. This structure is called the actin cortex. This is also a gel-like structure, and it is formed with spectrin. Spectrin is a long actin cross-linker and allows for filaments to be attached at large angles relative to one another[27]. Villin is another protein that controls the shape of the cell membrane [28]. This ABP is responsible for forming microvilli on the cell surface, which serve to dramatically increase the plasma membrane surface area[29]. These structures are more permanent than the fascin-cofilin filopodia.

Stress fibers are yet another multi-filament actin structure. However, there are several key differences between stress fibers and the structures discussed previously. The first is the abundance of non-muscle myosin II, an active motor protein. Even though stress fibers are long and thin, like filopodia, the actin filaments in stress fibers orient in both directions. Figure 1-4 illustrates how the various components in stress fibers are organized.

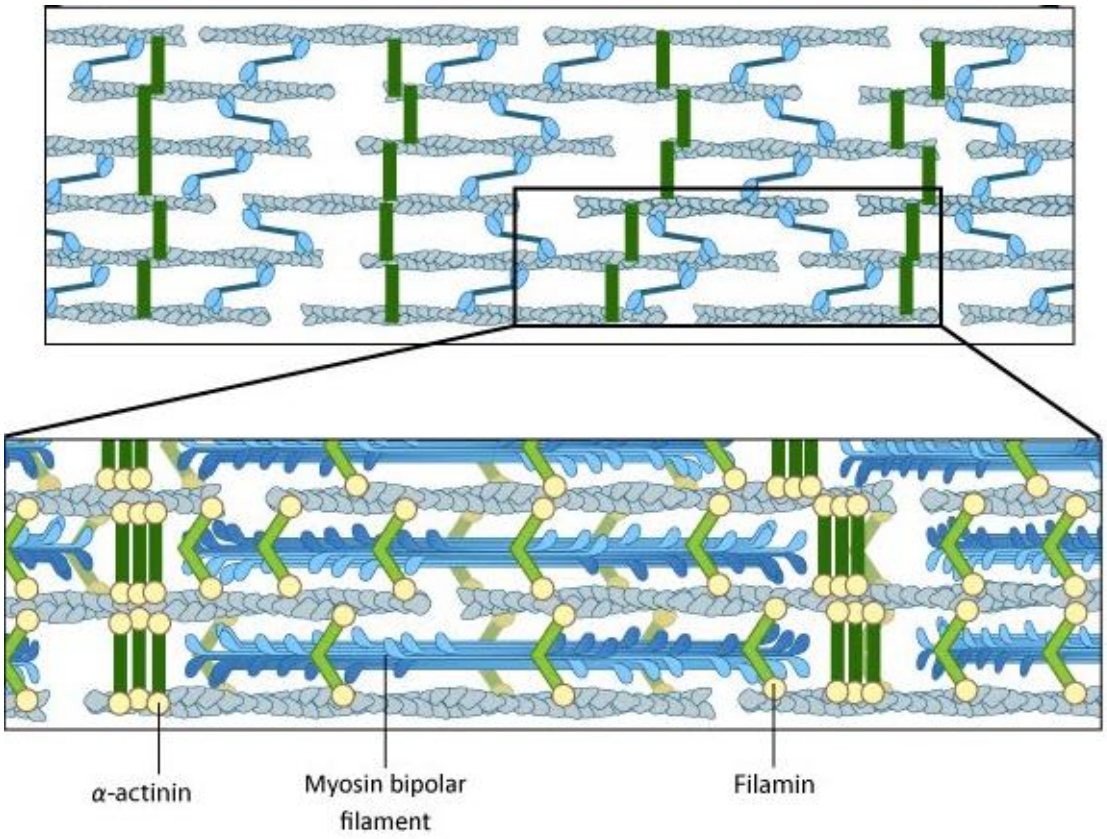

Figure 1-4 Diagram of stress fiber components and their organization. Actin filaments are in grey. Notice that the actin filaments point in both directions.

Figure used by permission from MBInfo: www.mechanobio.info; Mechanobiology Institute, National University of Singapore

Non-muscle myosin II can only bind to anti-parallel filaments, and hence, active contraction of the stress fibers can only occur if filaments in both directions are present. Stress fibers are also internally cross-linked by alpha actinin and palladin, two cross-linkers that do not bind actin filaments as tightly as fascin or villin. This allows for the myosin to function and actively contract the stress fibers from within. Thus, the dynamics of the stress fibers do not depend on active polymerization, like the other structures listed above, but instead rely on active motors within the structure itself. Stress fibers often anchor either end at a focal adhesion, a site where trans-membrane proteins attach to objects outside of the cell. Stress fibers can also be very long, often spanning the entire length of the cell.

1.3 Mechanical Properties of Living Cells

1.3.1 Techniques for Direct Measurement of Mechanical Properties

While cells are complex, they can be characterized by well-defined material properties which can be directly measured. A number of techniques have been used to do so, which we briefly describe below.

Atomic Force Microscopy (AFM) is a versatile technology that enables many types of physical interaction with cells. The first is nano-indentation. This simply uses a conical AFM tip to indent a cell on the surface. Conical indentations allow for an easy measurement of cell elasticity:

$$z - z_0 = \frac{F}{k} + \sqrt{\frac{\pi}{2}\frac{F(1-v^2)}{E\tan(\alpha)}} \qquad 1.7$$

Where z is the vertical displacement, F is the force, k is the tip spring constant, E is the Young's modulus, v is the Poisson ratio, and α is the conical angle. An AFM was successfully used to map the elasticity of a cell and compare it to the locations of various components of the cytoskeleton [30]. Interestingly, the microtubules, despite being the largest structures, showed the least contribution to local elasticity. Instead, high concentrations of actin and intermediate filaments were more strongly correlated with areas of high elasticity.

AFM tips may also be used to hook and pull various objects, such as stress fibers [31]. In this case, the internal tension of the stress fibers was estimated by pulling on them in a perpendicular direction to their length. By measuring the force and distance required for the displacement, an initial tension can be calculated.

Microrheology (MR) is a technique that embeds tracking particles in the cytoplasm and uses the particle movement as a measure of viscoelastic properties. One-point micro-rheology assumes that the mesh size of the material is smaller than that of the tracking particle, so that the particle is

not free to diffuse. The mean squared displacement (MSD) of the particle is measured over time. The movement of the beads also allows us to calculate the viscoelastic parameters of the surrounding materials. The complex modulus (a combination of the storage and loss moduli, G* = G' + iG'') can be computed directly from a numerical Laplace transform of the MSD [32,33].

$$G^*(\omega) = \frac{2\,k_B T}{3\pi a i\omega\,\mathcal{L}[\Delta r^2(t)]} \qquad 1.8$$

Two-point micro-rheology compares the displacement between pairs of points, rather than just the displacement of a single tracer. Correlations between movements of many pairs of tracer particles give an estimate of the viscoelastic properties by comparing them to the strain field of a single particle. Two-point micro-rheology does not require the mesh size to be smaller than the tracer particles, but suffers the disadvantage that it cannot give a local measurement, as is the case for single point. However, interactions such as tracer/actin collisions and the assumption that the media is incompressible lead to differing results between one- and two-point MR[34].

Magnetic tweezers are well suited to apply point forces tangent to the cell surface. Functionalized magnetic beads are allowed to adhere to the cell, and a computer-controlled electromagnet generates a magnetic field. With careful calibration, the distance between the magnetic tip and the bead can be used to determine the applied force. The position of the bead is recorded with a high-speed camera so that an accurate measurement of displacement can be made. Using a spring and dashpot model to approximate the cell allows stiffness measurements to be made by calculating the spring constant of the model. Furthermore, dashpots in the model give an estimate of the creep response. This method is another viable way to measure viscoelasticity[35].

Magnetic twisting cytometry (MTC) is similar to the magnetic trap, except the bead is magnetized in one direction and twisted in place by a field in another direction[36,37]. A magnetometer is used to measure how much the beads twist under an applied magnetic field. This allows for a time

dependent measurement of the stress-strain relationship. In this way, MTC is very similar to bulk rheology mentioned in section 1.2.4. The storage and loss moduli, G' and G'', can be computed by measuring the displacement and phase lag at various frequencies. MTC can be used to provide local measurements on individual cells.

Optical Tweezers exploit the fact that photons have momentum. A small transparent bead with an index of refraction different from its surroundings is held at the focal point of a converging laser beam. At this point, the photons in the beam experience the least change in trajectory possible, thus creating a stable resting point. A Gaussian beam distribution is used to create an approximate parabolic well, and thus the force actin on the bead is proportional to the distance of the bead from the center of the beam [38]. These devices typically exert forces in the range of 1-100pN. *Optical traps* are better suited for single molecule experiments, while devices like magnetic traps which exert higher forces are used for measuring the stiffness of larger systems, like live cells.

Micropipette aspiration is somewhat the opposite of AFM indentation. This technique uses negative pressure on the outside of a cell membrane and measures the curvature and displacement of the membrane as it is pulled into a micro-needle [39]. This technique can also be used on rounded cells that are not attached to a surface. This technique is especially useful on red blood cells and others that do not typically attach to their surroundings.

1.3.2 Relevant Models and Theory

The individual components of the cytoskeleton are well studied. However, developing a model that accurately predicts cell behavior is more challenging. The most basic models treat the cell as a material at equilibrium, and ignore the dynamics of individual cross-linkers. Such models fail to predict key material properties of live cells, such as stress stiffening, frequency dependent rheology, a power law displacement, and a prestress dependence [40–43].

Furthermore, models that attempt to explain how the properties of cytoskeletal components give rise to overall behavior should include thermal and non-thermal fluctuations.

Dashpot and spring models

These models are often used for their simplicity. They consist of dashpots and springs arranged in series and parallel configurations. The basic Maxwell model consists of a dashpot and spring in series. The modified Kelvin-Voigt model adds a dashpot in parallel with the spring. This second dashpot limits the rate at which the spring can deform and defines the time it takes for the model to transition from elastic deformation to viscous creep. Additional spring and dashpot elements can be added until the correct response shape is found. The membrane, actin cortex, and IF network may all contribute to the shape of the response curve [44]. Therefore, an accurate spring-dashpot model may require combining many spring and dashpot components in parallel.

However, the dashpot and spring models fail to predict several key elements of cell behavior. There is no prediction of stress hardening, and many spring and dashpot elements are required to get a good fit to data. With too many components it is no longer clear what each represents. Furthermore, this model is a top-down approach, meaning that it only mimics the result and does not attempt to explain how the interaction of cytoskeletal components gives rise to the observed behavior. Despite its shortcomings, it is a model that is easily fit to collected data. This is very useful because it makes it easy to compare mechanical properties of one cell type to another.

The Sol-gel model

The sol-gel model describes viscoelastic material as a two phase system. Disconnected polymers are in solution in the sol (solvent) state. As the polymers elongate they become cross-linked and entangled in the gel state. Stresses can cause a gel-sol transition and soften the

network. However, most biopolymers stress-harden. This model is more applicable to in-vitro actin networks and predicts the plateau modulus at low frequencies. However, it does not predict the power law dependence that live cells exhibit at low frequencies [44].

Soft glassy rheology (SGR) model

SGR is similar to the sol-gel model, however it incorporates driving forces from polymerization or myosin activity. The constituent parts of the cytoskeleton (actin filaments, and small bundles thereof) are assumed to be separate from each other but crowded, so that each part is trapped in place. A certain amount of energy is required to move one of these parts from its current position. This leaves each part of the cytoskeleton trapped in a series of energy wells. Thermal energy is typically not enough to move these parts from one well to another, but other active mechanisms such as polymerization or myosin motors raise the available energy to move the parts. The system will behave in an elastic manner when the added energy is lower than the barriers between the wells, but flow when it is above. This model does a good job explaining the simultaneous elastic/fluid behavior of cells[45]. However, it does not predict the stress-hardening observed in cells. It is possible that actin composes the soft-glassy component while other cell structures alter the overall mechanics.

Glassy worm-like chain model

The actin cytoskeleton is composed of semi-flexible polymers. These polymers naturally bend due to thermal fluctuations. This gives the impression of contraction, as the bending necessitates the two ends moving closer together. These polymers are also dynamically cross-linked, somewhat crowded, and tensioned by myosin. Individual filaments are usually modeled as a worm-like chain, however, this model may be extended to take the cross-links, tension and crowding into account[46,47].

A normal worm like chain is stretched by an external force, and it will return to a fluctuating bent state when the force is removed. However, by restricting the freedom of movement of the chain, the time required to return to the normal fluctuating state increases. This is exactly what is needed to explain the pre-stress dependence, which other models fail to do. Additional energy is required to make room for the new bends in the chain. Furthermore, interaction between chains can also affect their bending. These interactions essentially limit the energy that goes into the bending modes of the filaments. In this way, the interactions mentioned above can be incorporated into the model. A restrictive energy landscape affects how the worm-like chains can fluctuate, hence, this model is called the glassy worm-like chain.

These interactions appear to be necessary for explaining cell mechanics. Without both binding/unbinding and bending/unbending of the cross-linkers most models fail to predict the rate dependence of deformation in live cells. However, by placing restrictions on the fluctuation dynamics, the GLWC model does a very good job predicting both in vitro network rheology and live cell rheology[40,44].

Tensegrity model

Tensional elements can be used to create a stable structure, even when stiff, solid parts are not connected. In this model, microtubules bear compressive loads, while actin filaments and intermediate filaments bear tensional loads. Myosin motors are thought to introduce tension to the actin within the cell, so that even in a resting state, there is a certain amount of pre-stress within the cytoskeleton. Cells stiffen under high loads, which is a result predicted by the pre-stress of the components in the tensegrity model [48]. However, this model does not take into account myosin motors or thermal fluctuations and does not predict a rheological frequency dependence[44].

1.4 Cellular Response to Mechanical Stimuli

1.4.1 Overview

The cells in our bodies carry out many tasks, from signaling muscle movement to carrying oxygen to filtering toxins out of our blood. Some of these tasks are activated or regulated by mechanical stimuli. Touch, hearing, early development, cell differentiation, blood pressure regulation, bone remodeling, and wound healing are just some examples of force-sensitive processes. There are several mechanisms for sensing an applied force, as well as many different responses to said force. The entire process from force application to response can be studied for every cell type.

1.4.2 Examples of Responses to Force

There are many reasons that a cell might respond to external forces. Some must sense forces as quickly as possible, as in the case of sensory inputs like touch or hearing. Others respond over long time scales and use the forces as a guide for remodeling parts of the body.

Touch and hearing both make use of specialized cells that quickly translate mechanical stimuli into an action potential, which is transmitted through the nervous system to the brain. Cells in the ear grow vibration-sensitive structures using actin filaments. The length of these structures causes them to respond to different frequencies. As these structures, or microvilli, move, an actin tether opens or closes a channel that allows ions to pass in or out of the cell.

Other types of cells use external forces as a guide. For example, bones are constantly remodeled. Some cells actively destroy the bone, while others rebuild it. Osteoblasts, the bone makers, respond to applied forces and add bone where it is needed [49]. Similarly, arteries also remodel in response to blood pressure over long time scales [50]. In both cases external forces dictate the location and magnitude of cell activity.

1.4.3 Biochemical Signaling Pathways in Response to Mechanical Stimuli

There are many ways that a living cell can detect mechanical stimuli. In general, these events involve some kind of deformation, be it large-scale on the order of the size of a cell, or small-scale, localized to a handful of proteins. These deformations usually trigger a change in chemistry (in the case of stretch-sensitive ion channels) or trigger one or more signaling pathways by releasing sequestered proteins or molecules. Several examples are discussed below.

Integrin is a transmembrane protein consisting of an extracellular head and a pair of intracellular tails. The head binds readily to fibronectin, an ubiquitous extra cellular matrix (ECM) protein. The tails attach to the cytoskeleton inside the cell. Each tail has several binding sites, which can attach to many different actin-associated proteins, such as talin, vinculin, focal adhesion kinase, alpha-actinin, tensin, and others. Collectively, these components form focal adhesions. These are sites with high concentration of integrins that serve to anchor the internal structure of the cell to the ECM. Furthermore, these adhesion complexes can initiate signaling pathways which affect the behavior of the cell. One example, the Rho pathway leads to the formation of stress fibers. In some cases the Rho pathway can also lead to rapid cell stiffening in response to a shear force at the cell surface.

Filamin is another protein that can initiate a signaling response. The high flexibility of this molecule allows it to remain attached to the actin filaments even during very high strain. However, this high strain will cause the filamin to change shape and can lead to the detachment of filGAP [51]. FilGAP is a GTPase activating protein that affects the RAC signaling pathway to regulate cell spreading. This is an interesting ability because it allows the cell to sense internal deformation due to an external force, and therefore does not depend on specific binding to its environment.

Stretch-sensitive ion channels are another method cells use to detect force. These channels can actuate very quickly and are often used by sensory cells. These ion channels can also serve

as a starting point for a signaling cascade, which alters the cytoskeleton. Increased levels of calcium 2+ ions have been shown to affect calmodulin and caldesmon, leading to cell stiffening and cytoskeletal reorganization [52,53]. Due to their small size, ions can diffuse much more quickly through the cytoplasm than signaling protein counterparts. Other work has shown that bovine capillary endothelial cells exhibit different responses depending on the time duration of the applied force [54].

1.4.4 The Cell on Glass vs. In Situ

Cells may inhabit many different environments within the body. Skin, organs, bones, and cartilage all have varying properties. However, due to the constraints of light microscopy, it can be nearly impossible to examine cells in their natural environment. Unfortunately, the most convenient environment for imaging (glass: 2D and flat) bears little resemblance to the internal structure of a living organism. However, the glass does offer many advantages when studying live cells. It is optically transparent, extremely consistent, and due to its hardness we can be sure that any measurements we make solely due to the compliance of the cell.

The extra cellular matrix (ECM) consists of several materials. These materials are often what give tissue its structure. Polysaccharides and Collagen are two very common examples of ECM components. The ECM is maintained by various cells, most commonly fibroblasts, which live inside of the ECM. Other types of cells live connected to one another to form various organs or barriers within the body. With the exception of tooth enamel (Young's modulus 83GPa) and bone (up to 20 GPa)[55], there are few truly hard surfaces within the body. Most tissues are soft; skin for example has a Young's modulus below 200kPa [56] and cartilage below 600kPa[57]. The basement membrane has a Young's modulus of up to 4 MPa in mouse retinal tissue.

The internal structure of the ECM is a porous network of fibers, with spacing often on the order of the length of the cells. The cells may extend and connect to several different ECM

components simultaneously. This is a relatively soft 3D environment with an irregular structure. Glass, on the other hand, is extremely flat (surface features are only a few nanometers tall) and hard (Young's modulus 50GPa and higher). This environment is drastically different than those found within the body. Some studies suggest that this affects cell behavior, such as lifespan[58], molecule expression[59], differentiation[60–62], migration[63], cell stiffness, cell spreading, and cytoskeletal organization [64–66].

There are several methods used to investigate possible differences between glass and softer and environments. One such method is the use of lipid bilayers on the glass, and this provides interface that is more akin to another cell than functionalized glass. Furthermore, polyacrylamide gels are softer than glass but almost as optically transparent. These gels can be added to a coverslip to allow for a more compliant experimental surface. Surface flexibility can also be used for measurement with techniques such as traction force microscopy. Finally, several studies have used synthetic 3D environments to mimic the ECM or to study how specific constraints affect cell behavior [63,66,67].

Despite the limitations of a glass environment, many cell functions remain intact, and the cells continue to thrive in the proper media. For the purposes of this thesis, the downsides of glass substrates are ignored because the cytoskeletal structures remain intact. In fact, the glass provides a more consistent base from which to test the structural properties of live cells. While it may not be possible to extrapolate some conclusions drawn in vitro to in vivo systems, the advantages of a glass environment enable many experiments that would otherwise not be possible.

1.5 Summary and Motivation

Cell function often depends on structure. Shape, size, mobility, stiffness, and mechanical sensing all depend on the cytoskeleton. It is my goal to study specific parts of this system that

have not been studied before, namely, the actin cross-linker palladin. This is accomplished through both in vitro and in vivo studies.

This thesis builds on previous work by expanding previously developed techniques as well as taking a more comprehensive view of how cytoskeletal interactions give rise to cell behavior. We begin with an overview of the cytoskeleton, followed by a current summary of the field, explaining the various techniques used to measure the mechanical properties of cells and in vitro actin networks. From there, we explain our findings pertaining mainly to the actin binding protein palladin and pancreatic stellate cells, both of which are relatively novel objects of study. Using these specific subjects, we gain insight into the mechanisms by which individual interactions lead to organized processes within the cell.

Chapter 1 has provided an introduction to various aspects of the field. Chapter 2 gives an overview of in-vitro experiments with actin and various cross-linkers. Chapter 3 investigates the importance of palladin to the mechanical properties of live cells. Chapter 4 describes a new method for tracking a cell's response to an applied force, and attempts to probe the signaling pathway behind that response. Chapter 5 discusses in detail some of the computational methods required for the analysis of the collected data. Finally, Chapter 6 provides a summary of the work, and discusses its implications and possible future work to be pursued.

2 Relating Rheology and Morphology of In-Vitro Actin Networks in the Presence of Palladin and Alpha-actinin

2.1 Summary

Actin filaments and associated actin binding proteins play an essential role in governing the mechanical properties of eukaryotic cells. Even though cells have multiple actin binding proteins (ABPs) that exist simultaneously to maintain the structural and mechanical integrity of the cellular cytoskeleton, how these proteins work together to determine the properties of actin networks is not clearly understood. The ABP, palladin, is essential for the maintenance of cell morphology and the regulation of cell movement. Palladin coexists with α-actinin in stress fibers and focal adhesions and binds to both actin and α-actinin. We characterized the micro-structure and mechanics of actin networks crosslinked with palladin and α-actinin to study how mutually interacting actin crosslinking proteins modulate the properties of actin networks. We first showed that palladin crosslinks actin filaments into bundled networks which are viscoelastic in nature. Our studies also showed that composite networks of α-actinin/palladin/actin behave very similar to pure palladin or pure aactinin networks. However, we found evidence that palladin and α-actinin synergistically modify network viscoelasticity. To our knowledge, this is the first quantitative characterization of the physical properties of actin networks crosslinked with two mutually interacting crosslinkers.

2.2 Introduction

Palladin is a relatively novel actin binding protein, discovered in 2000 by [68] and again, independently, in 2001 by[69]. Palladin is ubiquitous in mammals, with multiple tissue-specific isoforms. Palladin is found in lamellar actin networks and stress fibers, structures that are critical for cell movement and sensing of the mechanical environment [68]. Two immunoglobulin-like domains (Ig3 and Ig4) bind F-actin with an apparent dissociation constant of 1-10 μM, and full

length palladin has been shown to bundle actin networks in vitro at very high concentrations [25]. Changes in the level of palladin expression changes the morphology of the actin cytoskeleton leading to defects in cell shape and movement [70,71]. Palladin knockout in mice is lethal during gestation, with defects stemming from aberrant cell motility during development [72,73]. Many isoforms of palladin are expressed mainly during development, but the 95 kDa isoform is still abundant in certain adult tissues.

α-actinin is a short dimer with an actin binding domain at each end. It can also bind to various other cellular components, such as vinculin, zyxin, integrins and many more[74]. It is difficult to assign it a primary purpose, as it is found in many different structures, such as stress fibers[75], dendritic spines[76], and the leading edges of migrating cells[77]. α-actinin only binds F-actin (not G-actin) and does not serve as a nucleation point for actin polymerization[78], so its role is not to direct actin filament growth. It appears to be almost as versatile in use as actin itself, and in general serves to stabilize structures with multiple filaments.

As the cellular cytoskeleton is extremely complex, elucidating the basic principles governing cytoskeletal mechanics in cells is difficult. In vitro studies where crosslinker composition and properties can be precisely controlled, are advantageous for the study of the mechanical behavior of actin networks. In-vitro studies typically consist of polymerizing actin in the presence of cross-linking proteins and observing the resultant structures. The size, shape, length and spacing of the actin bundles can all tell us about the interaction between the cross-linker and the actin filaments. Actin monomers assemble in vitro into filamentous networks that behave like weak viscoelastic solids [79]which stiffen in the presence of crosslinkers [14,23,24,80–85]. These networks exhibit remarkable material properties owing to the semi-flexible nature of the actin filaments as well as the structure, affinity and compliance of the individual crosslinkers [86]. Despite advances in the study of crosslinked actin networks, the

physical principles which lead to the formation of complex structures such as bundled networks are not well understood.

While many studies have focused on the mechanical properties of networks formed with a single cross-linker [14,16,17,20,87], the number of multiple cross-linker studies is fewer [24,85]. In living cells, several actin crosslinking proteins co-exist in the same subcellular region. The heterogeneous cytoskeletal structures seen in cells arise in part due to the simultaneous presence of multiple crosslinkers. In reconstituted networks each crosslinker species imparts a particular structure and mechanical character to the network in isolation. Depending on the cross-linkers used, the properties of the networks with multiple cross-linkers may be affected by their concentrations independently [85], or cooperatively [24]. A unique aspect of Palladin and α-actinin is that they also bind to each other [68], as well as colocalize in stress fibers and focal adhesions[26]. The interaction of these two proteins make them excellent candidates for in-vitro studies, as this will allow us to study their interaction in a simpler setting than that of a living cell.

The motivation for this work was two-fold: 1) to characterize the morphological and viscoelastic properties of actin networks crosslinked by palladin and 2) to study whether palladin modifies the network morphology and viscoelasticity of actin networks crosslinked by α-actinin. We found that palladin induces the formation of bundled actin networks as evidenced by morphology and rheological measurements. Increasing palladin concentrations led to changes in morphology of the network resulting in an enhancement of the linear network stiffness. We also found that α-actinin and palladin do not behave independently in modulating the mechanical properties of composite actin networks.

2.3 Materials and Methods

2.3.1 Protein Isolation

Acetone powder was prepared from frozen rabbit muscle (Pel- Freeze Biologicals, Rogers AR) to purify actin for in vitro studies according to protocols approved by the NHLBI Institutional Animal Care and Use Committee. Actin was extracted by dissolving acetone powder in G-buffer (2 mM Tris, 0.2 mM ATP, 0.1 mM CaCl2, 0.5 mM DTT, 1 mM NaN3). The solution was centrifuged at 25000 rpm for 30 min. and then filtered through glass wool to remove the powder. Polymerization was initiated and actin was removed from solution by centrifugation. The actin was again dissolved in G-Buffer and dialyzed for 2 days. For fluorescent labeling of actin networks either AlexaFluor-488- actin (Invitrogen, Carlsbad CA) or Rhodamine-actin (Cytoskeleton, Denver, CO) was obtained. α-actinin was purchased from Cytoskeleton Inc. (Denver, CO). Full-length palladin (90 kD isoform) was generated using the baculovirus expression system as detailed in [25]. The target gene was amplified via PCR. This portion of DNA was added to a plasmid and transfected into E. coli, which in turn was used to infect insect cells. After enough E. coli expressing palladin have been produced, the protein was isolated with immobilized nickel columns.

2.3.2 Actin polymerization

Unlabeled and labeled actin monomers, crosslinkers (a-actin and/or palladin) and G-buffer were mixed on ice to obtain the desired ratios of proteins. The final concentration of actin monomers ranged from 1 to 20 mM with 10% of the actin labeled with either Rhodamine or Alexa-Fluor-488. The concentration of ABPs varied from 0:01 mM to 2 mM. After polymerization was initiated by adding 3 ml of 10| polymerization buffer (1 M KCl, 20 mM MgCl2, 20 mM tris-HCl and 10 mM ATP), the samples were immediately pipetted into wells for imaging, or onto the bottom plate of the rheometer. Wells were made using 0.5 mm thick silicone spacers with circular holes (diameter 9 mm) placed on a No.1 coverglass and the top was sealed

with a microscope slide. The overall volume of each well was 30μl. After pipetting on to the rheometer bottom plate, the top cone was immediately lowered into the sample and surrounded by a solvent trap made using a metal surround with a sponge soaked in water.

2.3.3 Imaging

Images were gathered on a Zeiss LSM 510 or LSM 710 confocal microscope using a 63x oil immersion objective. A 543 nm HeNe laser line was used to excite Rhodamine labeled actin, and a 488 nm Argon line was used for exciting the Alexa488 labeled actin. The images were 512x512 pixels (73.1x73.1 mm) digitized at 8 bits per pixel. All data presented was corrected for any variation in the image acquisition settings. The slice thickness for confocal images varied from 0.24 to 1 μm between stacks, but each stack used a consistent spacing. Confocal microscopes are an essential tool because they can record the 3D structure of these in-vitro actin networks. Laser scanning confocal microscopy uses structured illumination to generate the 3D image of a sample one point at a time. A laser light source is focused to a sharp point by the objective lens on the microscope. A pair of mirrors upstream of the sample move this focal point quickly through the sample. The light intensity is too low outside of the focal point to cause the sample to fluoresce at an appreciable level. A photo multiplier tube measures the intensity of the fluorescing light as the focal point is moved through the sample and this allows the reconstruction of the image.

2.3.4 Image Analysis

Pore size distributions were calculated from confocal images. There is no generally accepted definition of pore size distribution, and some methods, such as peak to peak distance measures [83], can give biased estimates (e.g. in a directional network). We used a robust method that uses volumes of covering spheres to calculate pore sizes [88]. In this method, the confocal stack is first converted to a 3D binary image, with bundle voxels labeled as “1” and fluid voxels (background or empty space) labeled as “0”. A distance map is computed for every fluid voxel

representing the distance from each fluid voxel to the nearest bundle or 1 voxel. Then, starting from the voxels with the smallest distance value, covering spheres with centers on that voxel were generated (*Figure 2-1*).

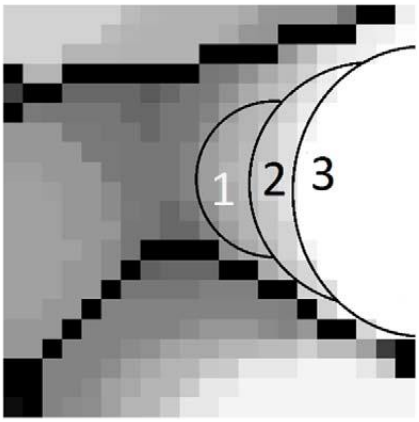

Figure 2-1 Close-up illustration of the covering spheres method. Black pixels represent actin bundles, gray and white pixels represent covering spheres of three different radii. The thin black lines show edges of representative spheres. Here, sphere 1 is partially covered by a larger sphere 2, and sphere 2 is partially covered by sphere 3. The voxels enclosed by a sphere, but left uncovered by a larger sphere, are those counted for the pore size analysis. For example, the 19 voxels whose centers are in the crescent shaped region (2) would contribute to the total for pores of 12 pixel diameters because that is the diameter of sphere 2, and it is the largest such sphere which covers those voxels.

The size of the sphere was chosen such that it is the largest possible sphere that did not cover a bundle or "1" voxel. All voxels within the sphere are given the same value as its center voxel, unless its distance map value was greater. This ensures that large spheres covered smaller ones. In the end, each background voxel is marked with the size of the largest sphere which covered it. These values are binned to produce the pore size distribution. In our studies, networks that were homogeneous throughout the confocal stacks were chosen for pore size analysis. Pores that reached the edge of the confocal stack were ignored, as an abundance of such pores causes the pore size analysis of these networks to fail.

2.3.5 Rheometry

Bulk physical properties of the networks were measured with a custom Anton Paar MCR-301 stress-controlled bulk rheometer. The upper portion is cone shaped so that the strain is

constant throughout the sample. A solvent trap was used to surround the sample and cone head of the rheometer in order to minimize evaporation. The sample (*70µl volume) rested on a plate at the base of the rheometer, and a 40 mm diameter, 1 degree cone was lowered into it from above with a 50 µm spacing. It was assumed that the sample does not slip on either surface. To characterize the linear viscoelastic response, small amplitude, oscillatory shear strain $\gamma \sim \sin(\omega t)$, was applied and the resultant oscillatory stress, $\sigma \sim \sin(\omega t + \delta)$, was measured, where $0 \leq \delta \leq \pi/2$ is the phase shift of the measured stress. The in-phase component of the stress response determines the shear elastic modulus, $G'(\omega) = (\sigma/\gamma) * \cos(\delta(\omega))$ which is a measure of how mechanical energy is stored in the material. The out-of-phase response measures the viscous loss modulus, $G"(\omega) = (\sigma/\gamma) * \sin(\delta(\omega))$ which is a measure of how mechanical energy is dissipated in the material. Yield tests are carried out at a continuous strain of $\dot{\gamma} = .1s^{-1}$. The force required to drive this deformation is recorded at 0.1 s intervals. The differential modulus (defined as $K = \partial\sigma/\partial\gamma$) is computed numerically from this data.

2.4 Results

2.4.1 Palladin crosslinks actin into bundled networks

We allowed actin filaments to polymerize in the presence of palladin and imaged them on a confocal microscope. We observed distinct morphological changes of the actin network depending on both the concentration of actin (c_a) and the actin-palladin ratio, denoted by $R_{pa} = c_{pa}/c_a$. Maximum intensity projections of fluorescent confocal images of networks with fixed c_a = 10µM and varying R_{pa} are shown in Figure 1. For very low concentrations of crosslinker ($R_{pa} \leq$ .005) the networks were visually indistinguishable from entangled F-actin networks (Figure 2-2). As the concentration of crosslinkers increases (above R_{pa} = .005), small bundles become apparent within the entangled F-actin network. The initial appearance of bundles was characterized by continuous groups of pixels with intensities greater than 1.5 × the average. The depletion of F-actin in the bundled phase appeared as a change in the contrast of the image (80–90% of the

dynamic range of the sensor for bundles versus 20% or below for entangled F-actin). Further increase in palladin concentration yielded networks with thicker bundles and larger spaces between bundles as indicated by a stronger depletion of F-actin in the dark regions between bundles and brighter fluorescence in the bundled regions (Figure 2-2, middle pictures). At higher crosslinker concentrations, above R_{pa} = .1, the bundles formed dense clusters (Figure 2-2, right), which seemed to be separated from each other and the network no longer appeared continuous across the sample.

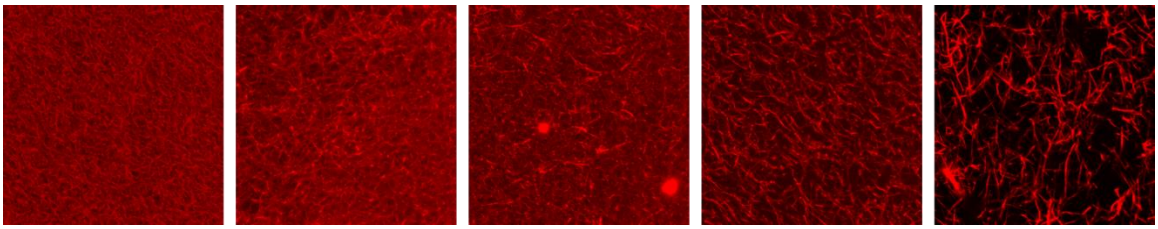

Figure 2-2: Maximum intensity projections of palladin/actin networks. Left to right R_{pa} = .007, .018, .035, .070, .120 respectively.

We next examined the effect of actin concentration on actin/ palladin networks. We fixed the palladin ratio, R_{pa} = .007, .018 .035 or .07 and varied the actin concentration from 2 μM to 20 μM (Figure 2-3). R_{pa} = .07 is a concentration regime where palladin forms homogenous, bundled networks well above the bundling threshold. At this ratio, filaments formed bundled networks that were initially sparse for low c_a and formed spanning networks with larger voids for increasing ca. At a very high actin concentrations (c_a = 20 mM), we found that palladin appeared to bundle actin extremely efficiently, forming numerous overlapping bundles as well as clusters where the bundle concentration is very high. Our observations indicated that above a critical concentration, palladin organized actin filaments into a crosslinked network of branched bundles which were slightly curved. Similar structural changes have also been observed in actin networks grown in the presence of filamin [84]. Actin filaments cross-linked by fascin form tight straight bundles. While in the presence of filamin they form long curved bundles and networks of branched bundles [85]. It is known that macroscopic network elasticity is linked to microscopic

network structure which can depend sensitively on the details of the interaction of crosslinkers with actin filaments [89]. It has been confirmed by electron microscopy that palladin bundles actin filaments, leading us to believe that the bright lines we see in our networks are indeed bundles rather than loose collections of filaments [25].

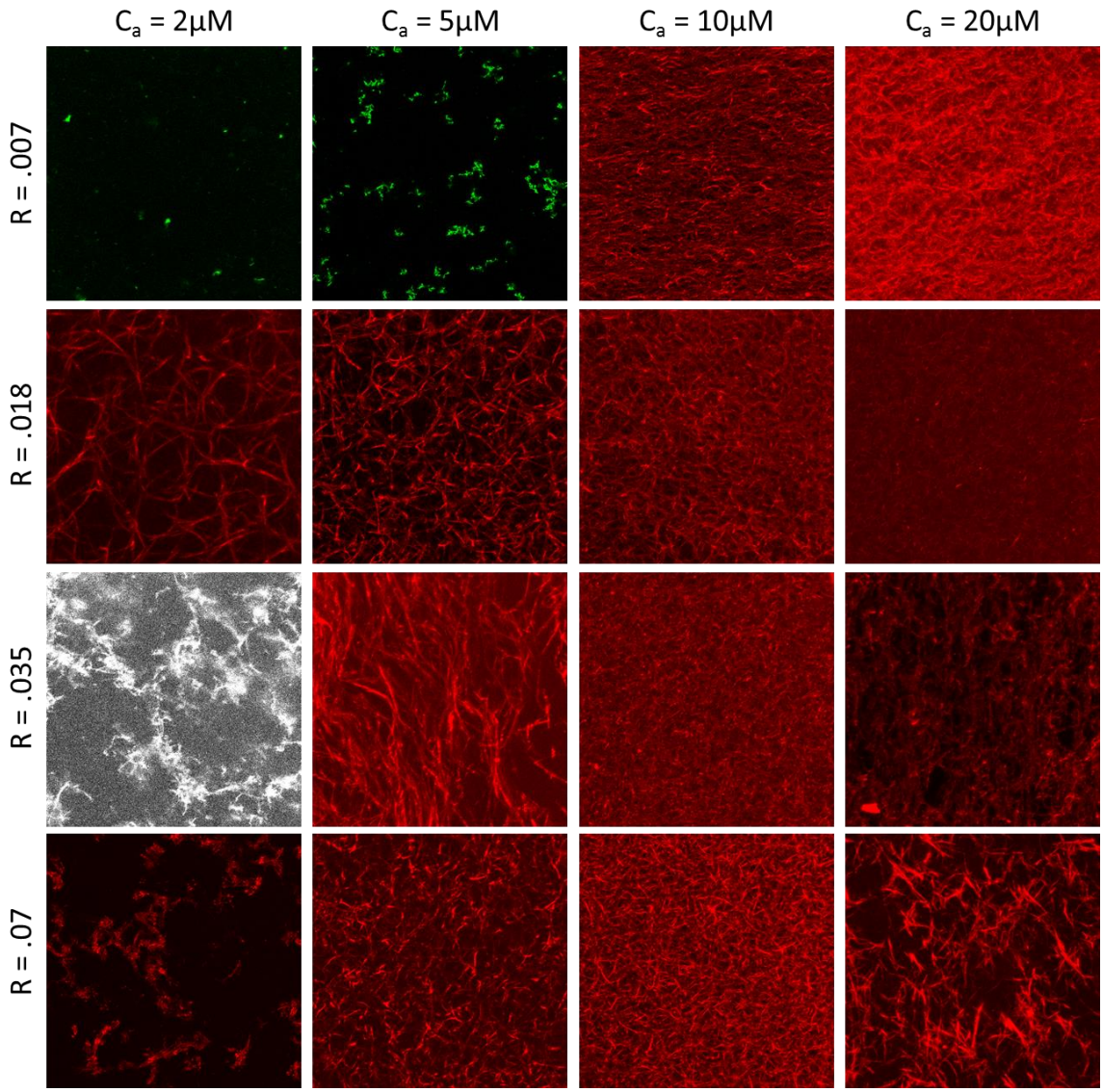

Figure 2-3: Maximum intensity projections of actin/palladin networks at various concentrations and palladin ratios. Some of the low concentrations of actin (C_a = 2μM and 5μM) show some artifacts due to thermal fluctuation in between consecutive image slices.The green images in the top left used alexafluor-488 label instead of the usual rhodamine. The black and white image was acquired from a different microscope and acquisition software (Leica) than was normally used.

A useful quantity to measure in a network of filaments is the mesh size, (also known as the pore size), which captures the characteristic distance between bundles of filaments in 3D networks. This is effectively the size of the spaces between bundles that are devoid of F-actin. Previous studies of crosslinked actin networks have characterized the network structure qualitatively using visual depiction of the types of bundles formed, or measured the average spacing between bundles from an estimate of peak-to-peak distance between bundles across one cross-section of the sample, thereby underestimating the pore size [89]. While there have been some studies to quantify collagen and other filamentous networks [88,90,91], to our knowledge, the mesh size of cross-linked actin networks has not been carefully characterized as a function of crosslinker concentration. We adapted a method based on a covering sphere algorithm to quantify the microstructure of actin networks from confocal image stacks (*Figure 2-1*; see Methods). This analysis is most useful for concentrations where there is a clear distinction between individual bundles and the background. The middle to right images in Figure 2-2 are good examples of the network morphology we can analyze. Figure 2-4 shows pore size calculations superimposed on a confocal slice. We show the results of the analysis for $c_a = 10\mu M$ and $c_a = 20\mu M$ in Figure 2-5.

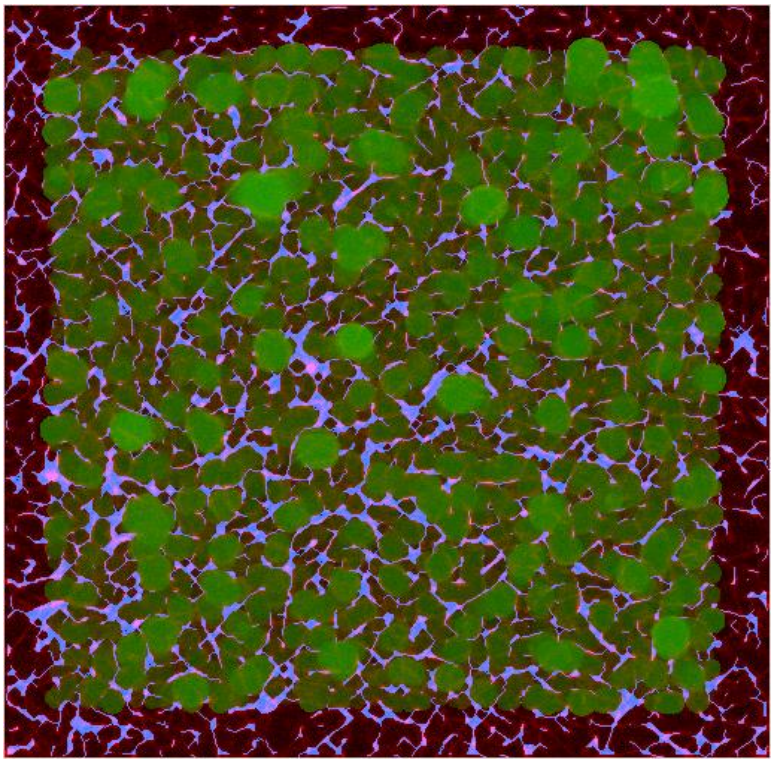

Figure 2-4: An example of pore size distribution. The red pixels are a confocal slice. The pale blue represents identified actin bundles. The green circles represent pore sizes. The brighter the green the larger the pore size. The missing border is by choice: rather than let spheres cover non-existent voxels, we chose to restrict our analysis to actual image data.

We found that networks with crosslinker concentrations below $R_{pa} \leq 0.01$ have pore-size distributions indistinguishable from pure F-actin networks. On the other hand, very high palladin concentrations, above R_{pa}~0:1, resulted in clusters of filament bundles several tens of microns across. The clusters were isolated from each other and no longer formed part of a continuous network of bundles throughout the sample. We found that with increasing palladin concentrations, $0.01 \leq R_{pa} \leq 0.1$, the peak of the pore size distribution shifted towards larger pore sizes. This implies that bundles get thicker as the spaces between bundles increase, and consequently the pore sizes become larger. Additionally, the pore size distribution also broadened to exhibit a prominent tail of large pores (Figure 2-5).

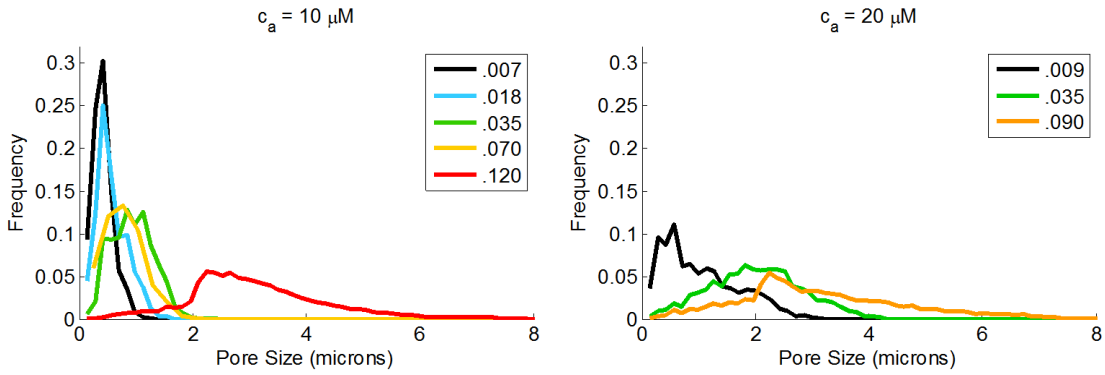

Figure 2-5 Pore size distributions for 10μM actin networks (left) and 20μM actin networks (right). Legends show values for R_{pa}. Note that in both cases higher cross-linker concentration leads to larger pore sizes.

For a higher actin concentration, c_a = 20 μM, the pore size analysis showed a similar trend, with larger R_{pa} leading to larger pore sizes (Figure 2-5). Under these conditions the overall pore sizes were larger than for c_a = 10 μM at similar palladin ratios. Higher actin concentration also led to a broader tail of the distribution, arising from stronger bundling by palladin and appearance of bundle clusters. Overall, we found that the average pore size scaled as $R^{0.4}$ for both actin concentrations. Our observations suggest that high palladin concentrations might lead to a cooperative effect in which the presence of smaller bundles facilitates the formation of further bundles, thereby increasing the preponderance of large pores. This effect was enhanced at larger actin concentrations (Figure 2-5, right). Actin/fascin networks show qualitatively similar behavior with larger crosslinker concentrations leading to an increase in the bundled phase [84]; actin/scruin networks show an increase of apparent pore size with concentration ~$R^{0.2}$ [83]. Such pore size distributions might be characteristic of networks of bundled actin filaments.

2.4.2 Palladin modifies viscoelastic properties of actin networks

Our next goal was to determine whether the structural changes correspond to changes in the viscoelastic properties of the actin networks. Applying a shear deformation to the network requires energy to be put into the system. Some of the energy is stored elastically (similar to a spring), while the rest is dissipated within the system. Two values, G' and G'', are typically used

to describe these properties. G' is known as the storage or elastic modulus, and measures the propensity of the network to rebound after deformation (energy stored). G'' is known as the loss modulus, and measures the amount of flow due to deformation (energy lost). For these measurements we used a sinusoidal 1% strain (within the linear elastic limit) at frequencies ranging from 10mHz to 10Hz. Actin concentrations were restricted to 10μM to ensure that samples were homogeneous for all R_{pa} tested. For several samples the frequency sweep was repeated. In all cases the results were nearly identical, indicating that the network has reached a stable state and the tests do not damage or alter the network.

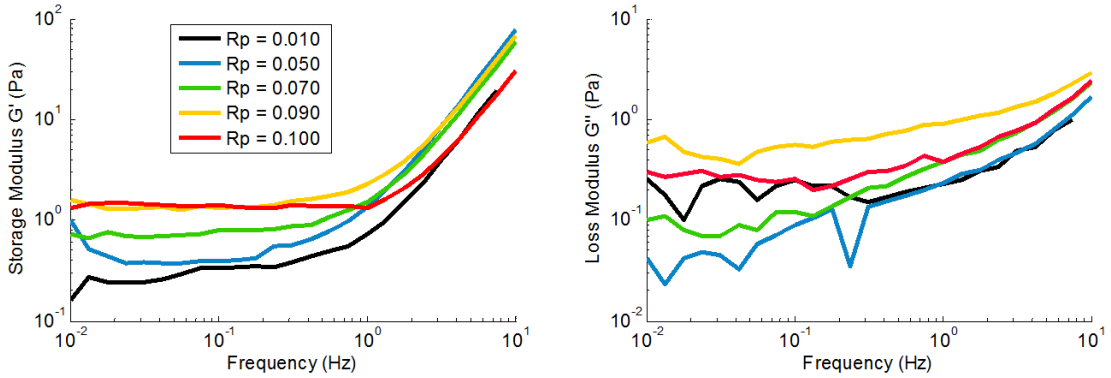

Figure 2-6: Storage (right) and Loss (left) Moduli of Actin/Palladin networks at C_a=10μM. The legend is valid for both graphs.

For all values of R_{pa} tested the G' frequency response remained mostly flat from 10mHz up to 1Hz. Above 1Hz the power law relation developed, where $G' \sim \omega^2$ (Figure 2-6). The value G_0, defined as the lower limit of G' as the frequency approaches 0 Hz, is a measure of the static stiffness of the system. There is approximately a linear dependence of G_0 on the palladin/actin ratio, for the range $0.01 < R_{pa} < 0.1$. Above $R_{pa} = 0.1$, G_0 no longer increases. This corresponds exactly to the transition from well-connected networks to disjointed clusters.

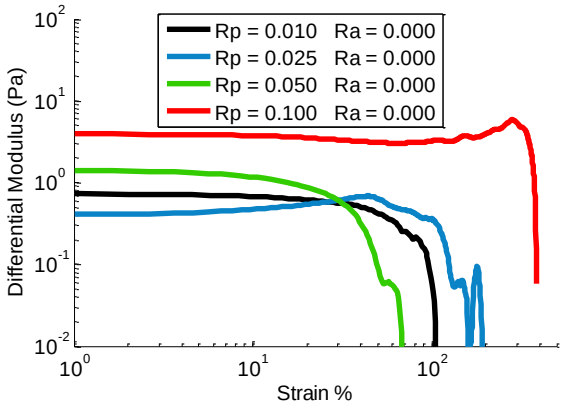

Figure 2-7: Differential modulus of actin networks at C_a = 10μM and varying palladin ratios. The differential modulus is the derivative of the stress/strain relationship. A flat curve shows a linear relationship. A positive slope shows strain hardening, while a negative slope shows strain softening.

Such enhancement of network stiffness with crosslinker concentration has been observed for other crosslinkers with a similar power-law dependence. The effect of palladin concentration on the linear elasticity of the network was smaller than that of some actin bundling proteins such as fascin or scruin [89,92], but similar to the that of filamin [17]. The networks were predominantly elastic, as shown by G' being larger than G'', however the viscous component is not negligible. G'' increases as ~ω as expected for viscous dissipation. Above 1Hz the separation between G' and G'' increases because G' begins to scale as ω^2. This transition to a clearly dominant elastic behavior at high strain rates is a hallmark of viscoelastic behavior.

At very high crosslinker concentrations (R ≥ 0.1), the formation of regions of dense bundle clusters interspersed with regions that have large gaps likely affected the continuity of the network, resulting in a decrease in overall stiffness of the network, as we observed. So, while palladin was efficient at creating bundled networks over a range of concentration values, there was a rapid transition to a phase where the structural integrity of the network collapsed and the network softened. This was in contrast to networks of filamin, fascin or scruin which form well-defined bundled networks with increasing network stiffness over a much larger concentration range up to (R=1). Since many actin crosslinkers have been shown to cause actin networks to

strain harden under large strains [17,93], an open question is whether actin/palladin networks also show significant nonlinear elasticity. One technique to study nonlinear behavior is to apply a constant shear rate dγ/dt and measure the differential modulus $K(\gamma) = \partial\sigma/\partial\gamma$ from the observed σ(γ). This method avoids viscous creep, which is typically non-negligible. A linear stress-strain relationship will appear flat, and any deviation from flatness will represent non-linearity. With increasing crosslinker concentration, R, we found that actin/palladin networks exhibited limited or no strain hardening for all R_{pa} values examined (Figure 2-7). We also found that at the highest palladin concentration, R_{pa}=0.1, the maximum strain that the network seems to be able to accommodate before rupturing is quite large. In general, the nonlinear mechanical response of semiflexible polymer networks may be influenced by several factors, such as the crosslinker density, unbinding kinetics, compliance of the crosslinker, actin concentration and the applied strain rate [94]. The lack of strain stiffening in palladin/actin networks may be due to a number of reasons. First, palladin may be overall a stiffer, less compliant crosslinker, unlike filamin which is a large flexible crosslinker [95]. Second, the lack of strain hardening at low R_{pa} may be attributable to the low abundance of bundles, and the network being able to accommodate any applied strain (for the applied strain rate) due to the relatively rapid unbinding of palladin from filaments (with the disassociation constant on the order of $1s^{-1}$), allowing for network rearrangement. Hence, most of the network may undergo remodeling and homogeneous stress redistribution, precluding any nonlinear elastic behavior, even at high strains [82,96]. On the other hand, the extensive bundle formation at higher R_{pa} and forced crosslinker unbinding between bundles again likely results in strain accommodation, similar to observations in fascin [92,97].

2.4.3 Structure and viscoelastic properties of composite networks

Given that palladin binds to α-actinin with a similar affinity as to F-actin, we reasoned that composite networks of palladin/α-actinin/ actin may exhibit distinct structural and mechanical properties compared to networks with only one type of crosslinker. In particular, we wished to examine whether the addition of either crosslinker supplements the effects of the other, i.e. whether the mutual interaction between palladin and a-actinin leads to a synergistic or antagonistic effect on the composite networks. Confocal images of a-actinin and composite a-actinin/palladin actin networks are shown in Figure 2-8. Qualitatively, the structures of networks formed by either crosslinker were very similar in terms of bundle curvature, branching, fluorescence intensity (apparent bundle thickness) and homogeneity (compared with pure palladin networks in Figure 2-3).

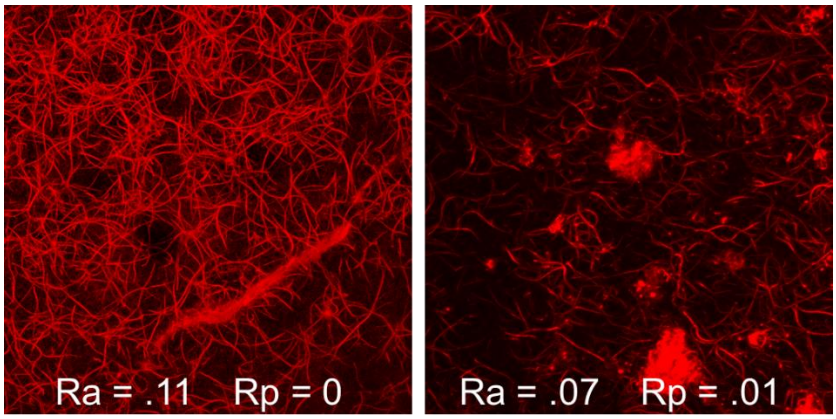

Figure 2-8 Maximum intensity projections showing that the addition of palladin leads to more efficient cluster formation. The morphological differences are also confirmed by the pore size analysis. C_a = 10μM.

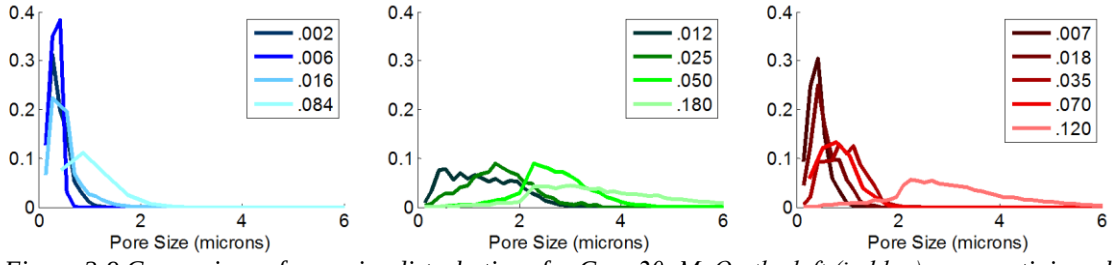

Figure 2-9 Comparison of pore size distrubutions for C_a = 20μM. On the left (in blue) are α-actinin-only networks. In the center (green) are composite networks. On the right (red) are palladin-only networks.

The transitions from entangled F-actin networks to bundles to clusters occurred at similar concentration ratios for all cases. We found that composite networks of a-actinin and palladin also have a morphology that is very similar to singly crosslinked networks. As we increased the total crosslinker to actin ratio (R_{total}), with equal amounts of α-actinin and palladin in the mixture, the networks transitioned from small, isolated bundles to homogenously bundled crosslinked networks and finally to heterogenous networks with large bundle clusters at high concentrations ($R_{total} > 0.1$) The bundling transition appeared to be at a slightly lower concentration for the composite network compared to the actin/α-actinin network, as evidenced by the pore size distributions in Figure 2-9. For pure α-actinin (R_{pa}=0, $R_{\alpha a}$=.07), networks had median pore size slightly less than 1 μM as shown in the distribution of pore-sizes, with very few large pores (Figure 2-10). Addition of small amounts of palladin ($R_{pa}/R_{\alpha a}$=.1) to the network shifted the pore-size distribution to the right, indicating larger pore sizes and more efficient bundling. However, higher palladin/α-actinin ratios resulted in a reduction of the median pore size and an overall leftward shift of the distribution. The pore size distribution for a pure palladin network was similar to that of pure α-actinin.

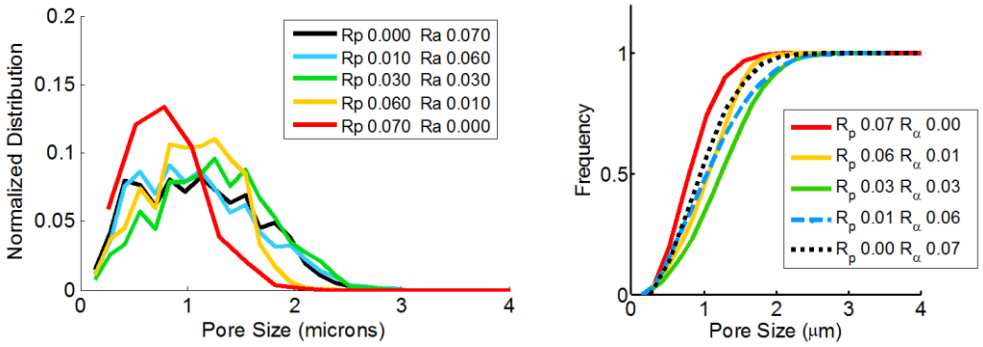

Figure 2-10 Left: Pore Size distribution for composite networks with C_a = 10μM at R_{total} = .07. Right: Cumulative distribution of the same data.

We next examined the mechanical properties of composite networks to determine whether the two crosslinkers behave synergistically or independently (

Figure 2-11, left and center). We fixed the total concentration of crosslinkers at R_{total}=.05 to ensure that the network was in a bundled regime. We found that the addition of palladin to pure a-actinin networks resulted in a biphasic effect on the network stiffness (

Figure 2-11, left). For $R_{pa}/R_{\alpha a}$~0.1, the network was considerably stiffer than for R_{pa}=0, $R_{\alpha a}$=.05. However, increasing R_{pa}=$R_{\alpha a}$ further, softened the network. The stiffness of pure palladin networks ($R_{\alpha a}$=0) was similar to that of the pure α-actinin networks (R_{pa}=0). This behavior of network stiffness appeared to parallel the dependence of pore size on crosslinker ratio, R_{pa}=$R_{\alpha a}$ at fixed R_{total} (Figure 2-9, and Figure 2-10). From these data, it appears that the effect of adding small amounts of palladin to an actin/a-actinin network is not the same as adding a small amount of α-actinin to an actin/ palladin network.

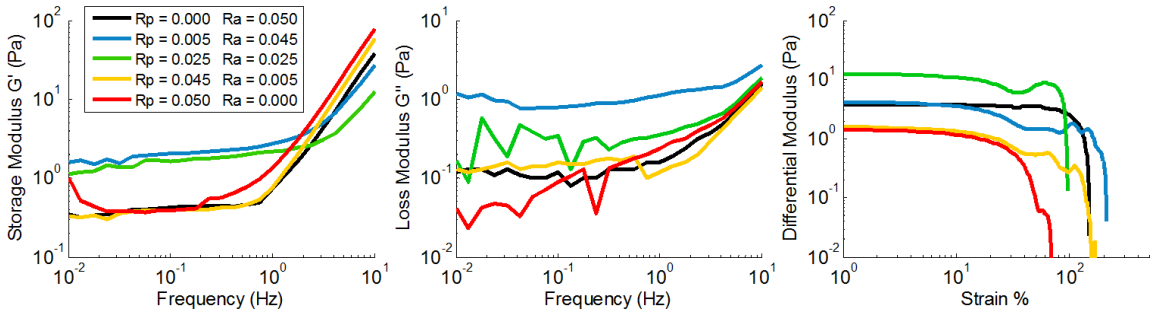

Figure 2-11 Viscoelastic measurements for composite networks, R_{total} = .05. Right: Storage Modulus (G') for composite networks, C_a = 10μM. Center: Loss Modulus (G'') of composite networks. Right: Differential modulus of composite networks.

The mechanical properties of composite networks can be compared by studying the static stiffness of the networks, or equivalently the plateau modulus, G_0, as a function of crosslinker composition. We found that a-actinin and palladin networks exhibited nearly identical changes of G_0 with respect to crosslinker concentration (Figure 2-12). G_0 was weakly dependent on concentration for Rw0:04 (corresponding to a low abundance of bundles in the confocal images) and increased as G_0~R for an intermediate range of R (majority of filaments were part of a crosslinked bundled network). For two independent crosslinkers, we would expect the plateau

modulus, $G_0(R_{\alpha a},R_{pa})\sim G_0(R_{pa})*G_0(R_{\alpha a}) / G_0(R=0)$ [85]. In this case, for a fixed Rtot, varying the ratio of the two crosslinkers would result in a monotonic change in the plateau modulus, rather than the biphasic behavior that we observed. Moreover, the independent model predicts that when two crosslinkers with similar $G_0(R)$ (such as palladin and α-actinin) are mixed, the overall network stiffness should not depend on the exact ratio of the two crosslinkers, whereas they should for the case when $G_0(R)$ differ. However, as shown in Figure 2-12, we found that the plateau moduli of composite networks was different for the same overall crosslinker ratio, depending on whether palladin or a-actinin was dominant. Yet the overall dependence of G_0 on R_{total} for the composite network was similar to that of either crosslinker alone. Finally, as with the case of pure palladin networks, the differential modulus showed that the addition of palladin to a-actinin did not result in strain-stiffening (

Figure 2-11, right)

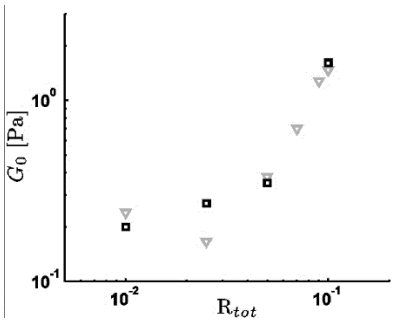

Figure 2-12 Plateau modulus, G_0 of pure palladin (gray triangles) and pure a-actinin (black squares) networks showing correlation between the total amount of crosslinker and stiffness, G_0.

2.5 Discussion

Palladin modifies the viscoelastic properties of in vitro actin networks. Palladin's effect on the linear elasticity is similar to that of α-actinin or filamin [17], but not as strong as scruin or fascin [89,92]. Filamin and α-actinin are both larger cross-linkers which create more flexible bonds. Scruin and fascin are both short in length (length) and create tight bundles. Though palladin has been less studied than α-actinin, we can conclude it likely has a similar size, as

previous studies have shown that cross-linker length largely determines macroscopic network properties [23].

Palladin concentration not only affects network stiffness, but can effect morphological transitions. As palladin concentration increases from zero the actin network transitions from a weakly cross-linked phase to a strongly bundled phase. Maximum elasticity occurs around R = .1 for both pure and composite networks. This is the highest concentration that does not induce disjoint cluster formation. Above this concentration the network disconnects and the actin filaments are all contained in tightly packed but separate clusters. Without a continuous network the forces applied by the rheometer cannot be transmitted, and therefore not stored by large portions of the network. Since both palladin and α-actinin are major components of stress fibers, we compared the function of palladin in vitro with α-actinin and also investigated composite networks crosslinked with palladin and α-actinin. We found that the morphology and viscoelastic properties of actin/palladin networks are qualitatively very similar to that of actin/α-actinin networks, despite differences in their actin binding domains (Ig-like domain for palladin [25] versus calponin-homology domain containing motifs for α-actinin [98]).

Palladin expression levels are likely to sensitively control cytoskeletal stiffness in vivo. Up-regulation of palladin leads to increased stress fiber formation, while a decrease in palladin expression leads to a loss of stress fibers as well as F-actin [68]. With the results in this study, where small amounts of palladin can enhance the stiffness of an alpha-actinin network in vitro, Palladin is likely essential for controlling mechanical properties of the cytoskeleton.

Composite networks showed cooperative behavior. The two cross-linkers used in this study form in vitro actin networks with nearly identical properties. However, the presence of both cross-linkers can enhance the stiffness of the actin network beyond what they would be able to accomplish separately. Networks formed with filamin and α-actinin show a similar behavior [24], while networks formed with filamin and fascin do not [85]. Palladin and α-actinin bind to

each other and colocalize in stress fibers[26], and perhaps their cooperative abilities play a role in controlling the mechanical properties of the stress fibers. α-actinin binds flexibly to actin filaments. This creates weakly coupled bundles, and allows the spacing between filaments to change depending on the angle at which it binds actin filaments. As discussed in the introduction, stronger coupling leads to higher bending stiffness. The addition of another cross-linker with a different length, or a different binding geometry may eliminate the freedom of motion within the bundle, leading to a stronger coupling. Additionally, palladin binding to α-actinin allows for more binding sites near the original two on α-actinin dimers. This could allow for up to five filaments to be attached at one point, rather than just two filaments as would be the case for a single α-actinin dimer. In either case, the presence of more than one cross-linker species would raise stiffness of the network components, and hence the network itself.

These studies suggest that the relative abundance of palladin and α-actinin might also be important in shaping cellular viscoelasticity. It remains unclear whether the distinct structural and viscoelastic properties of composite networks arise as a result of the mutual interaction between palladin and a-actinin or because of the difference in their actin binding domains. Studies with palladin mutants that lack α-actinin and/or actin binding sites may help elucidate the specific contributions of various protein-protein interactions to the overall network mechanics. Our study highlights the importance of mutual interaction among actin crosslinkers in determining the overall structure and mechanics of actin networks.

We have shown that palladin binds actin filaments to form viscoelastic networks. Increases in palladin concentration cause a transition from a weak, F-actin gel to a continuous network of bundles. Further increases in concentration cause another transition, one from a homogenous network of bundles to a heterogeneous collection of separated bundle clusters. We have also measured the corresponding changes in mechanical properties with varying concentrations. Finally, we have shown that palladin and α-actinin cooperate to enhance network

stiffness more efficiently than either cross-linker could separately. The addition of palladin to in-vitro actin/α-actinin networks affects dramatic changes in structural organization and mechanical stiffness. These two results strongly illustrate that palladin is very important for regulating cytoskeletal function.

3 Directly Measuring the Mechanical Properties of Human Pancreatic Stellate Cells

3.1 Summary

Cell stiffness plays an important role in cell behavior. Cell stiffness affects the cell's ability to sense mechanical stimuli, interact with its environment and indicates metastatic potential. In this study, we use a magnetic trap to measure the stiffness of pancreatic stellate cells (PSCs) by fitting the displacement data to a model system consisting of ideal springs and dashpots. PSCs maintain the structural integrity of the pancreas and are of vital importance to understanding pancreatic cancer, one of the most difficult types of cancer to detect and treat. We also account for pull direction, and pull angle, as well as test the effect of knocking down palladin, a protein which changes expression levels in malignant cells. We showed that cell stiffness is isotropic and consistent at various positions on the cell. Stiffness is independent of palladin expression levels and furthermore, bead displacement is not always parallel to the applied forces. Together, these results clearly illustrate the importance of thorough and careful analysis while trying to understand complex, living material.

3.2 Introduction

The internal structure of the cell depends on the organization of cellular actin networks which is largely determined by concentrations of a collection of actin crosslinking proteins. Palladin is an actin cross-linker which also binds alpha-actinin, and has been shown to play a role in organizing the cellular actin cytoskeleton [18,99]. Palladin is critical for embryonic development and cell migration and has been implicated in aberrant cell motility in pancreatic cancers. In spite of its important role in physiological function, the palladin's role in modulating cell stiffness has not been studied.

Cell stiffness is of great biological importance, as it can indicate many attributes, such as metastatic potential, increased ECM production, or responses to their environment. Cells will actively remodel their cytoskeleton to match their stiffness to that of the substrate. Responding to mechanical properties of their surroundings is critical for wound healing, metastisis, and proper migration during development. It is becoming increasingly clear that the stiffness of cells, tissues and their microenvironment is closely related to (or regulates) the progression of tumors and cancer metastases. Pancreatic cancer is among the most difficult types of cancer to detect and treat. Pancreatic stellate cells (PSC) are a major component of the pancreas and develop into tumors. PSCs help to maintain the extracellular matrix of the pancreas and assist in wound healing [100] while malignant cells, which overexpress palladin [101], have aberrant behavior such as increased motility and contractility [102]. Recent work has shown that individual cancer cells are softer than normal cells, while cancer tissue has been found to be stiffer than normal tissue due to fibrosis [103]. The softening of tumor associated fibroblasts is thought to aid metastasis [104,105], however the stiffness of pancreatic cells has not yet been directly measured, nor have any experiments investigated the importance of palladin in regulating cell stiffness.

Various methods, such as atomic force microscopy, cell stretching, micropipette aspiration, optical tweezers and magnetic tweezers, have been used for measuring cell stiffness in a number of different cell types [106]. These methods typically apply an external force to a part of the cell and measure its response. AFM studies, using an indentation method to probe the deformability of the cell, have shown that actin and intermediate filaments structures are most responsible for cell stiffness [30]. Magnetic twisting cytometry measures the response of magnetic beads to an external force in order to quantify local compliance [35]. Other magnetic bead systems use super-paramagnetic beads to apply a point shear force and quickly measure the transition from elastic deformation to viscous creep response of the membrane and underlying cytoskeleton [35,107].

Through the use of these techniques and others, it has been shown that cell stiffness can be a biomarker for disease, and therefore is an important parameter to measure.

3.3 Materials and Methods

3.3.1 Cell culture

PSCs were cultured in DMEM (Invitrogen), supplemented with 10% Fetal Bovine Serum, 1% penicillin/streptomycin, and 1% sodium pyruvate, at 37°C and 5% CO_2. Glass coverslips were coated with 0.5% fibronectin (Sigma) for two hours and washed with DBPS. Cells were plated on fibronectin coated coverslips and incubated overnight at 37°C.

3.3.2 Bead Coating and attachment

4.5 µm tosyl-activated dynabeads (Invitrogen) were coated with fibronectin following manufacturer's protocol with a slight modification (0.1% Tween-20 is added before buffer C to prevent irreversible clumping) and stored at 4°C. Fibronectin coated beads were vortexed briefly and then mixed with media at a concentration of 1%. Plated cells were treated with diluted bead solutions for 30 minutes at 37°C and washed with media to remove unbound beads. The culture medium was replaced with 100µl L-15 CO2 independent media (Invitrogen) for imaging.

3.3.3 Magnetic trap assay

A magnetic trap (obtained from UNC Center for Computer Integrated Systems for Microscopy and Manipulation (CISMM) [108]) was used to apply forces on 4.5 um fibronectin coated magnetic beads. Coverslips with plated cells were loaded into the trap chamber and cells were visualized with a phase contrast microscope (Nikon TE2000 PFS) at 40x magnification. Stiffness measurement experiments consisted of a series of four pulses (2s on and 2s off) typically at the maximum power. Creep measurements used single pulses for durations lasting up to several minutes.

The strength of the magnetic field was controlled by computer. The control signal was generated by a Matlab script and sent as a voltage by a National Instruments DAQ pci card. A custom built transconductance amplifier converted the control signal from a voltage to a current. The current passed through coils of wire embedded in the trap. The magnetic field was transmitted to the sample by super-paramagnetic mu-metal, arranged in a pole-flat configuration, which created a uniform magnetic field up to ±30° from center.

To calibrate the trap, magnetic beads were added to a Newtonian fluid, (Karo corn syrup, viscosity 3.4 Pa.s) and loaded into the trap chamber. Their positions were tracked at 200 fps by a JAI-pulnix camera. Bead positions were obtained using UNC's CISMM video spot tracker. The velocities of the beads were determined by the distance travelled between frames, and the time elapsed between frames. Finally, Stoke's law was used to calculate the force of the magnetic field acting on the bead.

	$F_d = 6\pi\,\mu\,r\,v$	*3.1*

Where F_d is the drag force, μ is the viscosity of the liquid, r is the radius of the bead, and v is the velocity of the bead.

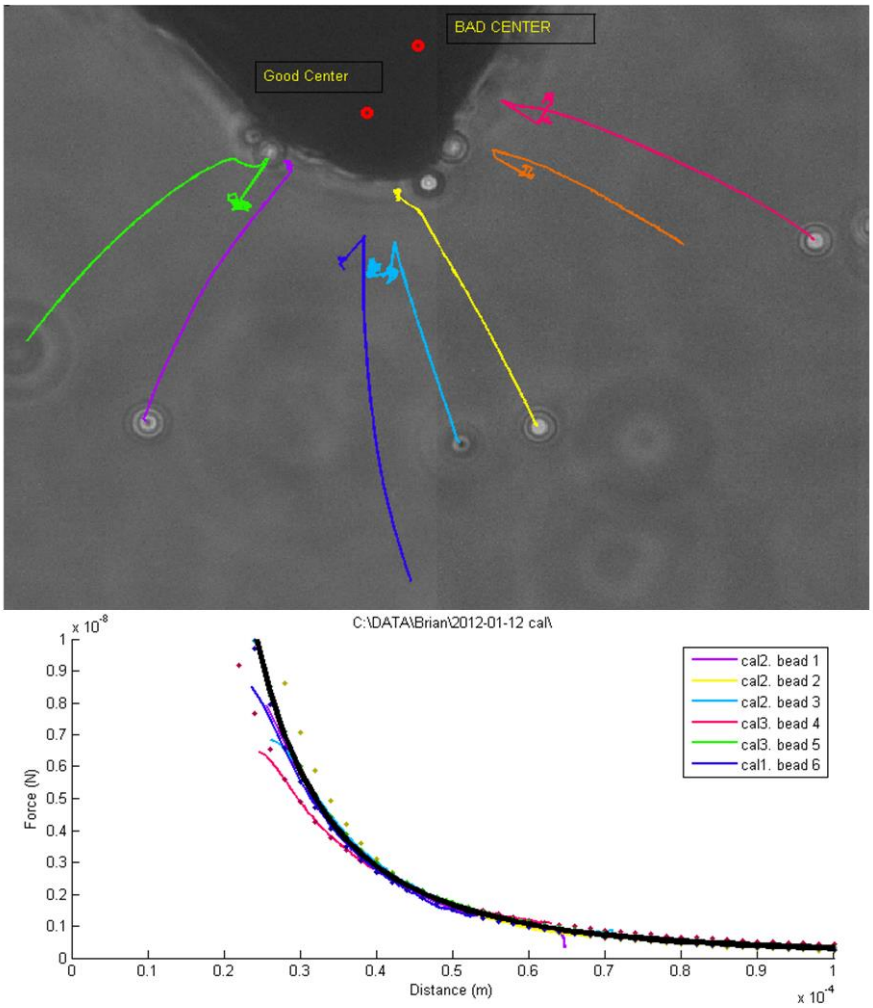

Figure 3-1 Top: Traces of magnetic beads as they are pulled through Karo Corn Syrup. The tip geometry requires a proper center point to be chosen, such that all the traces exhibit the same force – distance relationship. Bottom: The force – distance curves (colors) for all of the tracked beads overlap. The black overlay represents the average of all the tracks. This is used as the master force-distance relationship when calculating the forces acting on beads attached to cells.

The strength of the magnetic field (and hence, the force actin on the bead) depends on the distance from the pole center. The pole-flat configuration generates a magnetic field similar in shape to that of a monopole. Custom software finds the "monopole center" by minimizing the difference between the distance-velocity maps of the tracked beads (see Figure 3-1). The distance-velocity curves are averaged to make a master curve. Using this curve, the force actin on a bead can be determined by its location relative to the monopole center, and the voltage signal sent from the computer.

3.3.4 Analysis of Fits

$$x(t) = F\left(\frac{1}{k}\left(1 - e^{-kt/\eta_2}\right) + \frac{t}{\eta_1}\right) \quad 3.2$$

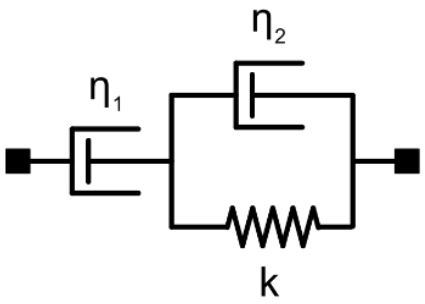

Figure 3-2: A modified Kelvin-Voigt system consisting of a parallel spring, k, and low viscosity dashpot, η_2, in series with a high viscosity dashpot, η_1. Equation 3.2 shows the displacement as a function of time, applied force, and model parameters.

We fit our data to a modified Kelvin-Voigt system that consists of two dashpots and a spring (shown above, Figure 3-2). The stiffness reported is the spring constant,k. The big dashpot, η_1, shows the rate of creep within the cell. The small dashpot, η_2, affects the transition time from elastic to viscous deformation. The displacement is a function of the applied force (assumed here to be a single step function), as well as the parameters of the model.

Another method used for curve fitting was a power law model, where

$$x(t) = Fa(t/t_0)^b \quad 3.3$$

The scale parameter, a, is a measure of compliance, and has units of m/N, the inverse of stiffness. The exponent, b, reflects the viscous/elastic relationship. For example, a purely elastic system would have an exponent of 0, while a system with only drag forces would have an exponent of 1 [109].

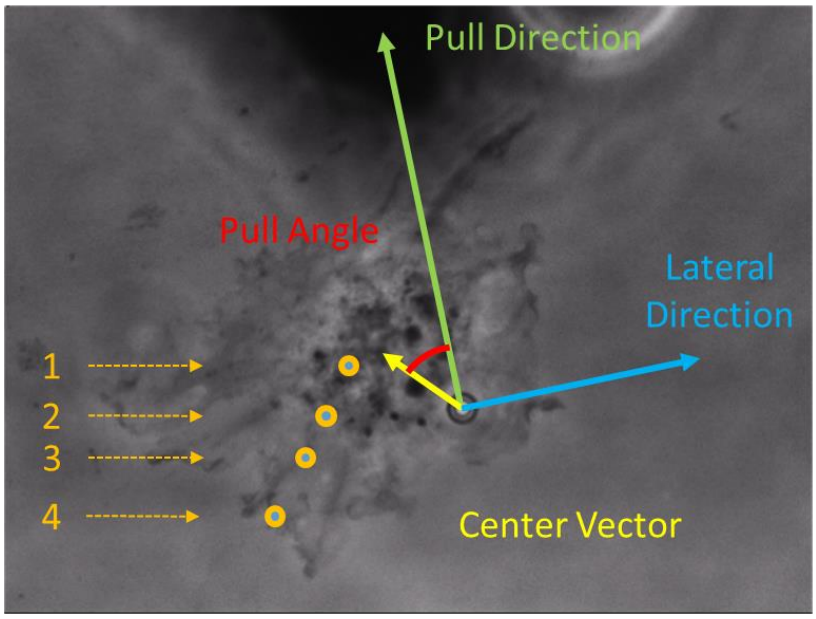

Figure 3-3 A diagram of bead locations and definitions for pull angle and the lateral direction. The bead locations are as follows: 1. Nucleus 2. Nuclear Edge 3.Lamellepodium 4.Cell Edge. The pull direction is defined by the vector pointing from the bead to the magnetic center of the tip. This is the direction of the applied force. The center vector points from the bead to the center of the nucleus. The pull angle is the angle between the pull direction and the center vector. The lateral direction is perpendicular to the pull direction.

The internal structure of cells varies across the cell body. The lamellipodia are flat and wide with highly branched actin networks near the edges, while the center of the cell is dominated by the nucleus. In order to determine the effect of cellular structures on measured stiffness, we recorded the location of each bead used for force application and the direction of the applied force, the (relative to the nuclear center). Bead locations were categorized as: nucleus (beads on top of nucleus), nuclear edge (beads overlapping the nuclear edge), lamella (beads on the lamellipodia) and edge (beads at the cell periphery). To measure the pull angle, we simply compare two vectors: one from the magnetic center of the tip to the center of the bead (pull vector), and the other from the center of the nucleus to the bead (center vector).

The lateral direction is defined as perpendicular to the pull vector. An isotropic, homogeneous material would only deform in the direction of the force. For all experiments, displacement is measured along the pull vector and along the lateral vector. Computing a normalized cross-correlation of the two quantifies their similarity. Furthermore, the ratio of

maximum displacement in the pull direction to the lateral direction are also computed. These measurements allow for comparison of bead locations and pull angles, and serve as an indication of the homogeneity and isotropy of the structure in the cells.

3.4 Results

3.4.1 HPSC cells show viscoelastic responses to applied forces

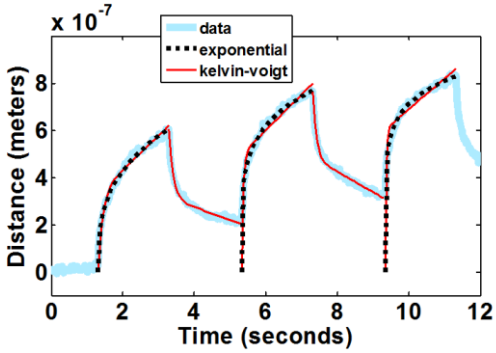

Figure 3-4 An example of data and fits for a typical stiffness measurement. The raw data in light blue is a measurement of total bead displacement. The bead position was determined by using UNC's CISMM video spot tracker software for sub-pixel spatial resolution. The red and black lines are fits to Equations 3.2 and 3.3 respectively.

Our first goal was to measure the mechanical stiffness of PSCs and compare with other known cells. Using a magnetic trap, we applied local tangential forces to cells via fibronectin-coated magnetic beads attached to the surface of spread cells. The shear force on the cell surface probes the mechanical properties of the underlying structure within the cell. The fibronectin coating on the beads binds to trans-membrane integrin receptors, which are in turn bound to actin filaments by α-actinin, talin, and other protein complexes. In this way, the bead is anchored to the actin cortex, which is a thin but very dense actin network just below the membrane.

The strength and duration of forces applied to the beads can be controlled using an electromagnet. Typical measurements involved sets of four two-second pulses spaced two seconds apart, as in [107]. The applied forces ranged from 50-2000pN. Bead displacements showed a typical viscoelastic response: a period of rapid elastic deformation, a transition period, and finally a

period of viscous creep (Figure 3-4). The data was fit to a modified Kelvin-Voigt model, which consists of one spring and two dashpots (Figure 3-2), and various parameters were derived from the fits. The reported stiffness of the cell is taken to be the spring constant, *k*, in the model. The rate of creep within the cell is determined by the viscosity of the big dashpot η_1. The small dashpot η_2 affects the amount of time to transition from elastic deformation to viscous creep. A plot of the stiffness as a function of increasing applied force (Figure 3-5, left) showed an increase in effective stiffness with applied force. We find the parameters of the Kelvin-Voigt model increase monotonically with increases in applied force. For small forces (~100pN), the spring constant averages 0.6 pN/nm. Around 1000pN, the spring constant averages 8pN/nm. The distribution of the data appears to be a log normal distribution. The geometric means at each of the forces listed above are 0.5pN/nm and 3.6pN/nm respectively. The arithmetic mean is skewed by one or two extremely high values. Therefore, the geometric mean better represents the expected value.

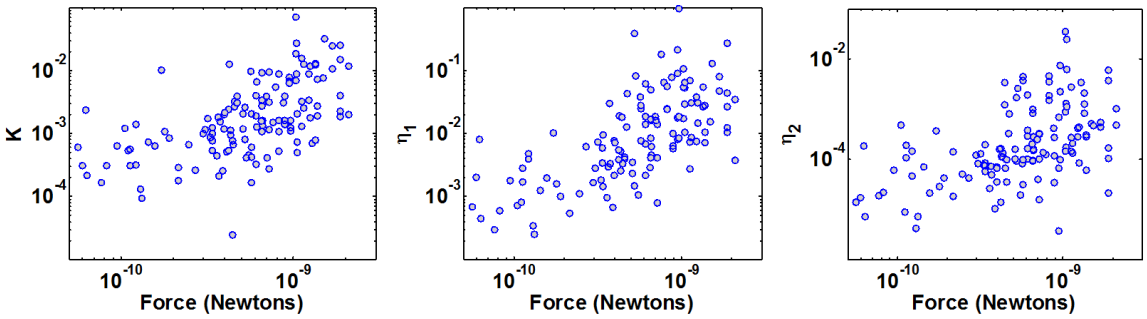

Figure 3-5 All stiffness measurements over a range of forces from 50pN to over 2000pN. From left to right are the parameters for the fits from the modified kelvin-voigt model, spring, k; large dashpot, η_1; and small dashpot η_2.

The values for the dashpots follow the same pattern, increasing with applied force. The geometric means for η_1 are 1.2 mPa*s and 27 mPa*s at 100pN and 1000pN respectively (Figure 3-5). The geometric means for η_2 are 0.07mPa*s and 0.47mPa*s at 100pN and 1000pN respectively (Figure 3-5). In both cases the viscosity increases by an order of magnitude along with the applied force. The values for these parameters can vary by an order of magnitude, also reported in [35]. We also

fit our data to a power law model, $\boldsymbol{x(t) = a(t/t_0)^b}$ as in [109].The value of the exponent was found to be 0.30±0.16 for the entire force range and did not show a dependence on applied force (Figure 3-6). The various parameter values measured for these cells display a typical viscoelastic response to an applied force.

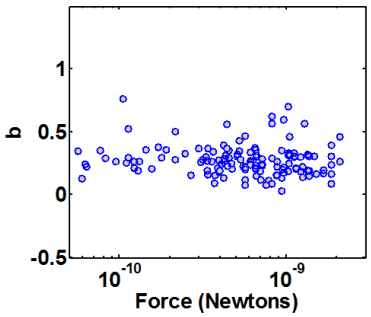

Figure 3-6 The exponent parameter b from equation 3.3, showing the balance between viscous and elastic behavior of the cells. A value below 0.5 means the system has a dominating elastic behavior.

3.4.2 Cell stiffness is independent of pull angle or bead location

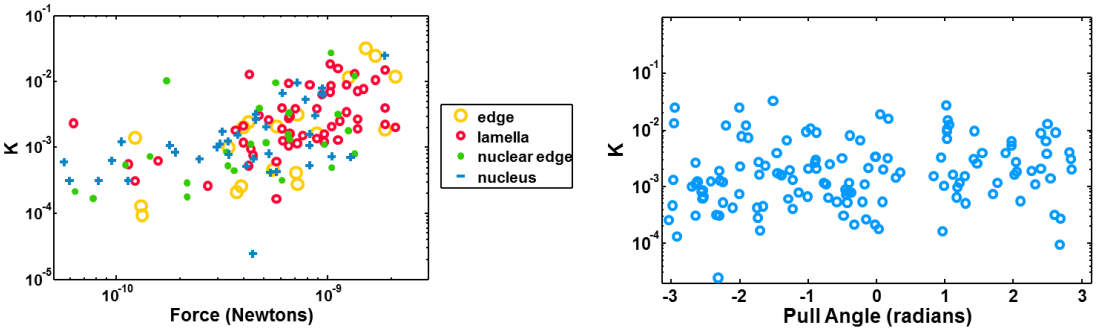

Figure 3-7 Left: The same plot as Figure 3-5, left, but with bead locations marked. Right: Measured Cell Stiffness as a function of pull angle. Zero represents the bead being pulled directly towards the nucleus center. ± π represents the bead being pulled directly away from the nucleus.

The internal structure of cells varies across the cell body. Lamellipodia are flat and wide with highly branched actin networks near the edges, while the center of the cell is dominated by the nucleus. In order to determine the effect of cellular structures in different parts of the cell or the

pull angle on the measured stiffness, we recorded the location of each bead used for force application and the direction of the applied force relative to the nucleus. Bead locations were categorized as: nucleus (beads on top of nucleus), nuclear edge (beads overlapping the nuclear edge), lamella (beads on the lamellipodia) and edge (beads at the cell periphery) (Figure 3-7). Despite the heterogeneous nature of the cytoskeleton, we found no significant difference in the range of measured stiffness or viscosity for different locations. The geometric means at 1000pN applied force were 2.3, 2.6, 4.0 and 1.6 pN/nm for the nucleus, nuclear edge, lamellipodia, and cell edge respectively. However, the standard deviations are all larger than the measured values due to the high variability in cell stiffness. Despite the different means from the data available, the graph clearly shows that all locations exhibit similar ranges of spring constants. The same held true for the dashpots as well as the exponent parameter, b. To measure the pull angle, we compare two vectors: one from the magnetic center of the tip to the center of the bead (pull vector), and the other from the center of the nucleus to the bead (center vector). We found that cell stiffness was independent of the direction of the applied force (Figure 3-7).These measurements allow for comparison of bead locations and pull angles, and serve as an indication of the homogeneity and isotropy of the structure in the cells.

3.4.3 Bead displacement is not always parallel to applied force

Our initial analysis measured the total displacement from the bead's origin. However, upon further observation, we found that the beads often moved in directions which were not parallel to the magnetic field (and hence applied force). This has been reported previously [37,109].

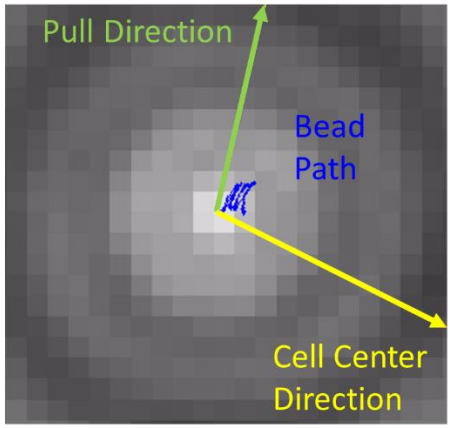

Figure 3-8 Image showing lateral displacement. The grayscale image is a close-up of a magnetic bead attached to a cell. The green line represents the direction of the applied force. The blue overlay is the track of the bead center over the course of the experiment. In this case there are four pulls and relaxations. The yellow line points to the center of the nucleus (not important for this figure).

To quantify this unexpected behavior, the movement of the bead is separated into two orthogonal directions, one in the direction of the magnetic field, and the other perpendicular to it (lateral direction). See Figure 3-3 for a diagram showing these directions and Figure 3-8 for an example of a bead track moving laterally to the applied force.

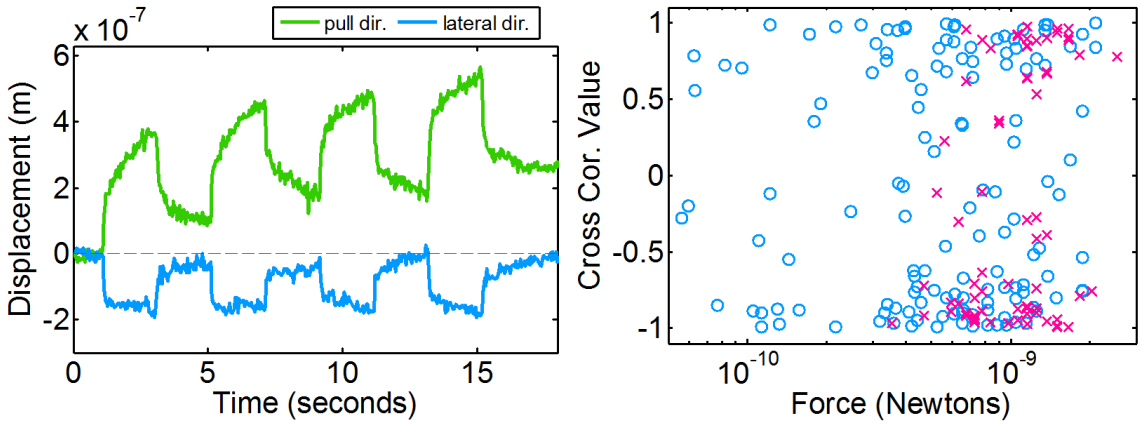

Figure 3-9 Left: An example of lateral displacement. The colors correspond to the directions in Figure 3-3, with green being in the direction of the applied force (pull direction) and blue being perpendicular to the applied force (lateral direction). Right: Maximum cross-correlation values between displacement in the direction of the applied force and perpendicular to it. A value of ±1 shows a perfect match between the shapes of the displacement curves in both directions. Blue circles indicate normal cells, red exes indicate palladin knockdown cells.

Analysis showed that the bead's motion in these two directions was highly coordinated with large displacements in one direction correlated with large displacements in the other (Figure 3-9). Further, the shape of the graphs for each orthogonal direction has the characteristic shape for a viscoelastic response as shown before. A cross correlation analysis showed a high degree of similarity in the shape of the graphs for each direction (> 0.7 cross-correlation) for a majority (~75%) of our experiments. The observed lateral bead movement may be due to interactions with internal cytoskeletal structures (such as stress fibers, microtubule bundles) as the bead is translated on the surface, which reorient the bead in a direction orthogonal to the applied force. One conjecture is that the internal structure of the cell is not homogeneous, and that the unexpected lateral motion of the bead is the result of separate regions of stiff actin bundles colliding with the cluster attached to the bead [37].

3.4.4 Cell stiffness decreases upon repeated force application

Cells often exist in environments where mechanical forces manipulate their shape and internal tension. Cells can adjust their own mechanical properties to better adapt to these external forces. For all of our experiments we used four measurements, which allowed us to observe short term changes in cell stiffness.

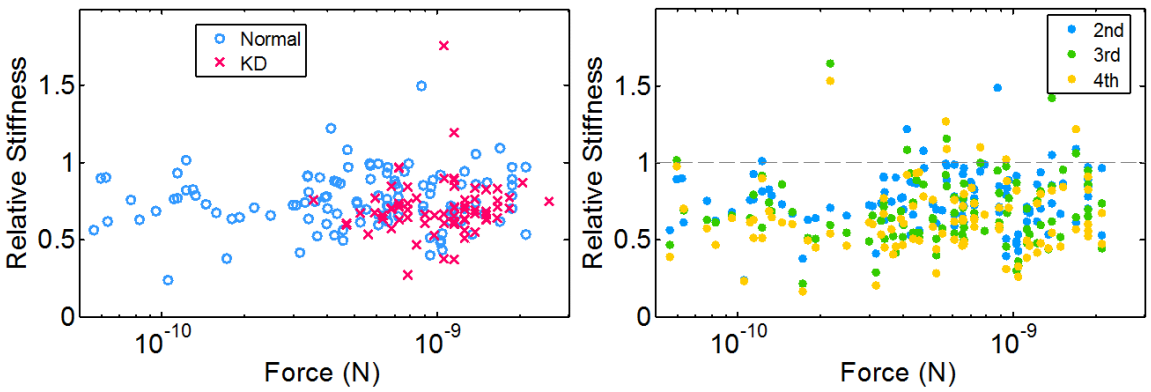

Figure 3-10 Left: Relative Stiffness as a function of applied force for both normal cells (blue circles) and palladin knockdown cells (red exes). Values shown are for relative changes between the first and second measurements. A value of 1 shows an identical stiffness measurement to the previous value. Right: Relative stiffness as a function of applied force for normal cells. Blue, green and yellow dots represent stiffness relative to the first measurement for 2nd, 3rd and 4th pulls respectively.

The relative stiffness was observed to decrease between each successive pull (Figure 3-10). Furthermore, we observed that strain induced softening does not depend on the applied force. Instead, the average loss in stiffness between the first and second pull is consistently 25% (±17%) across nearly two orders of magnitude of applied force. Each additional pull results in a typical loss of 10% from the previously measured value. As expected from our previous results for cell stiffness, the pull angle and position of beads on the cell have no effect on the amount of stiffness lost. Some cells show active stiffening in response to repeated application of forces [107]. However, in that study, cells showed a stiffening response only between the first and second pulls, while the subsequent pulls resulted in a slight decrease of stiffness. PSCs do not display the rapid active stiffening response, but behave similarly with respect to subsequent softening on repeated pulls. The cytoskeleton, which is responsible for cell structure and stiffness, is continuously reorganizing. High strains may temporarily soften the underlying structure because components of the cytoskeleton can unbind during these times, however the exact mechanism is still unclear.

3.4.5 Cell Stiffness is independent of palladin expression

Palladin is overexpressed in patients with pancreatic neoplasia, and a mutation leads to a unique form of pancreatic cancer [101]. While we are unable to test this mutation, we sought to determine the role of palladin expression levels on regulating the stiffness of PSCs. Changes in palladin levels have been shown to change viscoelasticity of reconstituted actin networks [18]. We therefore examined the effect of palladin expression levels on cell stiffness using palladin knockdown cells (Carol Otey's lab UNC-Chapel Hill). We measured the stiffness of knockdown

cells as described before. We found that, surprisingly, the level of palladin expression appeared to have no effect on cell stiffness or other parameters (Figure 3-11).

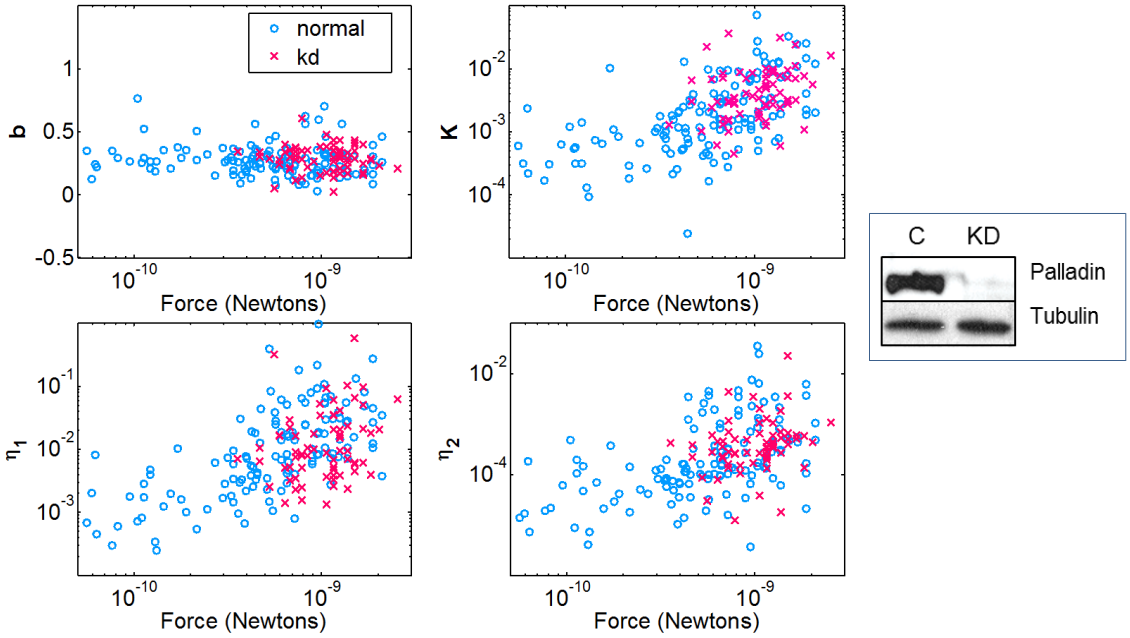

Figure 3-11 Model parameters for the exponential model (upper left) and kelvin-voigt model (all others). The blue circles represent normal cells. Red exes represent palladin knockdown cells. Right: a western blot confirming palladin knockdown (obtained from Dr. Carol Otey, UNC).

The exponent of the power law fit (b = 0.29 ± 0.1), cell stiffness as measured by the spring constant from the Kelvin-Voigt model (geometric mean: 3.7 pN/nm) or effective viscosity (η_1 = 11 mPa*s, η_2 = 0.36mPa*s)) were similar to the values obtained for normal cells. Furthermore, all of the parameters we tested, such as pull angle and bead location showed identical results to the wild type cells.

3.5 Discussion

We have investigated the mechanical properties of tumor associated fibroblasts from human pancreatic stellate cells. We found that PSCs exhibit a viscoelastic response to applied forces, like many other cell types. We further found that the mechanical properties of the cell such as effective stiffness were independent of the location or angle of force application. The effective stiffness of these PSCs are close to those of NIH 3T3 murine fibroblasts (5 pN/nm) [35],

F9 mouse embryonic carcinoma cells (5 pN/nm)[109], and others [37,107,110]. While cell stiffness has been measured using several different methods, the dependence of stiffness on cellular location and measurement parameters has not been well explored. Our results of homogenous stiffness across the entire cell suggest that internal forces are equalized in the cell. We have observed in these cells that stress fibers form upon cell spreading, and are usually present throughout the cell. The contractile activity of myosin II is known to be necessary for the formation of actin stress fibers. During our observations, these cells are largely unmoving, suggesting an equalization of tension across the cell, which may lead to a homogenous distribution of structural properties. Importantly, our results show that the cell can be described by effective mechanical properties, such as stiffness, which is independent of location and measurement parameters despite apparent differences in local morphology of the cell. Once the cell has becomes static, the tension has likely equalized, as an imbalance in forces would cause movement. Thus, this equalization in tension may serve to set up homogenous structural mechanics as well, which could explain why measurements at the cell edge are the same as those near the nucleus, despite vast differences in local morphology.

The high variability in the measurements however, could be explained by the heterogeneous nature of the underlying structure of the cell [30]. The magnetic beads are anchored to the cortex via integrin receptors, but the connectivity between the cortex and cytoskeleton is unknown. Some beads may be attached to parts of the cortex connected to larger cytoskeletal structures while others are not. The membrane and the actin cortex are somewhat fluid in directions tangent to the membrane surface, and therefore the results of our measurements may depend upon structures deeper within the cell.

The fact that palladin has no effect on the stiffness measurements also indicates that cells actively regulate their stiffness, and that it is not a result of stochastic assembly. Although palladin modifies the stiffness of in vitro actin networks, it does not appear to do so in vivo. This

result is counterintuitive, but cells are complicated machines. Palladin may simply be unnecessary in the scope of cell stiffness, or the lack of palladin may trigger a compensatory response, wherein other crosslinkers are upregulated. Palladin localizes to cell periphery, podosomes and to stress fibers. Therefore, it is also possible that the change in expression levels of palladin would not affect our measurements if the magnetic bead only engages structures without palladin. Furthermore, it could be that palladin may serve to organize actin filaments in a more efficient manner and allowing other crosslinkers to impart the structural integrity. Or, palladin might be primarily used to stabilize existing structures. While its exact purpose remains unknown, we have demonstrated that its role is distinct from other cross-linkers, and therefore that cross-linkers in general may do more than regulate the compliance of the cytoskeleton.

We also found that the displacement of the magnetic beads perpendicular to the applied force. The expected observation would be that displacement occurs only in the direction of the applied force. However, we frequently observe perpendicular displacement, similar to a previous study [37]. The cytoskeleton and cytoplasm may form a microgel. This means that the cytoskeleton is not one continuous structure across the cell, but rather a colloid system of smaller pieces. This has been observed in in vitro actin networks [81]. The evidence for this is that the amount of lateral displacement does not depend on pull direction or bead location. This rules out lateral displacement being a result of a stiffness gradient within the cell. Furthermore, the lateral displacement is highly correlated with the parallel displacement of the bead. That is to say, the extension and recovery occur in both directions at the same time. Internal structures acting as a ramp or wedge could explain this phenomena and would be consistent with previous observations [37,109].

Given the complexity of a cell and its finite size, variations in shape and local structure may influence measurements. Phenomenological models can be a powerful means of describing the data and provide quantifiable physical parameters. Using a modified Kelvin-Voigt model to

fit our data, we found that the effective viscosity and stiffness of the cell show a non-linear dependence on the applied force. This finding is consistent with other studies [109] and is also true for many materials subject to high strains. Here, higher forces lead to larger displacement (as is true of almost any system). But, due to the complexity of the cytoskeletal structure, higher strains engage a larger amount of material, and a larger number of structural objects within the cell. This may account for the apparent force dependence.

Actin crosslinking proteins play a key role in organizing the cellular cytoskeleton and may therefore be expected to modulate the mechanical properties of cells. For example, previous studies have shown that reduced expression levels of vinculin leads to softening of cells [109]. Reduced expression levels of alpha-actinin have been shown to increase the cellular traction forces, which would typically correlate with an increase in cell stiffness, though that has not been measured. It therefore seems that a simple relationship between cell stiffness and crosslinker expression levels does not exist, and that the particular nature of the crosslinker and the actin/adhesion structures it binds to may be important in determining the cellular properties. Here we found that knocking down palladin, an actin crosslinker which is important in many aspects of cell behavior, has no effect on the apparent cell stiffness. While palladin is an integral part of actin structures such as stress fibers, the presence of palladin in the actin cortex has not been investigated. Our measurements likely probe the cortical stiffness of cells, palladin may not be important in determining this parameter. Palladin has multiple roles in the cell including the formation of focal adhesions, serving as a scaffold for signaling molecules and modulating the dynamics of leading edge protrusions by interacting with actin regulatory proteins. Studies have shown that cells knocked down in palladin can respond with altered signaling pathways, such as decreased RAC activation [71]. Our results that palladin does not modulate cell stiffness, although unexpected, indicate that palladin's role is distinct from other actin crosslinkers.

In conclusion, we have made the first measurements of the effective stiffness of tumor associated fibroblasts which are a key component of the microenvironment of pancreatic cancer cells. Our results show that apparent cell stiffness does not vary across the cell in spite of significant structural heterogeneities. The cell may actively control its stiffness to maximize the mechano-sensitivity of the cytoskeleton. We have shown that these cells soften upon repeated application of external forces pointing to structural plasticity and a potential mechanism for adaptation to forces from the environment.

4 Pancreatic Stellate Cells Respond to Local Forces with Increased Global Stress Fiber Dynamics

4.1 Summary

During the cell stiffness experiments in the previous chapter, long duration creep measurements produced an active response from the cells. Minutes after applying the force, the cells' stress fibers simultaneously increased their contractile activity, as observed by increased movement of fluorescent markers in the stress fibers. This is a global response to a locally applied force, and it occurs about 90 seconds after the force is applied. It is common for cells to adjust their behavior due to external factors, so we wanted to investigate if this cell type was responding this way. There are many mechanisms by which a cell could alter its behavior as a response to an applied force, so we performed several perturbations of the system, including force duration, force magnitude, and various signaling inhibitions. We find that a minimum force magnitude and duration are required for the response, and also find that the response is independent of the bead/cell binding mechanism.

4.2 Introduction

The increased stress fiber activity may be related to the function of the pancreatic stellate cells (PSCs). PSCs maintain the structure of the pancreas. They organize the ductal and acinar cells, which create and transport digestive enzymes. To do this, PSCs generate ECM proteins. PSCs are more active in tissue with high inflammation or necrosis [100]. Furthermore, PSCs are found in similar activated states (meaning an increase in ECM generation, migration and proliferation) in disorders such as pancreatitis and pancreatic cancer. There have been many studies which explore the chemical regulation of this activated state. Growth factors, cytokines, hormones and other signaling modes can all lead to activation[100]. We want to explore another possible path of activation: an applied force may also lead to changes in cell behavior. Many

other studies have observed responses to applied forces in other cell types [44,107,111–114]. These responses range from rapid cell stiffening[107], to increased contractility[115], to altering transcription[116], to migration[106]. In this case, the PSCs respond with a coordinated movement within the cell's stress fibers. Stress fibers consist of 10 to 30 actin filaments bundled together by α-actinin, palladin, and myosinII-A. The actin filaments (which have a plus and minus end) point in both directions. However, they tend to be unidirectional at focal adhesions but are found in both directions in the center of the stress fiber [117]. Non-muscle Myosin IIa is the motor protein which drives stress fiber contraction. However, the filaments in the stress fibers are connected by many groups of myosin motors. Each stress fiber will be pulled in both directions along its length, and hence the myosin motors work against each other. The myosin motors are unable to break individual filaments because the filament's tensile strength is too high, but they do generate enough force to buckle individual filaments. Recent work suggests that this buckling is the symmetry breaking mechanism that allows the stress fiber to contract [118–120].

We track local strain in the stress fibers by using PSCs with GFP labelled palladin (See Figure 4-1). The palladin forms a regular pattern along the stress fibers. It colocalizes with α-actinin[68], but not with myosin IIa [117]. By measuring the distance between two palladin regions over time, we can observe the strain rate at any segment along the stress fiber. A stress fiber may have areas of positive strain (extension) and negative strain (contraction) simultaneously. Typically, the contraction takes place at the cell periphery, where the stress fibers have a higher concentration of myosin[121]. In addition, there is evidence that focal adhesions serve as activation sites for RhoA, and that diffusion from these sites leads to the heterogeneous distribution and activation of non-muscle myosin II-a [122,123]. The contractions we observe follow the same pattern, typically stretching at the center and contracting near the edges.

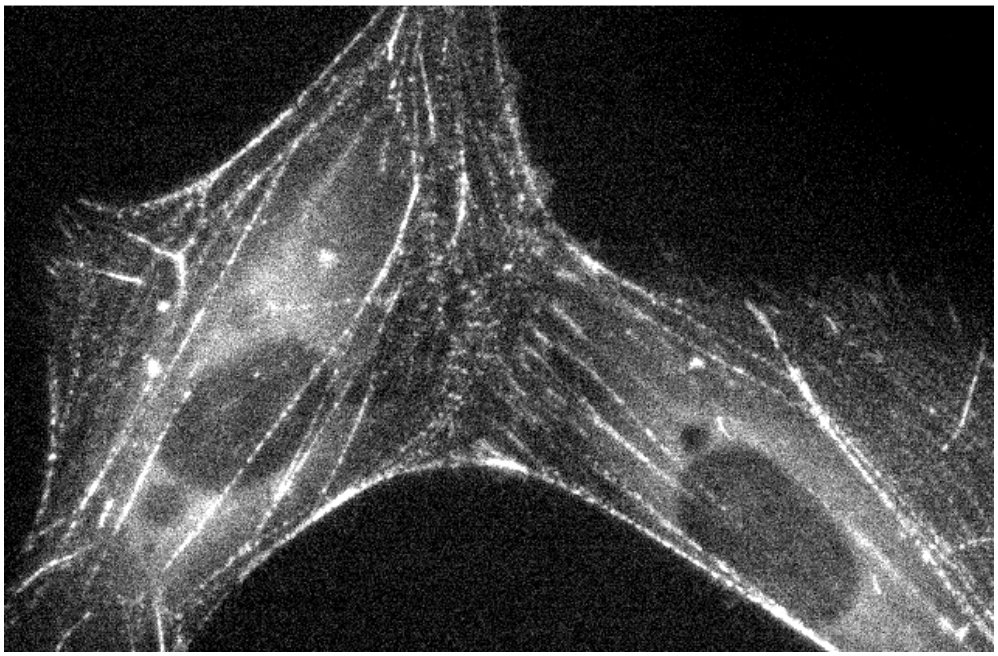

Figure 4-1 An epifluorescence image of Pancreatic stellate cells with EGFP palladin. Stress fibers are the long, straight, bright lines. Notice that the palladin tends to cluster into small spots.

We also wanted to determine which cellular components are required to activate the stress fiber response. The microtubule network[124,125], integrin receptors[110,126], and GEF - RhoA signaling pathways[107,114,123,127] are all essential parts of mechano-sensing pathways. In addition to driving stress fiber contraction, non-muscle myosin II-a actively reorganizes the cytoskeleton, and is essential for creating stress fibers [128]. We also sought to test its importance by direct activation or inhibition. Finally, we also test the importance of other factors, such as the magnitude and duration of the applied force.

4.3 Materials and Methods

4.3.1 Cell Culture and Spreading

See sections 3.3.1 and 3.3.2.

The success of this experiment depends completely on the ability to label stress fibers in such a way that their local strain rates can be tracked. PSCs were stably transfected with EGFP labeled

palladin (I would like to thank King Lam Hui for making these). This allows us to track local changes in length along the stress fibers.

4.3.2 Bead Coating

Tosyl-activated magnetic beads (dynabeads M-450, invitrogen) were coated with either fibronectin or poly-L-lysine according to manufacturer protocol, with the exception that 0.1% w/v Tween 20 was added before step 3 of the protocol to prevent excessive bead clumping.

4.3.3 Imaging

Images were collected on our Nikon TE2000 microscope, using Andor control software, a coolsnap HQ2 cooled CCD camera. We used a mercury lamp with appropriate filters to supply the blue light that excites the EGFP labelled palladin. We used a halogen lamp for bright field imaging in phase contrast mode. The cells are imaged in the epifluorescence channel every 4 seconds. Typically the cells are imaged for 5 minutes before the magnet is turned on, in order to establish a baseline level of stress fiber activity.

4.3.4 Force Application

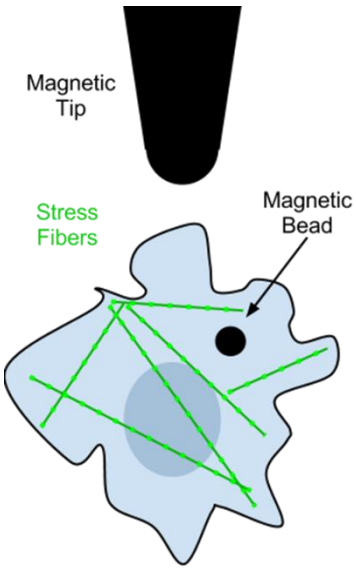

Figure 4-2 Diagram of experimental procedure. The magnetic bead is attached to the cell. The distance from the bead to the tip center is used to calculate the applied force on the bead. The bright segments on the stress fibers are tracked via software.

The setup employed is described in the chapter 3. Briefly, a transconductance amplifier converts an input voltage from the computer into a current which drives an electromagnet. Forces are applied ranging from 200 to 2000 pN, for durations of 1 to 10 minutes. We also pulsed forces (0.5 Hz square wave) for several experiments. Figure 4-2 shows a basic diagram of the experimental setup.

4.3.5 Pharmacological Treatments

Two drugs were used to inhibit specific cell functions. 10nM Calyculin-A (Cell Signalling Technologies, Boston, MA) was used to activate myosin-II motors in the absence of an applied force. These experiments were carried out in a well, as it is not possible to add fluid to cells in the magnetic trap. Cells were incubated for 30 minutes 2.5μM Nocodazole (Sigma, St. Louis, MO) to disassemble the microtubule network. Disassembly was verified by immunostaining cells with a mouse/anti-tubulin primary (Abcam, Cambridge, MA) and an alexafluor-594 labelled goat/anti-

mouse secondary (Invitrogen, Grand Island, NY). The complete immunostaining protocol may be found in the appendix.

4.3.6 Stress Fiber Tracking Algorithm

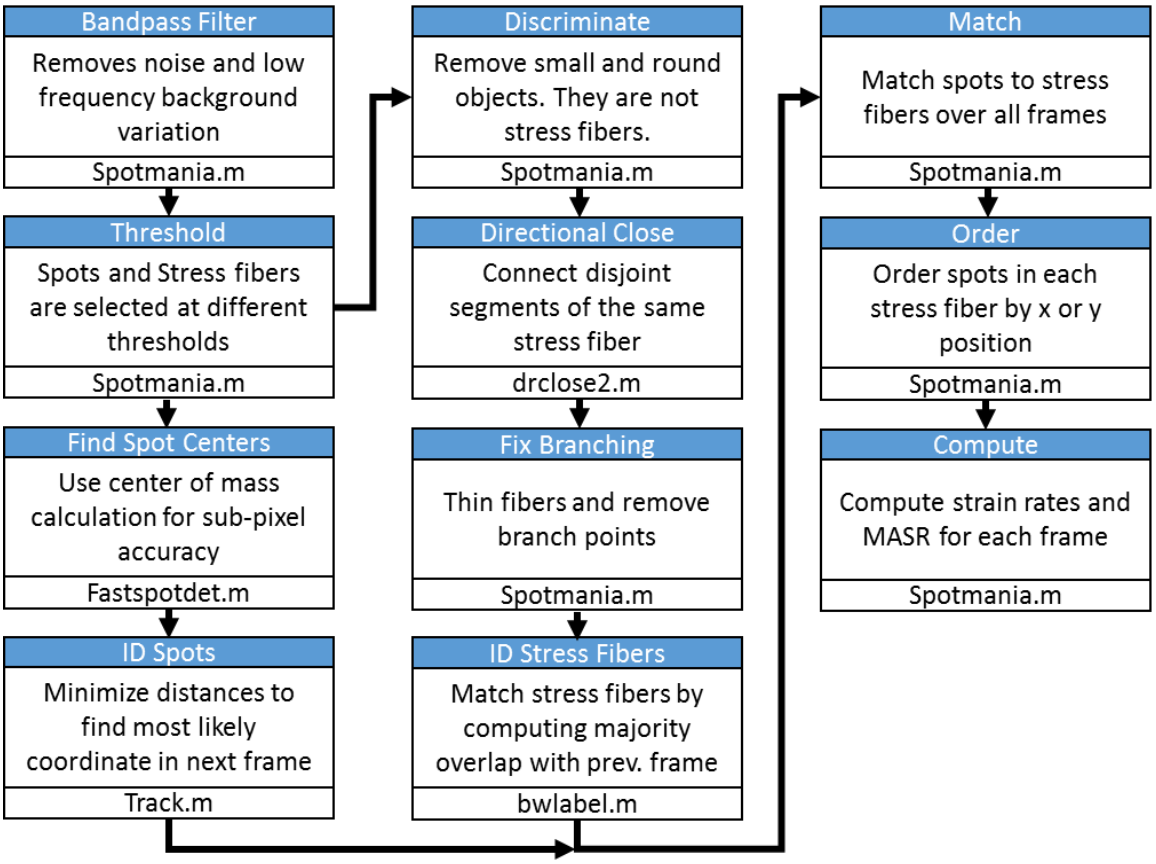

Figure 4-3 Block Diagram of the stress fiber strain rate tracking algorithm

The tracking algorithm consists of three main parts. Spot identification, stress fiber identification, and a matching/tracking algorithm. A more detailed outline is shown in Figure 4-3. To identify the spots on the stress fibers, the images are first run through a band pass filter to minimize the interference of noise and low-frequency background fluorescence. Then, local maxima above a threshold are found. For cases with local maxima closer than 3 pixels the larger is chosen and the smaller is ignored. Finally, we use a center of mass calculation in a window around the maxima to determine the spot location to sub-pixel precision. Spots are tracked from frame to frame using a very efficient track algorithm (Dan Blair, Georgetown University). To track stress fibers the

band pass filtered image is converted to a binary image. Using MATLAB's regionprops function, segments of stress fibers are identified along with their approximate direction. The stress fibers in our experiments are marked periodically by spots of GFP-palladin. Since these bright spots do not allow an easy adaptation of the bundle tracing method, additional smoothing is applied to the image, and a directional closing algorithm is used to connect disjoint segments of the same stress fiber. Normal closing connects parallel fibers that are actually distinct. Directional closing connects the segments, without connecting to adjacent stress fibers (Figure 4-4).

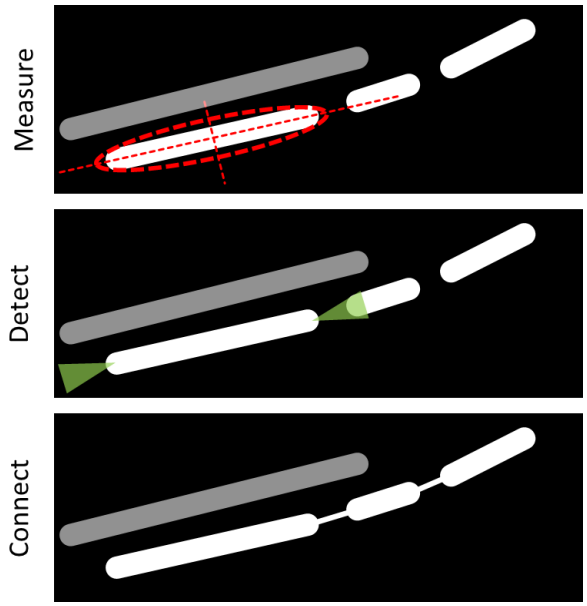

Figure 4-4 The steps in the directional closing algorithm. Segments from one stress fiber are grey, and the other white. This algorithm prevents parallel fibers from connecting to each other while connecting segments from the same stress fiber. Top: MATLAB's regionprops function determines the direction of the major axis. Middle: Each segment is extended along this axis to check for nearby segments of the same stress fiber. Bottom: The segments in the binary image are connected.

A secondary image is created with regions that overlap the stress fibers in the original. Distinct regions are identified. Regions are tracked frame to frame by calculating the amount of overlap between two regions in different frames. This is handled in such a way that temporary gaps in a region are prevented from splitting into two regions.

A direction specific closing algorithm is applied in order to better connect the identified stress fibers without merging parallel stress fibers (Figure 4-4). BWlabel is used to identify each

stress fiber region in the first frame. Subsequent frames are labeled by which stress fiber they overlap the most from the previous frame. The result is that every stress fiber tracked now has a region specified in every frame. The last part of the tracking algorithm uses these regions to determine which spots belong to which stress fibers, and orders the spots by location along the stress fiber. Strain rates are calculated by measuring the change in distance between pairs of spots from frame to frame. Spots that cannot be tracked for at least 120 frames are rejected. Furthermore, spots and stress fibers are re-identified every 20 frames to account for merging, splitting or overlapping stress fibers or spots. Spots and stress fibers that cannot be well tracked over these 20 frame intervals are not included for analysis during that interval.

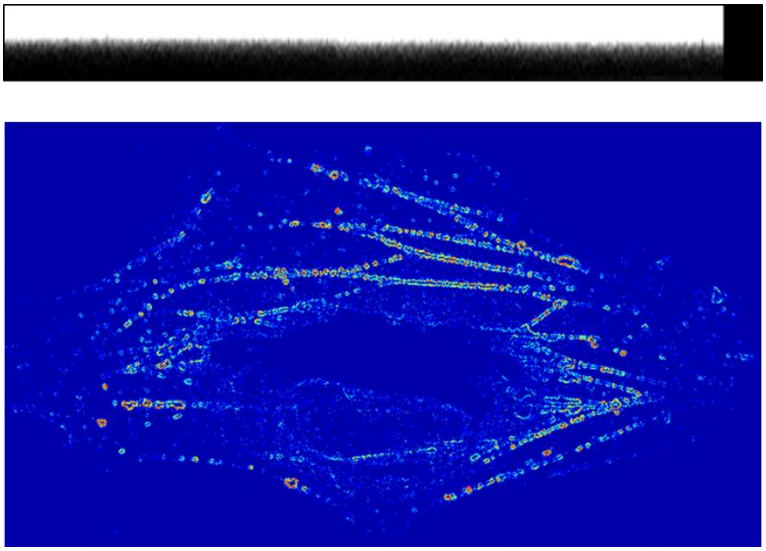

Figure 4-5 Top: a modified histogram used to assess focus consistency. A flat transition area between black and white regions (low and high contrast respectively) represents consistent focus throughout the movie. Bottom: heat map of the image gradient. Warm colors show high contrast.

Maintaining proper focus is essential for meaningful results. Both blur and image noise can affect the accuracy of the center finding algorithm. Figure 4-5 shows screen captures from software used to verify consistent focus. Movies that do not maintain focus and a good SNR are rejected, as well as movies with an insufficient number of trackable stress fibers. In this way, we can be sure that our responses are not artifacts of the shortcomings of image capture nor due to a small sample size.

4.3.7 Data Analysis

Our aim is to classify a response by measureable observations. We use local strain rates, calculated from observing changes in distance between adjacent palladin markers along the stress fibers. The stress fibers undergo positive and negative strain at different locations, so we calculate the absolute value of the strain rate (Figure 4-6). This avoids the problem of high strains averaging to zero, or near zero. The value we use to assess response levels is the mean of all absolute strain rates in a given frame. We call this the mean absolute strain rate (MASR). Both extension and contraction are included.

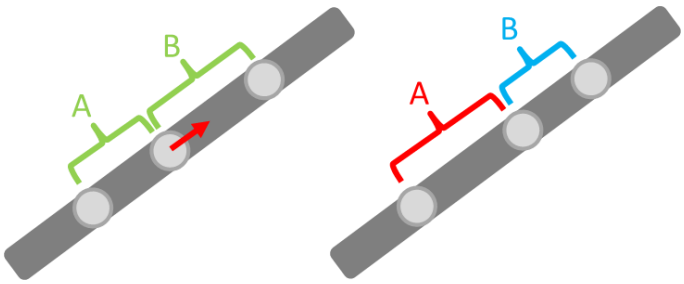

Figure 4-6 Diagram of image analysis. The grey bars represent the same stress fiber imaged at different times. The light circles represent palladin within the stress fibers. Software tracks the palladin and can be used to measure local strain rates within the stress fibers. The initial lengths A and B are shown on the left in green. On the right, A has expanded (red) and B has contracted (blue).

Stress fibers in PSCs are always dynamic, with EGFP-palladin structures exhibiting movement along the fibers, even in the absence of an external force. In order to establish the baseline level of activity and MASR, we imaged cells for several minutes prior to force application. The MASR fluctuates during this period, as the activity inside a cell is somewhat stochastic. Furthermore, image noise can have a small effect on locating the centers of the palladin spots. The baseline signal is described by its mean, and the standard deviation of the mean. The response level is determined by finding the absolute peak in the signal after the magnet has been turned on. The average of the peak is defined by averaging the signal on 30 seconds either side of the actual peak. The standard deviation is also calculated over this range. To compare the level of response to the baseline, we compute the ratio of the difference between the baseline and peak averages to

the standard deviation of the baseline. This ratio (peak to baseline ratio, or PBR) is similar to a signal to noise ratio and enables us to quantify the response. The PBR quantity allows us to categorize the response into one of three levels: non-response, possible response, or clear response.

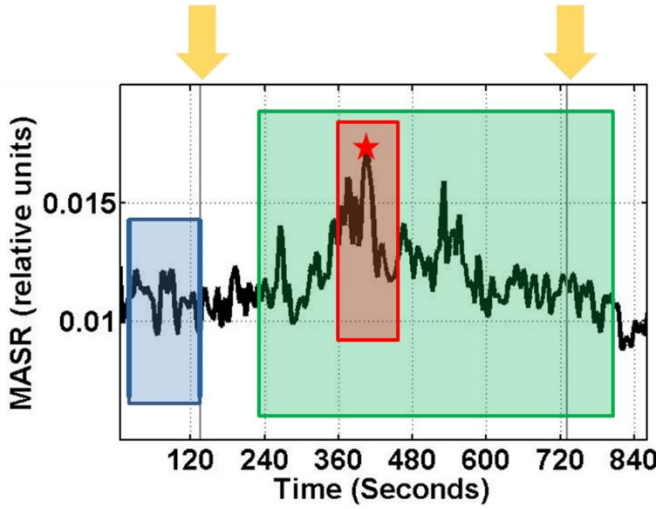

Figure 4-7 Magnet is on between yellow arrows. Cells have a base level of stress fiber motion (blue). The peak response region (red) is ± 30s of the overall max (red star). The Peak to Baseline Ratio (PBR) is computed as follows: (Peak Mean – Baseline Mean) / std. dev. of Baseline. The green box represents the typical range of time where the response occurs.

Calculating the peak response involves finding the absolute peak in the data and including it in the mean. For this reason, we always expect the peak mean to be above the baseline mean (See Figure 4-7). Therefore, we define thresholds for response as follows: PBRs below 2 are counted as non-responses, PBRs between 2 and 4 are counted as possible responses, and above 4 as clear responses. By grouping our results in this fashion, simple histograms can represent the likelihood of a response under various conditions. A t-test is used to compare the PBRs for each set of conditions to the control group, where the magnet is turned on for 5 minutes but without any beads attached to the cells' surface.

4.4 Results

4.4.1 The force response requires minimum magnitude and duration of applied force

We used PSCs with EGFP labelled palladin so that we could visualize the stress fiber movement in response to external forces. The forces were applied with fibronectin coated magnetic beads, which adhere strongly to the cell surface. Time lapse images allowed us to calculate the strain rates within the stress fibers. We first compared the cell's response to high forces (>2nN) and of 5 minute duration to the activity of cells without magnetic beads. This was our control, and it ensured that the response we observe was not an artifact of focus drift, image drift, exposure to light or the magnetic field, or just an occasional event that occurs naturally. The difference is apparent when plotting the MASR as a function of time (Figure 4-8). A typical experiment consists of a 5 minute continuous force, > 2pN and frequently exhibits a clear response (PBR>4). These conditions are referred to as a "Normal" experiment for the duration of the chapter. The control experiments, which are run under the same conditions as normal experiments except without magnetic beads, do not show strong increases in MASR (Figure 4-9).

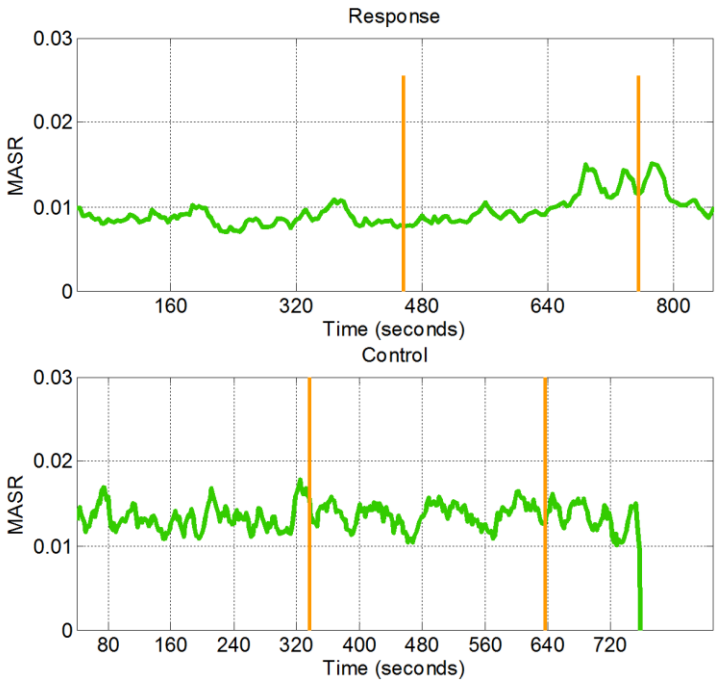

Figure 4-8 MASR is plotted in green as a function of time. The magnet was turned on during the time between the vertical orange bars. Above: Data from a standard experiment; a steady 5V control signal (>2pN force) for a duration of 5 minutes. Below: the same control signal applied to a cell without magnetic beads attached.

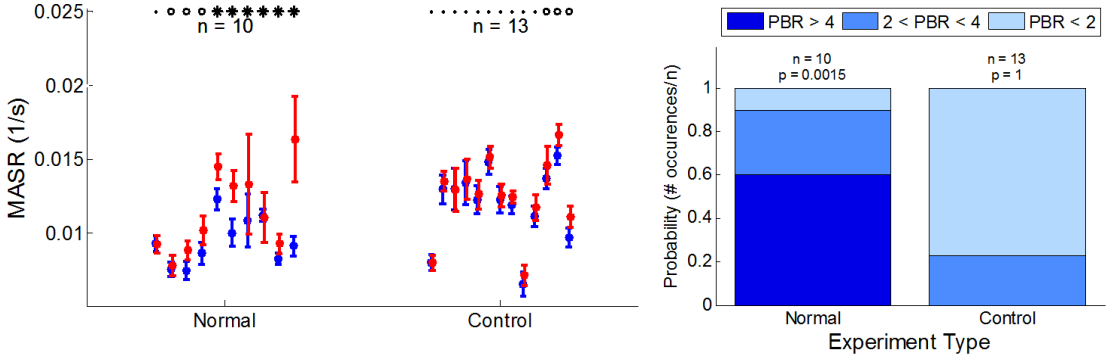

Figure 4-9 Left: The standard test vs. Control. The standard test consisted of 5 minute pulls exerting a constant force from 2.0 to 4.0nN. The controls use the same 5 minute pulls with the same magnetic fields but with no beads. The beads are coated with fibronectin, just like the glass surface. The blue markers represent the baseline MASR with bars showing standard deviation. The red markers show the mean MASR during peak response, again with bars showing standard deviation. The markers above the plots indicate the level of response. Dots for non responses, PBR < 2; circles for possible responses, 2 < PBR < 4; and stars for clear responses, PBR > 4. This convention is used for all subsequent figures. Right:The likelihood of obtaining a PBR in a given range for each experiment type. The number of experiments per group is denoted by n. Mean PBRs are compared using a t-test. The p-values against control are shown above each experiment type. These conventions hold for all subsequent graphs.

Our next goal was to determine whether response had a threshold for either the magnitude or duration of the applied force. Determining the threshold may help to elucidate the purpose of this response in the cell's natural environment. By adjusting the voltage signal sent to the amplifier, as well as the distance between the bead and the magnetic tip, we can vary the applied force from 50pN to 3000pN. Similarly, the time duration is easily controlled via software, and lasts from 1 to 10 minutes.

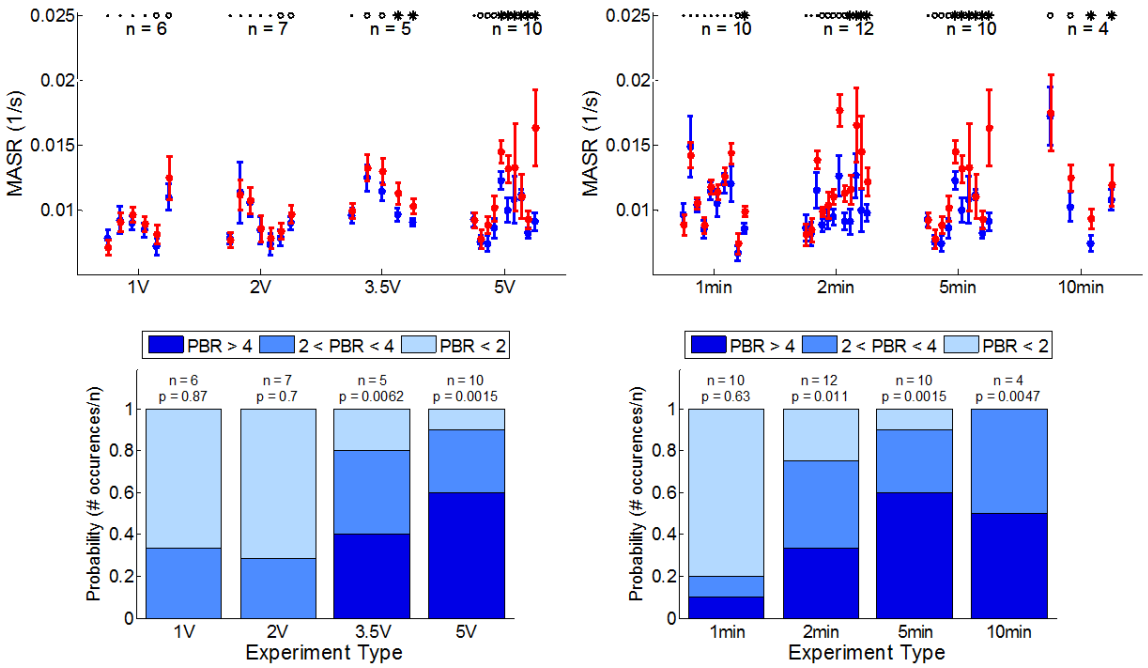

Figure 4-10 Top left: Force dependence tests. The range of forces tested are 0.4-0.8nN, 0.8-1.6nN,1.4-2.8nN and 2.0-4.0nN for 1V, 2V, 3.5V, and 5V control signals respectively. All experiments used 5 minute pulses. Top right: Time dependence tests. All experiments used 5V control signals (forces > 2nN). Bottom left and right: probabilities of response levels for the given experimental conditions.

Figure 4-10 shows the response data for applied forces of various strengths and durations. We found that the threshold for force response was in the range of 1nN (Figure 4-10, left). Below this value, there was no significant change in response levels when compared to control. Above this level, there was a very obvious increase in stress fiber strain rates, demonstrated by higher values for the PBRs. Additionally, Figure 4-10 (right) shows that a minimum duration of applied force (2 minutes) was required to illicit a response, even for forces above 1nN. All tests at lower forces

were carried out at 5 minute durations (more than double the minimum required time), so it is unlikely that lower forces would trigger a response at even longer durations.

4.4.2 Steady force application is more likely to trigger a response

During typical force application experiments the bead displaces at a slow, steady pace because it has transitioned to a creep response. However, the initial displacement during the elastic response is very rapid. In order to test which type of displacement was more effective at triggering the increased strain response in stress fibers, we applied a 0.5Hz square wave force profile, rather than a continuous force. In this way, the bead moves rapidly back and forth, causing it to cover a greater total distance (and almost completely the elastic regime), even though the net displacement is smaller.

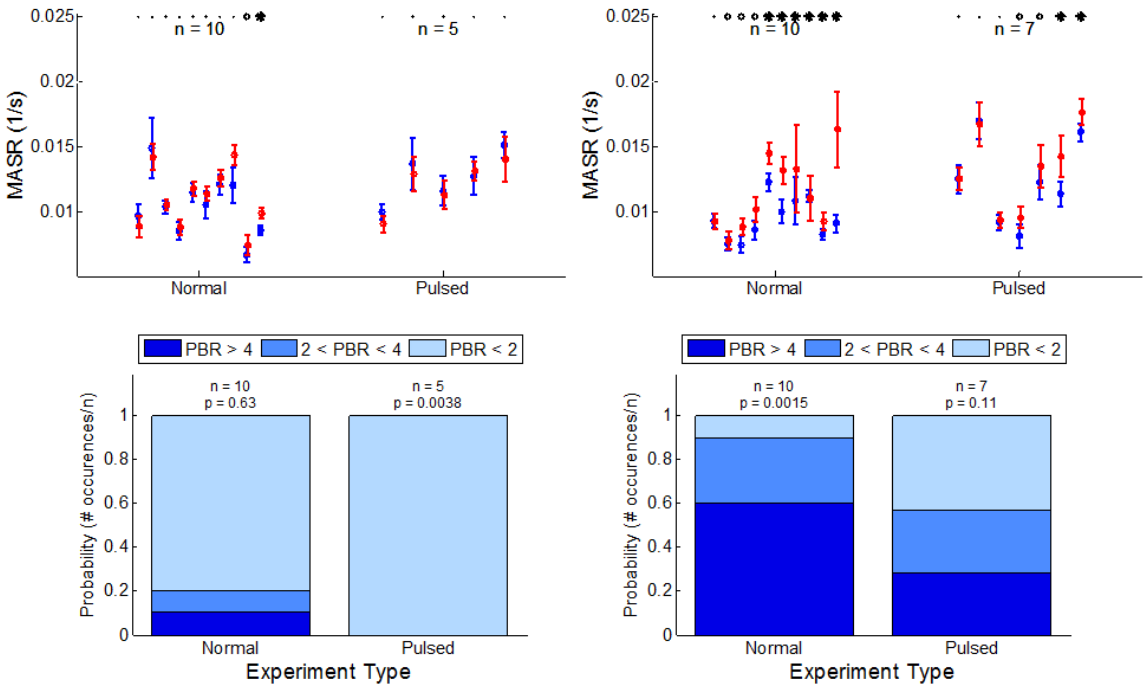

Figure 4-11 Left: Response to pulsed forces 2.0-4.0nN lasting 1 minute compared to responses to continuous forces of the same magnitude lasting 1 minute. Right: Responses to pulsed forces 2.0-4.0nN lasting 5 minutes compared to responses to continuous forces of the same magnitude lasting 5 minutes. Bottom left and right: probabilities of response levels for the given experimental conditions.

While we did see a slight increase in response levels for pulsed forces over the control for five minute tests, the difference was not statistically significant (Figure 4-11). One minute tests showed

no response whatsoever. Continuous forces trigger the response consistently than pulsed forces. This may be important as we search for the exact mechanism of the response, as well as its purpose.

4.4.3 An intact microtubule network aids response

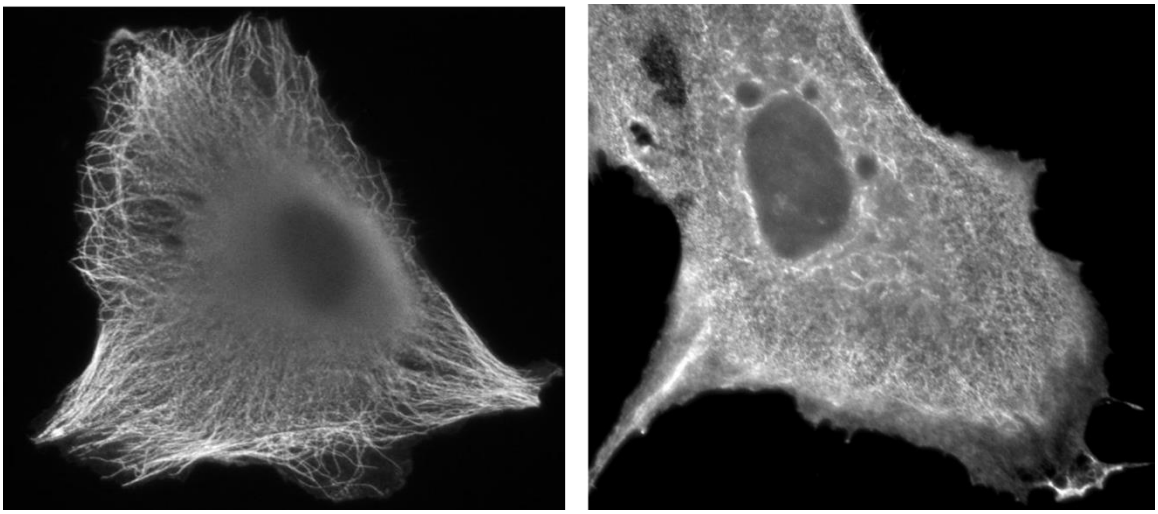

Figure 4-12 Epifluorescent images of PSCs with labelled tubulin. The image on the right shows an intact microtubule network, while the image on the left shows a disrupted microtubule network resulting from incubation with 2.5μM nocodazole for 45minutes.

An intact microtubule network can transmit forces throughout a cell. In some cases, it is essential for force transmission or cytoskeletal organization[124,129]. In order to test the role of the microtubule network in PSCs, we treated cells with 2.5 μM Nocodazole, which depolymerizes the microtubule network. Immunostaining cells allowed us to directly image the microtubule network. The disruption of a clear structure confirmed that the nocodazole treatment was successful (Figure 4-12).

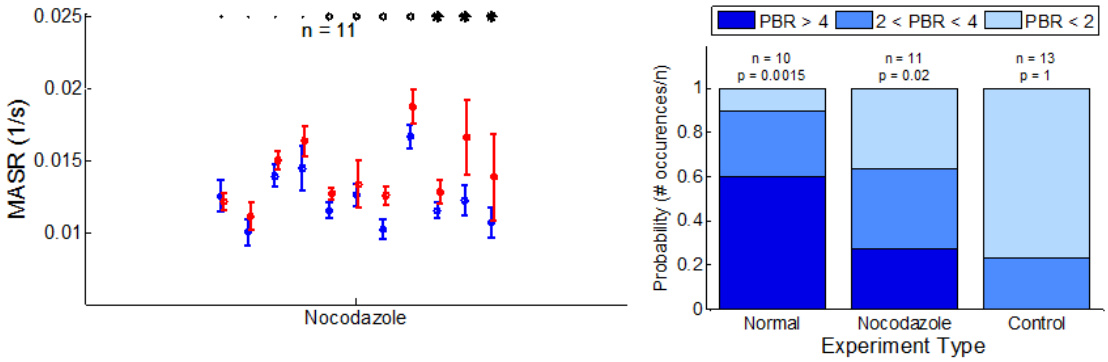

Figure 4-13 Right: Peak and baseline MASRs measured for PSCs treated with 2.5μM Nocodazole. Applied forces were in the 2.0-4.0nN range, all lasting 5 minutes. Left: probabilities of response levels for the given experimental conditions.

We found that increased stress fiber contraction does partially depend on the microtubule network (Figure 4-13Figure 4-13). The number of cells which respond, as well as the level of response fall between the control, and the untreated 5 minute, 5V response. This indicates that an intact microtubule network is required for a robust response.

4.4.4 The response is not integrin specific

Other studies have shown that force response can depend on specific mechanisms or parts of the cell. For example, integrin is a transmembrane receptor that binds to fibronectin, which is abundant in the ECM. Cells often use integrin-fibronectin binding as a means to attach to their surroundings. Stress applied to integrin receptors can initiate signaling cascades which alter cell behavior. In the case of aortic endothelial cells, the response to external forces is integrin specific [112]. We used poly-L-lysene coated beads (that bind electrostatically to the cell membrane) instead of the normal fibronectin coated beads to test whether or not PSCs' response also depends on integrin receptors. There are several types of proteins that anchor the membrane to the actin cortex (PIP_2, for example), so even though there is no longer a direct connection from the bead to the actin cortex via integrin receptors, the poly-L-lysine beads are still coupled to the actin cortex by other means. Stretch sensitive ion channels on the membrane may still be deformed and

external forces may still be transduced through the cytoskeleton, but the integrin receptors will not be activated.

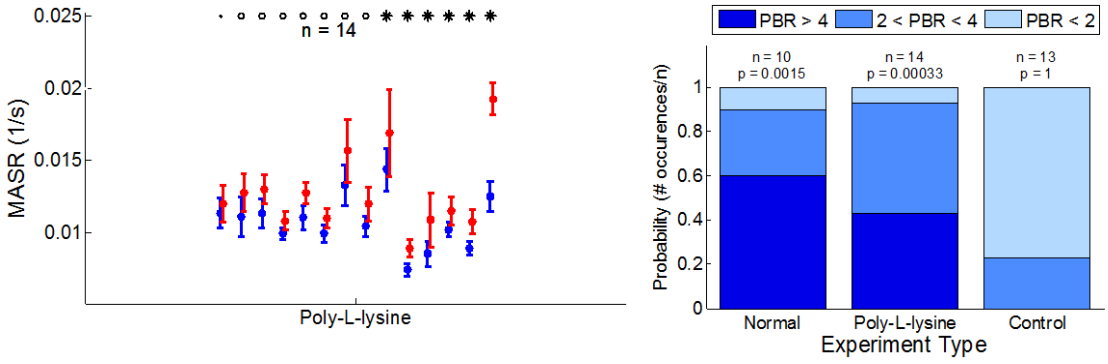

Figure 4-14 Right: Applied forces were in the 2.0-4.0nN range, all lasting 5 minutes. Poly-L-lysine coated beads were used instead of fibronectin coated beads. Left: probabilities of response levels for the given experimental conditions.

We found that PSCs responded similarly with either fibronectin of poly-L-lysine coated beads (Figure 4-14). This leads us to believe that the integrin signaling pathway is not involved in PSC's response to external forces. There are several other known force sensing mechanisms which could be used here, (see section 1.4.3).

4.4.5 Directly activating Myosin II shows a similar response

Finally, we wanted to confirm that myosin-II activity was responsible for the stress fiber contraction. Therefore, we used Calyculin-A, a protein phosphatase inhibitor that blocks myosin light chain phosphatase and increases myosin activity [130–132]. Similar increases in stress fiber strain rates would indicate that the stress fiber activity is indeed myosin driven. We see a nearly identical response in stress fiber contraction for direct activation as we do for force activation (Figure 4-15).

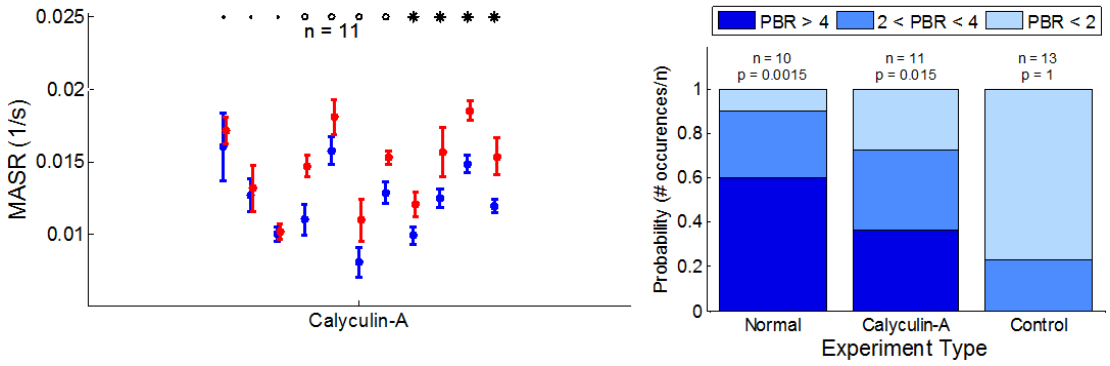

Figure 4-15 Right: Responses after pharmacological treatment with Calyculin-A. Left: probabilities of response levels for the given experimental conditions.

This leads us to believe that the response is indeed driven by myosin-II, and not a release of pre-tensioned stress fibers. We note that the calyculin-A driven response was not as robust as the standard 5 minute, high force pull. It could be simply that calyculin-A does not activate myosin-II as efficiently as the native signaling pathway, or it could be that there are other components involved, which also increase contractility.

4.4.6 Myosin inhibition prevents stress fiber formation

We also wanted to determine the role of myosin motors in the stress fiber response. Similar experiments were carried out with ML7, a myosin inhibitor. M L7 works by preventing myosin phosphorylation [133,134]. Without new ATP the myosin heads cannot trigger, but they do retain their actin binding properties. However, published work indicates that effective levels to inhibit myosin activity require concentrations above 10 μM. We were unable to plate functioning cells with intact stress fibers at any ML7 concentrations above 2.5μM. This is partially expected, as previous work with bovine PA endothelial cells showed that myosin II was responsible for maintaining the stress fiber integrity[128]. Thus, we were unable to directly test the role of myosin activity in stress fiber contraction, as we could not be sure that we were actually inhibiting myosin activity.

4.5 Discussion

We have shown that PSCs exhibit a global, cell-wide mechanical response to a local, external force. A sustained force of 2-4 nN resulted in stress fiber contraction throughout the cell which was mediated by myosin contractility. Remarkably, mechanical or biochemical signaling downstream of integrin receptors was not required to initiate this response. We also found that this response was engaged within 90 seconds of force application. A previous study which measured stress fiber dynamics in response to an applied force [124] also reported a zero net strain (as mentioned before, this is expected), but large strain fluctuations when the cell was subjected to a 20 nN applied force. The NIH3T3 mouse fibroblasts in that study responded after 30 seconds, as opposed to the 90 second lag that we observe. Furthermore, the PSC response only partially depends on an intact MT network, whereas the NIH3T3 cell's response completely depends on the MT network. These differences may arise from the different extracellular environments inhabited by these cells.

While we have implicated myosin contractility in mediating this response, the relevant signaling pathway linking the applied deformation to myosin contractility is not known. Mitogen activated protein kinase (MAPK) is part of a phosphorylation cascade that triggers proliferation of mammalian cells [135]. Inflammation and necrosis of the pancreas has been shown to increase proliferation and migration of PSCs. The observed stress fiber response may be the beginning stages of PSC activation (which includes ECM production, migration and proliferation). Inhibiting MAPK would indicate whether or not the MAPK pathway is involved with this response. This can be accomplished by adding either PD-98059 or U-126MEK inhibitors[136]. MEK directly phosphorylates MAPK, so its inhibition is essentially the same as inhibiting MAPK directly. Interestingly, the MAPK pathway also depends on the structural integrity of the actin cortex [137].

Although we were unable to conclusively test the direct role of myosin activity in the cellular response to external forces, it is highly likely that myosin contractility is essential for this response. While our experiments with the myosin light chain kinase inhibitor ML7 were not conclusive, as stress fibers in PSC were disrupted even with lower concentrations of ML7, there are examples of successful experiments using other cell types. E.g. in bovine capillary endothelial cells ML7 application successfully inhibited myosin motors without eliminating stress fibers [138]. Laser dissection of stress fibers and real time tracking showed that retraction after the fiber is severed is too slow to be completely elastic. We observed stress fiber contraction similar to the descriptions from this study. Furthermore, they found that active myosin light chain kinase (MLCK) was required for contraction, but that interrupting the ROCK pathway with Y27632 had little effect. So there is indirect evidence that myosin contracts stress fibers in PSCs as well. Our experiments confirm the well-known fact that myosin activity is required for stress fiber formation and stability. Furthermore, Peterson et al. found higher concentrations of MLC (myosin light chain) at the periphery of the cell, near the focal adhesions compared to the central regions of the cell. The high concentrations of MLC are in the same regions with high contraction [121]. The central regions where the stress fibers typically elongate have lower concentrations of MLC. Our observations are consistent with these previous findings. While we were unable to directly show that eliminating myosin activity would eliminate the observed force response, other evidence suggests that myosin likely drives the stress fiber contraction.

Our experiments have investigated the nature of the cellular response to externally applied forces and enabled us to examine the process of force transmission through the cytoskeletal network in a cell. To further elucidate how external forces are transmitted and how this is coupled to the physical organization of the cytoskeleton, future experiments could include measuring the force response of cells spread on soft elastic surfaces. As mentioned earlier in this thesis, the stiffness of the substrate can alter cell behavior. We may therefore expect that the response of

cells will be modulated by the stiffness of the underlying substrate. Furthermore, elastic gels facilitate the use of traction force microscopy (TFM) to directly measure forces exerted by cells. Using TFM in conjunction with the magnetic trap would be a novel way to examine how an externally applied local force modulates the forces exerted by cells and whether the external force is transmitted across the cell to the substrate. An outstanding question in the field is how forces are transmitted through the dense cytoskeletal network of a cell. High speed imaging of the stress fiber dynamics may also help to reveal the timescales involved in this process.

5 Machine Vision for Data Analysis

5.1 Overview

As computation power increases, so does our ability to analyze data in a time- and cost-effective manner. Understanding computational methods allows for more efficient use of the computation power available to us. This section gives a brief overview of the image analysis used in my experiments, from the way images are stored in memory up to the algorithms used to process the image data. While the conclusions drawn in this thesis do not require a knowledge of image processing techniques, these techniques are nonetheless necessary for data analysis.

5.2 Digital Images

The translation from reality to image data naturally causes the captured image to be less than perfect for several reasons. First are the flaws in the optical pathway between the sample and the imaging chip, but these are minimized by modern technology. Second is the chip itself. The image is essentially a histogram. Each pixel counts the photons that enter, but cannot distinguish a photon that hits dead-on in the pixel center from a photon which hits at an angle near the edge. Thus, the pixel size can limit the resolution of the image. Furthermore, due to the diffraction limit, a photon may by chance interact with a neighboring pixel instead of its true pixel. Therefore, simply shrinking the pixel size cannot improve resolution past the diffraction limit. The sensor is not perfect either. Just as photons may stray from their intended path, so too may electrons in the sensor's circuits. These electrons affect the photon counts in each pixel and are known as noise. The data we collect in the form of images are thus approximate representations of reality. It is from these representations that we infer truths about our specimens.

Images in the digital age are comprised of a grid of pixels (or a 3D grid of voxels). Each pixel stores a brightness value for its location in the image. Pixels may have values described by

8, 10, 12 or 14 bits. Eight-bit values may be stored in a single byte, but the rest require two bytes per value. The image is an array of pixels describing brightness values. These arrays can be any dimension in use but are stored in 1D arrays in computer memory. Knowledge of the size of the array allows the pixels to be ordered correctly for display. For example, a 3D image with multiple color channels and multiple time points would be a 5D array in practice, but still stored as a 1D array in memory. This can become important when optimizing code. Accessing a group of neighboring pixels requires calculating their indices based on the original pixel's indices. This is much easier (and faster!) to do in one dimension than in several.

5.3 From Images to Data

The purpose of taking images is to measure them. We can measure brightness, distance, size and shape. We can measure all of these things at different times to measure change and rates of change. The advantage of using a machine over the human eye quickly becomes apparent when hundreds or thousands of measurements are required. Taking out a ruler and measuring the distance between two points is easy and accomplished in seconds. However, suppose the goal was to measure distances between hundreds of points, over hundreds of images for every experiment run. Making all of these measurements would be a tedious task, and errors in bookkeeping are practically guaranteed.

Machine vision is the answer to this problem—specifically, getting a machine to recognize features within the image and keep track of them. Computers, despite their speed, cannot intuitively process visual information the way that humans can. All a computer can do is compare numbers and perform calculations. We must therefore simplify 'seeing' into a list of rules or instructions. Calculations and comparisons (something that computers can do very quickly), can be used to identify, locate and track features in the image. This can be a very complicated task, especially when noise is present, or the shapes are complicated. However, it is not impossible. The first step is usually to apply a bandpass filter to the image. The filter is created by subtracting

a broad guassian distribution from a narrow one. The result is a so called 'Mexican hat' function (Figure 5-1). Convolving this function with the image accentuates objects that are the correct size for tracking

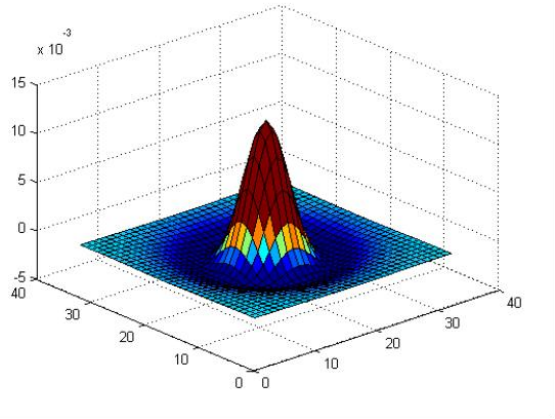

Figure 5-1 An example of a bandpass filter.

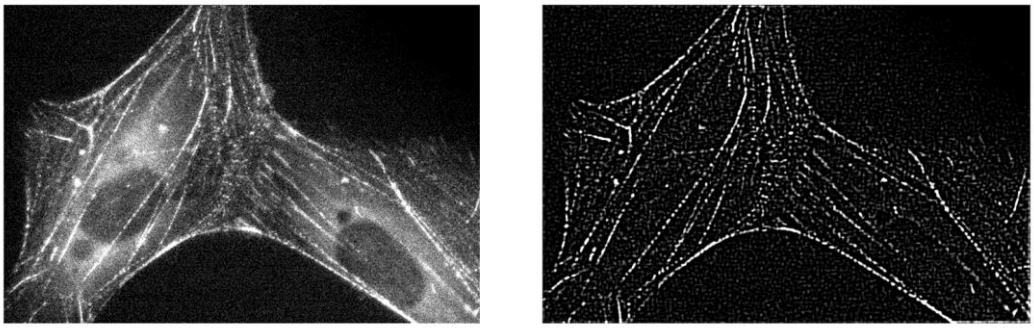

Figure 5-2 Left: original image from the microscope. Right: the same image after a bandpass filter has been applied.

Broad features such as excess brightness around the nucleus or uneven illumination across the frame are muted. Similarly, small features such as image noise are smoothed over. This typically makes the objects that we are trying to track the brightest in the resulting image (see Figure 5-2). Next, a threshold is applied, and distinct objects can be further discriminated by size and shape. By adjusting the parameters for each step listed above, it is possible to find different types of objects in a cell or actin network. For example, small, point-like objects may be clusters of a

specific protein, and long, slender objects may be stress fibers. With these simple steps, objects are identified and located within the image. Now it is possible to begin further quantification and analysis.

5.4 Feature Finding

Many proteins within the cell naturally cluster. When fluorescently labelled, these proteins appear as bright spots in the images, usually covering several pixels at once. After using the filtering methods above, these spots become easy to identify. Beyond identification, it is also possible to extract a location to greater precision than the pixel size. This can be accomplished in a number of ways. If the intensity profile is a known function (most commonly a Gaussian distribution), the pixel values may be fit to the function. A faster method is finding the local maxima of the bright spot, then selecting a window around it. All pixels within the window are used in a center of mass calculation.

Great care must be taken to avoid pixel locking, or location bias. Essentially, some algorithms will favor certain locations within the pixel to be marked as centers. This will introduce systematic error into the measurements. To check for pixel locking, one must count the fractional parts of the pixel locations. Typically, pixel locking will favor the edge or the center of the pixels. An even distribution of the fractional parts indicates a lack of bias.

In this thesis a bright spot's center is determined to sub-pixel accuracy by a center of mass calculation. To minimize pixel locking, a background subtraction method is employed [139]. Beads in the magnetic trap are tracked by UNC's CISMM's Video Spot Tracker software, using a symmetric tracking kernel. The diffraction pattern of the beads under bright field microscopy changes with their height. As such, they may have bright, dark, or neutral centers. However, their pattern is always radially symmetric. The kernel uses concentric rings and tries to minimize the variance in brightness around the rings by adjusting their center.

5.5 MATLAB and MEX functions

Advances in science are often made possible by advances made in technology, specifically computation power. MATLAB is a fantastic tool for scientists because it has many built-in functions and handles many necessary tasks behind the scenes to keep the user from accidently crashing the computer. However, these conveniences come with the cost of computational efficiency. I will take a moment to explain MATLAB's shortcomings, and the MEX function, which is a useful workaround.

Computer programs are just a set of instructions. These instructions have to be written such that the computer hardware can understand them. As stated before, computers only use ones and zeros. These instructions are nearly impossible for a human to read. Briefly, a bit is a one or a zero, a byte is a set of 8 bits, and a word is a set of bytes that may vary in size, depending on the data type. Instructions for machine hardware are just a series of words. Words can represent a numerical value, addresses in memory, or a function. Adding two numbers would consist of one word for the add command, then a word for each of the two numbers to add, and a final word for where to put the answer.

For example, we could type the following:

A = B + C

Somehow it must be translated to something like this:

00110011 - 11001010 - 00011101 - 11011010

This process is called compiling. Compiled code is a set of instructions ready for the machine to run, and a computer will follow these instructions blindly.

MATLAB uses what is known as an interpreted language. Programs written in MATLAB are not compiled, but rather read line by line by another program. This program interprets the

code and decides which machine calls to make. This program will also do many checks to make sure that what it has been asked to do is allowed, will not result in errors, can be done within available memory, is using the correct variable types, etc. This can actually be quite a long list, but it prevents the computer from crashing and often provides useful information about errors it encounters. Each of these checks will involve one or more machine instructions. Now, the simple **add** command may become vastly larger than the four words as shown above. Processing very large data sets with an interpreter will therefore require vastly larger amounts of time. One trick is to avoid for-loops and use matrix multiplication or built-in MATLAB functions instead, as this can sometimes avoid repeating certain steps while the code is interpreted. However, this is not always possible. If MATLAB does not have your algorithm, you must write your own. Every step in your algorithm will require interpretation, which can lead to prohibitive computation time. Another good practice is to pre-allocate variables. If elements are added to a variable that extend that variable beyond its current size in memory, a new larger variable must be created and the data must be copied to the new variable. This can quickly become very computationally expensive.

One solution to decreasing compute time in MATLAB is a faster computer. Another is the MATLAB executable, or MEX function. By compiling a set of instructions before the MATLAB code is run, many of the inefficiencies of using an interpreted language disappear. The code may be written in Fortran, C, or C++ and compiled into a MEX function. MATLAB then uses the MEX function as a normal command, except that instead of performing all of its normal checks during every step of the algorithm, it performs a few and then passes information about where and how the data is stored to the MEX function. The MEX function runs, and then returns to MATLAB. Thus, large steps can be run entirely in machine code without the interpreter intervening, and considerable time can be saved.

A considerable amount of my time has been spent optimizing code and developing image processing algorithms. Many of the algorithms here were optimized using the techniques listed above. In some cases, the lack of optimization would have required a prohibitive amount of time to process the data. In my opinion, understanding computation is just as important to science as knowing mathematics or how to operate a microscope. My hope is that scientists will learn to program *well* so that they may access more computation power already available to them, and that this will allow their work to progress at a higher rate.

6 Discussion

6.1 Chapter Summaries

6.1.1 Summary Chapter 2

We have shown that palladin binds actin filaments and organizes them into bundled networks that have viscoelastic properties. This behavior is common to many actin binding proteins, such as α-actinin, filamin, fascin, spectrin and others. The network morphology depends on the ratio of palladin to actin. Other work has shown that palladin also binds to α-actinin, another actin cross-linker. An interesting result is that small amounts of palladin can enhance the stiffness of an actin – α-actinin network more efficiently than additional α-actinin. The hinged junction that α-actinin forms with actin may be stabilized by palladin, thereby enhancing the coupling of parallel filaments, which in turn leads to stiffer bundles.

6.1.2 Summary Chapter 3

We have measured the viscoelastic properties of live pancreatic stellate cells with and without palladin. We find that, in contrast to the previous chapter, palladin has no appreciable effect on cell stiffness. The actin network is a large part of the cytoskeleton. As the previous chapter demonstrates, palladin concentration determines network properties *in vitro*. However, we have shown here that this is not the case *in vivo*. We have also shown that the measured cell stiffness does not depend on the direction of the force application nor the location of the bead relative to cellular features. It seems that pancreatic stellate cells are able to maintain a very consistent tension throughout. More in depth experiments could be carried out with multi-directional magnetic traps. It is difficult to find cells with multiple beads suitably spaced for measuring stiffness at different locations and for different directions. Nonetheless, the number of experiments performed here clearly demonstrate the lack of directionality, location dependence and palladin dependence.

6.1.3 Summary Chapter 4

We have found that pancreatic stellate cells actively respond to an applied force. This is directly observed by changes in strain rates along actin stress fibers. GFP labelled palladin has enabled stress fiber tracking without the need for a photo-bleaching laser. Our results have elucidated many aspects of the response, including which parts of the cell are involved and the necessary parameters of the applied force. We also know that PSCs are less dependent on an intact MT network than NIH3T3 fibroblasts. While the responses show similarities, the differences indicate that different cell types may sense external forces in different ways. This further illustrates the importance of studying biomechanics, in addition to biochemistry. Continued progress requires the joining of many disciplines in order to achieve a truly comprehensive understanding of the cell.

6.1.4 Summary Chapter 5

Understanding computational methods has enabled most of the data analysis performed in this thesis. Just as advances in technology enable new means of data analysis, so too can advances in algorithm efficiency. MATLAB is an extremely versatile tool, but because it is an interpreted language it suffers in speed. Being able to code in other languages can be the difference between having the computing power to run the analysis or not.

6.2 Conclusions and Future Work

Our studies have shown that the actin crosslinker palladin modifies viscoelastic properties of in vitro actin networks. We have demonstrated that the morphology and mechanical properties of the network depend on crosslinker concentration. Palladin also binds α-actinin, another actin crosslinker. We have also demonstrated that these two cross-linkers cooperatively enhance

network stiffness. These are the first *in-vitro* studies of actin networks cross-linked with palladin, as well as networks cross-linked with mutually interacting cross-linkers. Further work is required to elucidate whether the effect on the mechanical properties of composite networks arise due to mutual interaction between palladin and α-actinin or due to differences in their actin binding domains.

Our work has also shown that palladin does not modify viscoelastic properties of live PSCs. This result is counterintuitive given the results with *in vitro* actin networks. Although palladin can regulate properties of reconstituted actin networks, it does not regulate the apparent stiffness of the live cells on glass. However, cells have been shown to adapt their stiffness to match their surroundings, which means that palladin may have an effect on cells spread on softer substrates. The experiments described here could be repeated on soft poly-acrylamide gels to investigate this possibility. Another possibility may be that the expression levels of α-actinin or other crosslinkers in the cell increase to compensate for the loss of palladin. Further experiments are required to fully investigate palladin's ability to modulate cells' mechanical properties.

Unpublished work from our lab (Azatov, et al.) has shown that cells lacking palladin recover their cytoskeleton more quickly, and exert higher forces on the substrate than cells with normal expression levels. Therefore, palladin may negatively regulate myosin generated forces, and by extension, regulate cytoskeletal dynamics rather than apparent stiffness. Other work has demonstrated that stress fiber dynamics depend on the ability of filaments in the stress fiber to buckle [118,119]. Palladin rich regions are located between myosin rich regions along the stress fiber. The palladin rich regions are the locations where the filaments might buckle. Palladin may stabilize the stress fiber and limit the rate of buckling, and by extension, force generation and contraction. The experiments that have demonstrated the buckling process could be repeated with the addition of palladin to investigate palladin's role in regulating stress fiber dynamics.

Work in this thesis has also demonstrated that palladin rich structures on stress fibers undergo a dynamic response upon application of an external force. This response is likely important for regulating the mechanism of force transmission through the cellular cytoskeleton. Myosin based contraction of stress fibers plays an important role in force transmission in the cell. Independently, other work in our lab (Azatov et al) has shown that stress fiber formation is affected by palladin knockdown. While palladin may not be involved in setting the overall cell stiffness, its role in establishing parameters of force transmission in cells is yet to be determined and a topic worthy of future study. The results of this thesis suggest the possibility that a critical role for palladin may be to modulate myosin contractility within stress fibers for efficient force transmission in cells and raise the question of palladin's potential role in cellular mechanosensing.

Appendix A Matlab Code: Examples and descriptions

A.1 fastSpotDet.m: An example of linear indexing

This code uses a center of mass algorithm to find spots in an image. This is much faster than attempting to fit a Gaussian profile. The narrow spot sizes (a few pixels) and image noise do not allow for any gains in accuracy of one method over the other. Masks and relative indexes are pre-calculated as 'linear indices'. A value would be referenced from a 100x100 image as a(505) rather than a(5,5). This saves time having to compute indices for neighboring pixels.

```
function drs = fastSpotDet(img, thresh)
%this function was written to be compatible with SpotDetector by
Francois Aguet, March 2010
%However, this code has been optimized for the specific images used in
the
%stress fiber project, and is all original code by Brian Grooman.

%create bandpass filter
lp2 = fspecial('gaussian',[7 7],2);
lp = fspecial('gaussian',[7 7],4.5);
bp = lp2-lp;

s = size(img);
%make an index neighborhood to sum intensities.
nh = ones(5,5); nh([1,5,21,25]) = 0;
[x y] = find(nh);
nh = sub2ind([s(1),s(2)],y,x);
offset = nh(11);
nh = nh - nh(11);

%make distance neighborhoods to sum vertical and horiz distances
nhorz = ones(5,5); nhorz([1,5,11,12,13,14,15,21,25]) = 0;
nvert = nhorz';

[x y] = find(nhorz);
nhorz = sub2ind([s(1),s(2)],y,x);
nhorz = nhorz - offset;

[x y] = find(nvert);
nvert = sub2ind([s(1),s(2)],y,x);
nvert = nvert - offset;

%weights for subpixel calculation
dhorz = [-2 -2 -2 -1 -1 -1 -1 -1 1 1 1 1 1 2 2 2];
dvert = [-1 1 -2 -1 1 2 -2 -1 1 2 -2 -1 1 2 -1 1];
```

```
%adding .1 prevents values less than zero
im2 = imfilter(img,bp) + .1;

%fast way to find peaks
c = im2 == imdilate(im2, ones(7,7));
%keep only peaks above thresh
a = c & (im2 > thresh);

%zero pad edges
a([1:5 end-4:end],:) = 0;
a(:,[1:5 end-4:end]) = 0;

%code here to reject peaks too close together.
%create rough circle mask
q = ones(9,9);
q([1,2,3,7,8,9,10,18,19,27,41,55,63,64,72,73,74,75,79,80,81]) = 0;
[x y] = find(q);

%nh2 is a neighborhood defined by linear index of points in the array
nh2 = sub2ind([s(1),s(2)],y,x);
offset = sub2ind([s(1),s(2)],5,5);
nh2 = nh2 - offset;

%sort peaks in order of brightness
[crap idx] = sort(im2(a),1,'descend');
g = find(a);
g = g(idx);

%starting with brightest peak, delete all others which are too close
%deleted peaks get skipped
for i = 1:length(g)
    if a(g(i))
        a(nh2 + g(i)) = 0;
    end
end

%final list of peaks as 1d array and subindex
idx = find(a);
[y1, x1] = find(a);

%  find center of mass
drs.nComp = length(idx);
y = zeros(1,length(idx));
x = zeros(1,length(idx));

%center of mass calcs,  ibase = base intensity, subtracted to prevent
pixel%locking.
for j = 1:length(idx)
    ibase = min(img(idx(j) + nh));
    itotal = sum(img(idx(j) + nh) - ibase);
    x(j) = (dvert * (img(idx(j) + nvert)-ibase) ) / itotal;
    y(j) = (dhorz * (img(idx(j) + nhorz)-ibase) ) / itotal;
end

%output struct compatible with SpotDetector mentioned above.
```

```
drs.xcom = x1+x';
drs.ycom = y1+y';
```

A.2 Fast Distance mapping

BWDISTSC - Yuriy Mishchenko JFRC HHMI Chklovskii Lab JUL 2007

This code was borrowed from the MATLAB file exchange. It uses a very fast marching algorithm to compute a distance map, and makes it trivial to calculate distances for data with non-isometric aspect ratios. Briefly, instead of computing the distance for each voxel by searching for its nearest zero neighbor, this algorithm marches through the image and continuously updates the distance map during the march. This is done along each dimension, in both directions. Therefore, each voxel is visited only twice per dimension, and compared only to its current value. In this way, the algorithm scales as O(n), where n is the number of voxels. Matlab's function scales as $O(n^2)$, and is substantially slower. A more in depth explanation of the algorithm is in [140].

A.3 Tracking particles

Track.m – John C. Crocker and Daniel Blair 1999/2005

This code is used to track particles from frame to frame. The code is very robust and fast. The following explanation is taken from the comments in the code:

```
PROCEDURE:
% ; Given the positions for n particles at time t(i), and m possible
% ; new positions at time t(i+1), this function considers all possible
% ; identifications of the n old positions with the m new positions,
% ; and chooses that identification which results in the minimal total
% ; squared displacement. Those identifications which don't associate
% ; a new position within maxdisp of an old position ( particle loss )
% ; penalize the total squared displacement by maxdisp^2. For non-
% ; interacting Brownian particles with the same diffusivity, this
% ; algorithm will produce the most probable set of identifications
% ; ( provided maxdisp >> RMS displacement between frames ).
% ; In practice it works reasonably well for systems with oscillatory,
% ; ballistic, correlated and random hopping motion, so long as single
% ; time step displacements are reasonably small.
```

Appendix B Additional Protocols

B.1 Immunostaining protocol

1. At time point, add 250µl 4% paraformaldahyde (PFA), 2% sucrose to fix cells, 20 min

2. Remove the 250µl and wash well 3 times with 450µl PBS

3. Remove the 450µl and add 400µl PBS with .5% Triton X-100 5 min

4. Remove the 400µl and add 200µl 1% BSA in PBS, 60 min

5. Remove the 200µl and add 200µl anti-tubulin antibody (1:500) in PBS, 20 min ON ICE

6. Remove the 200µl and wash well 3 times with 400µl PBS for 15 min each

7. Remove 400µl; add 200µl AF-546 goat anti-mouse IgG2b (1:250) in PBS, 20 min ON ICE

8. Remove the 200µl and wash well 3 times with 400µl PBS for 15 min each

9. Remove the 400µl and add 250µl 4% paraformaldahyde (PFA), 20 min

10. Remove the 250µl and wash well 3 times with 450µl PBS

11. Remove the 450µl of PBS and add 300µl PBS for storage at 4˚C.

References

[1] M. Bindschadler, E.A. Osborn, C.F. Dewey Jr, J.L. McGrath, A mechanistic model of the actin cycle, Biophys. J. 86 (2004) 2720–2739.

[2] I. Fujiwara, S. Takahashi, H. Tadakuma, T. Funatsu, S. Ishiwata, Microscopic analysis of polymerization dynamics with individual actin filaments, Nat. Cell Biol. 4 (2002) 666–673.

[3] P.A. Kuhlman, Dynamic changes in the length distribution of actin filaments during polymerization can be modulated by barbed end capping proteins, Cell Motil. Cytoskeleton. 61 (2005) 1–8.

[4] A. Mogilner, G. Oster, Force generation by actin polymerization II: the elastic ratchet and tethered filaments, Biophys. J. 84 (2003) 1591–1605.

[5] A. Upadhyaya, J.R. Chabot, A. Andreeva, A. Samadani, A. van Oudenaarden, Probing polymerization forces by using actin-propelled lipid vesicles, Proc. Natl. Acad. Sci. 100 (2003) 4521–4526.

[6] A. Mogilner, G. Oster, Cell motility driven by actin polymerization, Biophys. J. 71 (1996) 3030–3045.

[7] M.J. Footer, J.W. Kerssemakers, J.A. Theriot, M. Dogterom, Direct measurement of force generation by actin filament polymerization using an optical trap, Proc. Natl. Acad. Sci. 104 (2007) 2181–2186.

[8] J. Howard, Mechanics of motor proteins and the cytoskeleton, Sinauer Associates, Publishers, Sunderland, Mass., 2001.

[9] B. Alberts, Molecular biology of the cell, Garland Science, New York, 2008.

[10] A. Ott, M. Magnasco, A. Simon, A. Libchaber, Measurement of the persistence length of polymerized actin using fluorescence microscopy, Phys Rev E. 48 (1993) R1642–R1645.

[11] C.G. Dos Remedios, D. Chhabra, M. Kekic, I.V. Dedova, M. Tsubakihara, D.A. Berry, et al., Actin binding proteins: regulation of cytoskeletal microfilaments, Physiol. Rev. 83 (2003) 433–473.

[12] S. Suetsugu, H. Miki, T. Takenawa, Spatial and temporal regulation of actin polymerization for cytoskeleton formation through Arp2/3 complex and WASP/WAVE proteins, Cell Motil. Cytoskeleton. 51 (2002) 113–122.

[13] M.L. Gardel, Elasticity of F-actin Networks, Harvard University Cambridge, Massachusetts, 2004.

[14] Y. Tseng, E. Fedorov, J.M. McCaffery, S.C. Almo, D. Wirtz, Micromechanics and ultrastructure of actin filament networks crosslinked by human fascin: A comparison with α-actinin, J. Mol. Biol. 310 (2001) 351–366.

[15] D. Breitsprecher, S.A. Koestler, I. Chizhov, M. Nemethova, J. Mueller, B.L. Goode, et al., Cofilin cooperates with fascin to disassemble filopodial actin filaments, J. Cell Sci. 124 (2011) 3305–3318.

[16] D.H. Wachsstock, W.H. Schwartz, T.D. Pollard, Affinity of alpha-actinin for actin determines the structure and mechanical properties of actin filament gels, Biophys. J. 65 (1993) 205–214.

[17] M.L. Gardel, F. Nakamura, J.H. Hartwig, J.C. Crocker, T.P. Stossel, D.A. Weitz, Prestressed F-actin networks cross-linked by hinged filamins replicate mechanical properties of cells, Proc. Natl. Acad. Sci. U. S. A. 103 (2006) 1762–1767.

[18] B. Grooman, I. Fujiwara, C. Otey, A. Upadhyaya, Morphology and Viscoelasticity of Actin Networks Formed with the Mutually Interacting Crosslinkers: Palladin and Alpha-actinin, PLoS ONE. 7 (2012) e42773.

[19] M. Bathe, C. Heussinger, M.M.A.E. Claessens, A.R. Bausch, E. Frey, Cytoskeletal Bundle Mechanics, Biophys. J. 94 (2008) 2955–2964.

[20] M.M.A.E. Claessens, M. Bathe, E. Frey, A.R. Bausch, Actin-binding proteins sensitively mediate F-actin bundle stiffness, Nat. Mater. 5 (2006) 748–753.

[21] J.H. Shin, L. Mahadevan, P.T. So, P. Matsudaira, Bending Stiffness of a Crystalline Actin Bundle, J. Mol. Biol. 337 (2004) 255–261.

[22] J. Howard, J.F. Ashmore, Stiffness of sensory hair bundles in the sacculus of the frog, Hear. Res. 23 (1986) 93–104.

[23] B. Wagner, R. Tharmann, I. Haase, M. Fischer, A.R. Bausch, Cytoskeletal polymer networks: the molecular structure of cross-linkers determines macroscopic properties, Proc. Natl. Acad. Sci. 103 (2006) 13974–13978.

[24] O. Esue, Y. Tseng, D. Wirtz, α-Actinin and Filamin Cooperatively Enhance the Stiffness of Actin Filament Networks, PLoS ONE. 4 (2009) e4411.

[25] R.D.S. Dixon, D.K. Arneman, A.S. Rachlin, N.R. Sundaresan, M.J. Costello, S.L. Campbell, et al., Palladin Is an Actin Cross-linking Protein That Uses Immunoglobulin-like Domains to Bind Filamentous Actin, J. Biol. Chem. 283 (2008) 6222–6231.

[26] M. Rönty, A. Taivainen, M. Moza, C.A. Otey, O. Carpén, Molecular analysis of the interaction between palladin and α-actinin, FEBS Lett. 566 (2004) 30–34.

[27] G.-Y. Huh, S.B. Glantz, S. Je, J.S. Morrow, J.H. Kim, Calpain proteolysis of αII-spectrin in the normal adult human brain, Neurosci. Lett. 316 (2001) 41–44.

[28] S.P. George, Y. Wang, S. Mathew, K. Srinivasan, S. Khurana, Dimerization and Actin-bundling Properties of Villin and Its Role in the Assembly of Epithelial Cell Brush Borders, J. Biol. Chem. 282 (2007) 26528–26541.

[29] E. Friederich, Villin Function in the Organization of the Actin Cytoskeleton. CORRELATION OF IN VIVO EFFECTS TO ITS BIOCHEMICAL ACTIVITIES IN VITRO, J. Biol. Chem. 274 (1999) 26751–26760.

[30] H. Haga, S. Sasaki, K. Kawabata, E. Ito, T. Ushiki, T. Sambongi, Elasticity mapping of living fibroblasts by AFM and immunofluorescence observation of the cytoskeleton, Ultramicroscopy. 82 (2000) 253–258.

[31] S. Machida, T. Watanabe-Nakayama, M. Saito, R. Afrin, A. Ikai, Fabricated cantilever for AFM measurements and manipulations: Pre-stress analysis of stress fibers, Micron. 43 (2012) 1380–1389.

[32] T. Mason, K. Ganesan, J. van Zanten, D. Wirtz, S. Kuo, Particle Tracking Microrheology of Complex Fluids, Phys. Rev. Lett. 79 (1997) 3282–3285.

[33] D. Wirtz, Particle-Tracking Microrheology of Living Cells: Principles and Applications, Annu. Rev. Biophys. 38 (2009) 301–326.

[34] J.C. Crocker, M.T. Valentine, E.R. Weeks, T. Gisler, P.D. Kaplan, A.G. Yodh, et al., Two-point microrheology of inhomogeneous soft materials, Phys. Rev. Lett. 85 (2000) 888.

[35] A.R. Bausch, F. Ziemann, A.A. Boulbitch, K. Jacobson, E. Sackmann, Local measurements of viscoelastic parameters of adherent cell surfaces by magnetic bead microrheometry, Biophys. J. 75 (1998) 2038–2049.

[36] M. Puig de Morales Fusté, M. Grabulosa Descals, J. Alcaraz Casademunt, J. Mullol i Miret, G.N. Maksym, J.J. Fredberg, et al., Measurement of cell microrheology by magnetic twisting cytometry with frequency domain demodulation., J. Appl. Physiol. 2001 Vol 91 Num 3 P 1152-1159. (2001).

[37] A.R. Bausch, W. Möller, E. Sackmann, Measurement of local viscoelasticity and forces in living cells by magnetic tweezers, Biophys. J. 76 (1999) 573–579.

[38] R.M. Simmons, J.T. Finer, S. Chu, J.A. Spudich, Quantitative measurements of force and displacement using an optical trap, Biophys. J. 70 (1996) 1813–1822.

[39] R.M. Hochmuth, Micropipette aspiration of living cells, J. Biomech. 33 (2000) 15–22.

[40] P. Kollmannsberger, B. Fabry, Linear and Nonlinear Rheology of Living Cells, Annu. Rev. Mater. Res. 41 (2011) 75–97.

[41] K. Kasza, G. Koenderink, Y. Lin, C. Broedersz, W. Messner, F. Nakamura, et al., Nonlinear elasticity of stiff biopolymers connected by flexible linkers, Phys. Rev. E. 79 (2009).

[42] N. Rosenblatt, A. Alencar, A. Majumdar, B. Suki, D. Stamenović, Dynamics of Prestressed Semiflexible Polymer Chains as a Model of Cell Rheology, Phys. Rev. Lett. 97 (2006).

[43] P. Fernández, P.A. Pullarkat, A. Ott, A master relation defines the nonlinear viscoelasticity of single fibroblasts, Biophys. J. 90 (2006) 3796–3805.

[44] B.D. Hoffman, J.C. Crocker, Cell Mechanics: Dissecting the Physical Responses of Cells to Force, Annu. Rev. Biomed. Eng. 11 (2009) 259–288.

[45] K.E. Kasza, A.C. Rowat, J. Liu, T.E. Angelini, C.P. Brangwynne, G.H. Koenderink, et al., The cell as a material, Curr. Opin. Cell Biol. 19 (2007) 101–107.

[46] L. Wolff, P. Fernandez, K. Kroy, Inelastic mechanics of sticky biopolymer networks, New J. Phys. 12 (2010) 053024.

[47] C. Semmrich, T. Storz, J. Glaser, R. Merkel, A.R. Bausch, K. Kroy, Glass transition and rheological redundancy in F-actin solutions, Proc. Natl. Acad. Sci. 104 (2007) 20199–20203.

[48] P. Canadas, V.M. Laurent, P. Chabrand, D. Isabey, S. Wendling-Mansuy, Mechanisms governing the visco-elastic responses of living cells assessed by foam and tensegrity models, Med. Biol. Eng. Comput. 41 (2003) 733–739.

[49] D.J. Hadjidakis, I.I. Androulakis, Bone remodeling, Ann. N. Y. Acad. Sci. 1092 (2006) 385–396.

[50] A.R. Pries, Remodeling of Blood Vessels: Responses of Diameter and Wall Thickness to Hemodynamic and Metabolic Stimuli, Hypertension. 46 (2005) 725–731.

[51] A.J. Ehrlicher, F. Nakamura, J.H. Hartwig, D.A. Weitz, T.P. Stossel, Mechanical strain in actin networks regulates FilGAP and integrin binding to filamin A, Nature. 478 (2011) 260–263.

[52] D.M. Helfman, E.T. Levy, C. Berthier, M. Shtutman, D. Riveline, I. Grosheva, et al., Caldesmon inhibits nonmuscle cell contractility and interferes with the formation of focal adhesions, Mol. Biol. Cell. 10 (1999) 3097–3112.

[53] J. Sadoshima, T. Takahashi, L. Jahn, S. Izumo, Roles of mechano-sensitive ion channels, cytoskeleton, and contractile activity in stretch-induced immediate-early gene expression and hypertrophy of cardiac myocytes., Proc. Natl. Acad. Sci. 89 (1992) 9905–9909.

[54] B.D. Matthews, Cellular adaptation to mechanical stress: role of integrins, Rho, cytoskeletal tension and mechanosensitive ion channels, J. Cell Sci. 119 (2006) 508–518.

[55] J.Y. Rho, R.B. Ashman, C.H. Turner, Young's modulus of trabecular and cortical bone material: ultrasonic and microtensile measurements, J. Biomech. 26 (1993) 111–119.

[56] Xing Liang, S.A. Boppart, Biomechanical Properties of In Vivo Human Skin From Dynamic Optical Coherence Elastography, IEEE Trans. Biomed. Eng. 57 (2010) 953–959.

[57] F. Boschetti, G. Pennati, F. Gervaso, G.M. Peretti, G. Dubini, Biomechanical properties of human articular cartilage under compressive loads, Biorheology. 41 (2004) 159–166.

[58] H. Rubin, Cell aging in vivo and in vitro, Mech. Ageing Dev. 98 (1997) 1–35.

[59] A.Y. Liu, L. LaTray, G. van Den Engh, Changes in cell surface molecules associated with in vitro culture of prostatic stromal cells, The Prostate. 44 (2000) 303–312.

[60] H.J. Kong, T.R. Polte, E. Alsberg, D.J. Mooney, FRET measurements of cell-traction forces and nano-scale clustering of adhesion ligands varied by substrate stiffness, Proc. Natl. Acad. Sci. U. S. A. 102 (2005) 4300–4305.

[61] A.J. Engler, S. Sen, H.L. Sweeney, D.E. Discher, Matrix elasticity directs stem cell lineage specification, Cell. 126 (2006) 677–689.

[62] K. Saha, A.J. Keung, E.F. Irwin, Y. Li, L. Little, D.V. Schaffer, et al., Substrate modulus directs neural stem cell behavior, Biophys. J. 95 (2008) 4426–4438.

[63] P. Friedl, E.-B. Bröcker, The biology of cell locomotion within three-dimensional extracellular matrix, Cell. Mol. Life Sci. CMLS. 57 (2000) 41–64.

[64] D.E. Discher, P. Janmey, Y. Wang, Tissue cells feel and respond to the stiffness of their substrate, Science. 310 (2005) 1139–1143.

[65] B.N. Mason, J.P. Califano, C.A. Reinhart-King, Matrix Stiffness: A Regulator of Cellular Behavior and Tissue Formation, in: S.K. Bhatia (Ed.), Eng. Biomater. Regen. Med., Springer New York, New York, NY, 2012: pp. 19–37.

[66] T. Elsdale, J. Bard, Collagen substrata for studies on cell behavior, J. Cell Biol. 54 (1972) 626–637.

[67] E. Cukierman, Taking Cell-Matrix Adhesions to the Third Dimension, Science. 294 (2001) 1708–1712.

[68] M.M. Parast, C.A. Otey, Characterization of palladin, a novel protein localized to stress fibers and cell adhesions, J. Cell Biol. 150 (2000) 643–656.

[69] O.-M. Mykkänen, M. Grönholm, M. Rönty, M. Lalowski, P. Salmikangas, H. Suila, et al., Characterization of human palladin, a microfilament-associated protein, Mol. Biol. Cell. 12 (2001) 3060–3073.

[70] S. Goicoechea, D. Arneman, C. Otey, The role of palladin in actin organization and cell motility, Eur. J. Cell Biol. 87 (2008) 517–525.

[71] S. Goicoechea, Palladin binds to Eps8 and enhances the formation of dorsal ruffles and podosomes in vascular smooth muscle cells, J. Cell Sci. 119 (2006) 3316–3324.

[72] H. Luo, X. Liu, F. Wang, Q. Huang, S. Shen, L. Wang, et al., Disruption of palladin results in neural tube closure defects in mice, Mol. Cell. Neurosci. 29 (2005) 507–515.

[73] L. Jin, T. Yoshida, R. Ho, G.K. Owens, A.V. Somlyo, The Actin-associated Protein Palladin Is Required for Development of Normal Contractile Properties of Smooth Muscle Cells Derived from Embryoid Bodies, J. Biol. Chem. 284 (2008) 2121–2130.

[74] B. Sjöblom, A. Salmazo, K. Djinović-Carugo, α-Actinin structure and regulation, Cell. Mol. Life Sci. 65 (2008) 2688–2701.

[75] R. Zaidel-Bar, S. Itzkovitz, A. Ma'ayan, R. Iyengar, B. Geiger, Functional atlas of the integrin adhesome, Nat. Cell Biol. 9 (2007) 858–867.

[76] H. Nyman-Huttunen, L. Tian, L. Ning, C.G. Gahmberg, alpha-Actinin-dependent cytoskeletal anchorage is important for ICAM-5-mediated neuritic outgrowth, J. Cell Sci. 119 (2006) 3057–3066.

[77] B. Knight, C. Laukaitis, N. Akhtar, N.A. Hotchin, M. Edlund, A.R. Horwitz, Visualizing muscle cell migration in situ, Curr. Biol. CB. 10 (2000) 576–585.

[78] T. Ohtaki, S. Tsukita, N. Mimura, S. Tsukita, A. Asano, Interaction of actinogelin with actin. No nucleation but high gelation activity, Eur. J. Biochem. FEBS. 153 (1985) 609–620.

[79] J. Käs, H. Strey, J.X. Tang, D. Finger, R. Ezzell, E. Sackmann, et al., F-actin, a model polymer for semiflexible chains in dilute, semidilute, and liquid crystalline solutions, Biophys. J. 70 (1996) 609–625.

[80] Y. Tseng, T.P. Kole, J.S.H. Lee, E. Fedorov, S.C. Almo, B.W. Schafer, et al., How actin crosslinking and bundling proteins cooperate to generate an enhanced cell mechanical response, Biochem. Biophys. Res. Commun. 334 (2005) 183–192.

[81] M. Tempel, G. Isenberg, E. Sackmann, Temperature-induced sol-gel transition and microgel formation in α-actinin cross-linked actin networks: a rheological study, Phys. Rev. E. 54 (1996) 1802.

[82] S.M.V. Ward, A. Weins, M.R. Pollak, D.A. Weitz, Dynamic viscoelasticity of actin cross-linked with wild-type and disease-causing mutant alpha-actinin-4, Biophys. J. 95 (2008) 4915–4923.

[83] M.L. Gardel, J.H. Shin, F.C. MacKintosh, L. Mahadevan, P. Matsudaira, D.A. Weitz, Elastic behavior of cross-linked and bundled actin networks, Science. 304 (2004) 1301–1305.

[84] K.M. Schmoller, O. Lieleg, A.R. Bausch, Structural and Viscoelastic Properties of Actin/Filamin Networks: Cross-Linked versus Bundled Networks, Biophys. J. 97 (2009) 83–89.

[85] K. Schmoller, O. Lieleg, A. Bausch, Cross-Linking Molecules Modify Composite Actin Networks Independently, Phys. Rev. Lett. 101 (2008).

[86] F.C. MacKintosh, J. Käs, P.A. Janmey, Elasticity of semiflexible biopolymer networks, Phys. Rev. Lett. 75 (1995) 4425–4428.

[87] R.K. Meyer, U. Aebi, Bundling of actin filaments by alpha-actinin depends on its molecular length., J. Cell Biol. 110 (1990) 2013–2024.

[88] W. Mickel, S. Münster, L.M. Jawerth, D.A. Vader, D.A. Weitz, A.P. Sheppard, et al., Robust Pore Size Analysis of Filamentous Networks from Three-Dimensional Confocal Microscopy, Biophys. J. 95 (2008) 6072–6080.

[89] J.H. Shin, M.L. Gardel, L. Mahadevan, P. Matsudaira, D.A. Weitz, Relating microstructure to rheology of a bundled and cross-linked F-actin network in vitro, Proc. Natl. Acad. Sci. U. S. A. 101 (2004) 9636–9641.

[90] S.B. Lindström, D.A. Vader, A. Kulachenko, D.A. Weitz, Biopolymer network geometries: characterization, regeneration, and elastic properties, Phys. Rev. E Stat. Nonlin. Soft Matter Phys. 82 (2010) 051905.

[91] A.M. Stein, D.A. Vader, L.M. Jawerth, D.A. Weitz, L.M. Sander, An algorithm for extracting the network geometry of three-dimensional collagen gels, J. Microsc. 232 (2008) 463–475.

[92] O. Lieleg, A. Bausch, Cross-Linker Unbinding and Self-Similarity in Bundled Cytoskeletal Networks, Phys. Rev. Lett. 99 (2007).

[93] M. Gardel, F. Nakamura, J. Hartwig, J. Crocker, T. Stossel, D. Weitz, Stress-Dependent Elasticity of Composite Actin Networks as a Model for Cell Behavior, Phys. Rev. Lett. 96 (2006).

[94] C. Storm, J.J. Pastore, F.C. MacKintosh, T.C. Lubensky, P.A. Janmey, Nonlinear elasticity in biological gels, Nature. 435 (2005) 191–194.

[95] G.M. Popowicz, M. Schleicher, A.A. Noegel, T.A. Holak, Filamins: promiscuous organizers of the cytoskeleton, Trends Biochem. Sci. 31 (2006) 411–419.

[96] O. Lieleg, M.M.A.E. Claessens, Y. Luan, A.R. Bausch, Transient binding and dissipation in cross-linked actin networks, Phys. Rev. Lett. 101 (2008) 108101.

[97] O. Lieleg, K.M. Schmoller, M.M.A.E. Claessens, A.R. Bausch, Cytoskeletal Polymer Networks: Viscoelastic Properties are Determined by the Microscopic Interaction Potential of Cross-links, Biophys. J. 96 (2009) 4725–4732.

[98] E. Borrego-Diaz, F. Kerff, S.H. Lee, F. Ferron, Y. Li, R. Dominguez, Crystal structure of the actin-binding domain of alpha-actinin 1: evaluating two competing actin-binding models, J. Struct. Biol. 155 (2006) 230–238.

[99] M. Boukhelifa, M. Moza, T. Johansson, A. Rachlin, M. Parast, S. Huttelmaier, et al., The proline-rich protein palladin is a binding partner for profilin, FEBS J. 273 (2006) 26–33.

[100] M.B. Omary, A. Lugea, A.W. Lowe, S.J. Pandol, The pancreatic stellate cell: a star on the rise in pancreatic diseases, J. Clin. Invest. 117 (2007) 50–59.

[101] S.M. Goicoechea, B. Bednarski, C. Stack, D.W. Cowan, K. Volmar, L. Thorne, et al., Isoform-Specific Upregulation of Palladin in Human and Murine Pancreas Tumors, PLoS ONE. 5 (2010) e10347.

[102] S.M. Goicoechea, B. Bednarski, R. García-Mata, H. Prentice-Dunn, H.J. Kim, C.A. Otey, Palladin contributes to invasive motility in human breast cancer cells, Oncogene. 28 (2008) 587–598.

[103] S.E. Cross, Y.-S. Jin, J. Rao, J.K. Gimzewski, Nanomechanical analysis of cells from cancer patients, Nat. Nanotechnol. 2 (2007) 780–783.

[104] W. Xu, R. Mezencev, B. Kim, L. Wang, J. McDonald, T. Sulchek, Cell Stiffness Is a Biomarker of the Metastatic Potential of Ovarian Cancer Cells, PLoS ONE. 7 (2012) e46609.

[105] V. Swaminathan, K. Mythreye, E.T. O'Brien, A. Berchuck, G.C. Blobe, R. Superfine, Mechanical Stiffness Grades Metastatic Potential in Patient Tumor Cells and in Cancer Cell Lines, Cancer Res. 71 (2011) 5075–5080.

[106] H. Huang, R.D. Kamm, R.T. Lee, Cell mechanics and mechanotransduction: pathways, probes, and physiology, Am. J. Physiol. Cell Physiol. 287 (2004) C1–11.

[107] C. Guilluy, V. Swaminathan, R. Garcia-Mata, E. Timothy O'Brien, R. Superfine, K. Burridge, The Rho GEFs LARG and GEF-H1 regulate the mechanical response to force on integrins, Nat. Cell Biol. 13 (2011) 724–729.

[108] J.K. Fisher, J. Cribb, K.V. Desai, L. Vicci, B. Wilde, K. Keller, et al., Thin-foil magnetic force system for high-numerical-aperture microscopy, Rev. Sci. Instrum. 77 (2006) nihms8302.

[109] C.T. Mierke, P. Kollmannsberger, D. Paranhos Zitterbart, J. Smith, B. Fabry, W.H. Goldmann, Mechano-Coupling and Regulation of Contractility by the Vinculin Tail Domain, Biophys. J. 94 (2008) 661–670.

[110] A.R. Bausch, U. Hellerer, M. Essler, M. Aepfelbacher, E. Sackmann, Rapid stiffening of integrin receptor-actin linkages in endothelial cells stimulated with thrombin: a magnetic bead microrheology study, Biophys. J. 80 (2001) 2649–2657.

[111] L. Guolla, M. Bertrand, K. Haase, A.E. Pelling, Force transduction and strain dynamics in actin stress fibres in response to nanonewton forces, J. Cell Sci. 125 (2012) 603–613.

[112] C. Collins, C. Guilluy, C. Welch, E.T. O'Brien, K. Hahn, R. Superfine, et al., Localized Tensional Forces on PECAM-1 Elicit a Global Mechanotransduction Response via the Integrin-RhoA Pathway, Curr. Biol. 22 (2012) 2087–2094.

[113] L.M. Hoffman, C.C. Jensen, A. Chaturvedi, M. Yoshigi, M.C. Beckerle, Stretch-induced actin remodeling requires targeting of zyxin to stress fibers and recruitment of actin regulators, Mol. Biol. Cell. 23 (2012) 1846–1859.

[114] X.-H. Zhao, C. Laschinger, P. Arora, K. Szaszi, A. Kapus, C.A. McCulloch, Force activates smooth muscle -actin promoter activity through the Rho signaling pathway, J. Cell Sci. 120 (2007) 1801–1809.

[115] K.E. Kasza, F. Nakamura, S. Hu, P. Kollmannsberger, N. Bonakdar, B. Fabry, et al., Filamin A is essential for active cell stiffening but not passive stiffening under external force, Biophys. J. 96 (2009) 4326–4335.

[116] A.G. Passerini, D.C. Polacek, C. Shi, N.M. Francesco, E. Manduchi, G.R. Grant, et al., Coexisting proinflammatory and antioxidative endothelial transcription profiles in a

disturbed flow region of the adult porcine aorta, Proc. Natl. Acad. Sci. U. S. A. 101 (2004) 2482–2487.

[117] S. Pellegrin, H. Mellor, Actin stress fibres, J. Cell Sci. 120 (2007) 3491–3499.

[118] M. Lenz, M.L. Gardel, A.R. Dinner, Requirements for contractility in disordered cytoskeletal bundles, New J. Phys. 14 (2012) 033037.

[119] M. Lenz, T. Thoresen, M.L. Gardel, A.R. Dinner, Contractile Units in Disordered Actomyosin Bundles Arise from F-Actin Buckling, Phys. Rev. Lett. 108 (2012).

[120] T. Thoresen, M. Lenz, M.L. Gardel, Reconstitution of Contractile Actomyosin Bundles, Biophys. J. 100 (2011) 2698–2705.

[121] L.J. Peterson, Z. Rajfur, A.S. Maddox, C.D. Freel, Y. Chen, M. Edlund, et al., Simultaneous stretching and contraction of stress fibers in vivo, Mol. Biol. Cell. 15 (2004) 3497–3508.

[122] A. Besser, U.S. Schwarz, Coupling biochemistry and mechanics in cell adhesion: a model for inhomogeneous stress fiber contraction, New J. Phys. 9 (2007) 425–425.

[123] S.-M. Lim, J.P. Trzeciakowski, H. Sreenivasappa, L.J. Dangott, A. Trache, RhoA-induced cytoskeletal tension controls adaptive cellular remodeling to mechanical signaling, Integr. Biol. 4 (2012) 615.

[124] A.E. Pelling, D.W. Dawson, D.M. Carreon, J.J. Christiansen, R.R. Shen, M.A. Teitell, et al., Distinct contributions of microtubule subtypes to cell membrane shape and stability, Nanomedicine Nanotechnol. Biol. Med. 3 (2007) 43–52.

[125] J. Engelberth, Mechanosensing and signaltransduction in tendrils, Adv. Space Res. 32 (2003) 1611–1619.

[126] K.A. DeMali, K. Wennerberg, K. Burridge, Integrin signaling to the actin cytoskeleton, Curr. Opin. Cell Biol. 15 (2003) 572–582.

[127] K. Burridge, K. Wennerberg, Rho and Rac take center stage, Cell. 116 (2004) 167–179.

[128] Z.M. Goeckeler, P.C. Bridgman, R.B. Wysolmerski, Nonmuscle myosin II is responsible for maintaining endothelial cell basal tone and stress fiber integrity, AJP Cell Physiol. 295 (2008) C994–C1006.

[129] N. Wang, J.P. Butler, D.E. Ingber, Mechanotransduction across the cell surface and through the cytoskeleton, Science. 260 (1993) 1124–1127.

[130] L. Fabian, J. Troscianczuk, A. Forer, Calyculin A, an enhancer of myosin, speeds up anaphase chromosome movement, Cell Chromosome. 6 (2007) 1.

[131] H. Ishihara, H. Ozaki, K. Sato, M. Hori, H. Karaki, S. Watabe, et al., Calcium-independent activation of contractile apparatus in smooth muscle by calyculin-A, J. Pharmacol. Exp. Ther. 250 (1989) 388–396.

[132] E.L. Barnhart, K.-C. Lee, K. Keren, A. Mogilner, J.A. Theriot, An Adhesion-Dependent Switch between Mechanisms That Determine Motile Cell Shape, PLoS Biol. 9 (2011) e1001059.

[133] P.T. Yam, C.A. Wilson, L. Ji, B. Hebert, E.L. Barnhart, N.A. Dye, et al., Actin-myosin network reorganization breaks symmetry at the cell rear to spontaneously initiate polarized cell motility, J. Cell Biol. 178 (2007) 1207–1221.

[134] M. Parizi, E.W. Howard, J.J. Tomasek, Regulation of LPA-promoted myofibroblast contraction: role of Rho, myosin light chain kinase, and myosin light chain phosphatase, Exp. Cell Res. 254 (2000) 210–220.

[135] G. Pearson, F. Robinson, T.B. Gibson, B. Xu, M. Karandikar, K. Berman, et al., Mitogen-activated protein (MAP) kinase pathways: regulation and physiological functions, Endocr. Rev. 22 (2001) 153–183.

[136] J.D. Laporte, P.E. Moore, J.H. Abraham, G.N. Maksym, B. Fabry, R.A. Panettieri Jr, et al., Role of ERK MAP kinases in responses of cultured human airway smooth muscle cells to IL-1beta, Am. J. Physiol. 277 (1999) L943–951.

[137] A.E. Aplin, R.L. Juliano, Integrin and cytoskeletal regulation of growth factor signaling to the MAP kinase pathway, J. Cell Sci. 112 (1999) 695–706.

[138] S. Kumar, I.Z. Maxwell, A. Heisterkamp, T.R. Polte, T.P. Lele, M. Salanga, et al., Viscoelastic Retraction of Single Living Stress Fibers and Its Impact on Cell Shape, Cytoskeletal Organization, and Extracellular Matrix Mechanics, Biophys. J. 90 (2006) 3762–3773.

[139] Y. Feng, J. Goree, B. Liu, Accurate particle position measurement from images, Rev. Sci. Instrum. 78 (2007) 053704–053704.

[140] P. Felzenszwalb, D. Huttenlocher, Distance transforms of sampled functions, Cornell University, 2004.